Study of the Dicke model: From phase space approach to quantum trajectories

Felipe Dimer de Oliveira

A thesis

submitted in partial fulfilment

of the requirement of the degree

of

Doctor of philosophy

at the

University of Auckland

Auckland – New Zealand

August 20, 2008

To Paula ...

Acknowledgments

I would like to express my gratitude to my supervisor, Prof. Howard Carmichael, for being so patient and always ready to provide any help; I'm in great debt to him for making my PhD in New Zealand possible. I would like to thank my co-supervisor, Dr. Scott Parkins, for making all effort to help me during these 3 years, as well as kindly correcting the many mistakes I did while writing this thesis.

My relation with the University of Auckland comes from 2001, when I started my masters degree supervised by a former student of Prof. Dan Walls, Murray Olsen, who I whish to thank for his friendship and moral support during my stay in Auckland. My thanks also to Prof. Chris Tindle for making me feel welcome when I arrived in NZ in 2004, as well as all the staff, specially Francie Norman and Nigel Lewin, for helping me to carry my duties as LTT.

I wish to thank the good friends I made while in Auckland. They helped me a lot in raising my morale during the long time I spent away from home. Specially Chang-Suk, Pablo German, Levente Horvath, Andy Chia, Benoit Estienne, Malkhaz Meladze, Frederique and Stephane.

A special thanks for my family for all support I received from them during these long three years.

Felipe Dimer de Oliveira

Abstract

In this thesis we study the Dicke model outside the rotating wave approximation (RWA), by employing phase space techniques and the quantum trajectory theory. We present a review of the basic models of open systems in quantum optics and present an experimental proposition justifying the model to be studied. We use the phase space approach to study, among other subjects, entanglement, squeezing and fluctuations across a quantum phase transition. Three different phase space representations are used and their strengths and weaknesses compared. The quantum trajectory theory is applied to visualise the global quantum fluctuations and to learn how different measurement schemes will affect the creation of entanglement.

Contents

List of Figures

1. Introduction

The main objective of quantum electrodynamics (QED) is to describe the interaction between light and matter; indeed it is regarded as one of the (if not the) most precise theories of physics in its agreement with experimental results. Despite its exceptional explanatory power, QED still has unexplored areas; one of these concerns systems with many particles – a rich field of research even in classical mechanics. For example, the subtle limit between microscopic (quantum) and macroscopic (classical) systems is a fundamental problem in many-body quantum mechanics, yet to be fully understood. One of the main difficulties in dealing with many-body problems in quantum mechanics is computational. For a number N of two level atoms, 2^N states are needed to fully describe the state of the system, and one must seek approximation methods. In the quantum optics context the main tool to deal with macroscopic problems is the quantum-to-classical correspondence, which maps a discrete many-body system onto a description in terms of a continuous probability distribution, generating partial differential equations to be solved or simulated. One of the aims of the present work is to explore the "traditional" quantum optics methods for many body problems, namely: the Holstein-Primakoff representation, the Haken representation, and the atomic coherent states representation.

The methods *per se* have no meaning if there is no relevant physical system being studied. Quantum optics experimental setups are composed mainly of lasers, cavities, and atoms. In the archetypical experiment, one or several atoms are held within a cavity and illuminated by a laser. The objective is, ultimately, to control precisely the state of the atoms by a suitable choice of the experimental configuration. One of the

obstacles faced arises through the coupling between the system and the many degrees of freedom of the environment surrounding the system; specifically, in quantum optics, this introduces irreversible losses due to the coupling of the atoms to the many modes of the electromagnetic field of free space. The purpose of the cavity is to provide a high intensity electric field, which interacts coherently with the atoms, and a common mode for all atoms to couple to at once. The cavity is also coupled to the environment and photons may be lost irreversibly from it. The role of the laser is to coherently drive the atoms to the excited state. We identify a balance between the atom-cavity field interaction, i.e. atoms exchanging photons with the cavity mode, and losses – photons being lost from the atoms and cavity to the environment (spontaneous emission and cavity losses respectively). In the past, in the optical regime, cavity losses overcame the coherent interaction between the field and the atoms [2]; in this situation, the system behaves as an overdamped pendulum – the atoms lose photons to the cavity and the cavity loses photons to the environment faster than they can be reabsorbed. In recent years, however, improvements in experimental techniques have made it possible to achieve cavities with finesse – the number of times photons bounce back and forth before leaving the cavity – several orders of magnitude higher than what was done in early quantum optics experiments. In this regime, coherent dynamics dominate the evolution of the state of the system before dissipation takes place; photons are coherently absorbed, emitted and reabsorbed by the atoms several times before leaving the cavity.

Having presented the methods and the experimental context we are aiming at, now we turn our attention to describe the specific configuration treated in this thesis. Our interest is to combine many-body quantum problems and cavity quantum electrodynamics in the strong coupling regime. We are inspired by the pioneering work of Dicke [3]. In that work, a collection of atoms, assumed to be sufficiently far apart that the inter-atomic interactions may be neglected, is considered to be coupled to a common single-mode field. It was thought that without direct interaction (dipole-dipole), the atoms should act independently of each other, and the maximum intensity of emitted radiation should be proportional to the number of atoms N. Dicke realized that the field is also a mediator

of the inter-atomic interactions. The resulting effect is that the atoms act collectively, in the same way as a set of coupled harmonic oscillators can swing in or out of phase with one another. The emission pattern in this case shows a burst of intense radiation with intensity proportional to N^2; this phenomenon is known as Dicke superradiance. Dicke's work did not consider cavities and lasers. Instead, its experimental context was that of a cloud of two level atoms excited by means of a intense source of coherent (microwave) radiation – a maser. The emitted radiation field of each atom provides the common field the atoms need to act collectively. Without the cavity, the energy in the atoms is lost irreversibly to the many modes of the free space electromagnetic field. The common field will enhance these losses when compared with the single atom (or independent emitters) case. As noticed by [4], the system is nothing but an open laser, with the common field playing the role of the cavity field.

The application of the Dicke model to the present background in quantum optics experiments in the strong coupling regime should be obvious: a cloud of two level atoms inside a cavity is excited by a laser. As in the original work of Dicke, we have to consider the atoms well separated so dipole-dipole interactions are negligible. The cavity mode provides the common field the atoms need to act collectively [1]. Within the strong coupling regime, the full coherent atomic dynamics becomes relevant. The light-atom interaction is modeled by the Tavis-Cummings Hamiltonian, and an exact solution for this many atoms case is known [5]. In this way the interesting quantities, like fluorescence spectra, correlation functions and entanglement can be easily calculated.

We have presented our methods, experimental context and system of interest. The physical system, as can be seen from the references, is a well established example studied previously in quantum optics. Our intention is to study the quantum optics version of the Dicke model adding something new to the existing framework. Up to now, little attention has been paid to the Dicke model outside the rotating wave approximation

[1] Actually, as we explain in chapter 4, ring cavities must be used in order to achieve the regime where all atoms couple to the same field. In a cavity with parallel mirrors, the atoms would need to be at the anti-nodes of the field, or the atomic cloud have dimensions much smaller than the wavelength. These setups are experimentally difficult for the optical domain.

(RWA). Consider the Hamiltonian modeling the atom-photon dipole interaction through the atomic dipole moment (with $\hbar$ set to unity),

$$\hat{H} = \omega \hat{a}^\dagger \hat{a} + \sum_i \frac{1}{2}\omega_0 \sigma_{iz} + \sum_i \lambda \left(\hat{a}^\dagger + \hat{a}\right)(\sigma_{i+} + \sigma_{i-}), \tag{1.1}$$

where ω is the frequency of the field, ω_0 is the frequency of the atomic transition, λ is the (dipole) coupling strength between the field and the atoms (depending on the intensity of the cavity electric field), the operators $\hat{a}^\dagger$ and $\hat{a}$ are the usual field creation and annihilation operators, respectively, σ_{iz} is the Pauli matrix representing the energy of atom i, and $\sigma_{i\pm}$ are the Pauli matrices representing the dipole moment of this atom. The rotating wave approximation consists in neglecting the terms $\hat{a}^\dagger\sigma_+$ and $\hat{a}\sigma_-$, given the condition $\omega, \omega_0 \gg \lambda$, which is easily satisfied at optical frequencies ($\omega \approx 10^9$ MHz against $\lambda \approx 10$ MHz [6]). By introducing the RWA into Hamiltonian (1.1) the system becomes integrable, i.e., its energy eigenstates have a closed solution as a linear combination, with finite number of terms, of states $|n\rangle|\pm\rangle$, where $|n\rangle$ are eigenstates of $\hat{a}^\dagger\hat{a}$, and $|\pm\rangle$ are eigenstates of σ_z. Also, the Hamiltonian in the RWA conserves the total number of quanta in the system, hence, if the system experiences any damping, its steady state is one of no energy left in the field.

The inclusion of the counter rotating terms in a regime where $\omega, \omega_0 \approx \lambda$ changes this situation. The energy eigenstates have no closed solution as in the RWA case described above. In a situation where the RWA is not valid, the total number of quanta is not conserved. With the inclusion of damping, in this case the system may or may not, depending on the strength of the coupling λ, have a steady state with non-zero flux of output photons. We must observe that this non-zero net photon flux at steady state is a consequence of the fact that the full non-RWA model we present is an effective model, derived from what is in fact an open system. As we show in Chapter 4, to realize the full non-RWA model we must introduce an external source of energy, which accounts for the non-zero output of photons in the steady state. In the limit where the number of atoms goes to infinity, the passage from the non-radiating to the radiating regime, as the coupling reaches a critical value, occurs through a non-analyticity in the equations for the mean values of operators. This indicates the presence of a quantum phase transition,

with which is associated the appearance of entanglement [7, 8]. The study of a phase transition in the Dicke model is not novel. Hepp and Lieb reported the existence of such a transition in the early 1970s [9], where the focus was on the interplay between the common field as an ordering factor for the atomic system and the disordering introduced by thermal fluctuations of the environment at non-zero temperature. The Hepp and Lieb phase transition exists whether or not the RWA is made.

To our knowledge, there is no work that considers the non-RWA Dicke model in a phase space approach, nor any attempt to study this system for a finite number of atoms under a more complete theory of open quantum systems, like quantum trajectory theory, which allows us to study the behaviour of the system when subjected to a specific measurement scheme.

The lack of attention paid to this system in the regime we propose to study is largely due to the non-existence of a suitable experimental realization which would justify further interest in a quantum optics approach. The obvious approach – making the coupling constant λ of Hamiltonian (1.1) large enough – would not work. To start with, there is the experimental difficulty in achieving this regime, which would require a large cavity field. Then, even if it is achieved, Hamiltonian (1.1) is no longer a good description for the system. The electric dipole Hamiltonian presented above has its origin in the atomic Hamiltonian

$$\hat{H} = \frac{1}{2\mu} \left(\mathbf{p} - e\mathbf{A} \right)^2 ,$$

where μ is the reduced mass of the nucleus-electron system, $\mathbf{p}$ is the momentum operator, e is the electron charge, and $\mathbf{A}$ is the potential vector. In the usual regime, where the RWA is valid, the self energy term $e^2\mathbf{A}^2$ is negligible [10, Section III.D.1]. The inclusion of this term for large cavity fields has been shown to destroy the thermodynamic phase transition of Hepp and Lieb [11, 12, 13, 14, 15].

We propose in this thesis a system whose effective Hamiltonian is given by equation (1.1), and where the field-atom coupling can be adjusted so the regime $\omega, \omega_0 \simeq \lambda$ can be explored. Our proposal consists of an atom coupled to a cavity mode through a pair of Raman transitions, which are driven by external lasers. In contrast to the approach

of Hepp and Lieb, we deal with an open system with external driving lasers and cavity dissipation. The non-zero photon flux in the dissipative case is a consequence of the continuous input of energy from the external lasers. The thermal equilibrium phase transition in the sense of Hepp and Lieb is not relevant to the model we propose.

Once our proposal for an experimental realisation of the Dicke model has been presented and justified, we focus on the application of quantum optics methods for many-body systems to the proposed model. The inclusion of the counter-rotating terms makes the system non-integrable – there is no closed solution for its eigenvalues and eigenvectors. To study this system in the thermodynamic limit (i.e. number of atoms $N \to \infty$) we adopt three approaches: (i) the Holstein-Primakoff representation [16] (ii) the Haken representation [17] and (iii) the atomic coherent state representation [18]. All approaches are developed using the Positive-P representation [19]. Each one of these techniques has its own advantages and disadvantages. The Holstein-Primakoff approach is used to study entanglement, squeezing and the fluctuations of the system across the phase transition. We show how the Haken representation, in its linearized form, fails to conserve angular momentum, but nevertheless returns correct results for the fluctuations of the cavity field. The atomic coherent state representation is treated for completeness, since it yields a Fokker-Planck equation for a finite number of atoms (without the need for linearisation).

The thermodynamic limit is useful to learn about the global behaviour of the system, as quantum fluctuations become negligible in this limit. Quantum fluctuations usually scale with $N^{-1/2}$, and become important when we are dealing with a small number of atoms strongly coupled to a cavity mode, which today is a feasible experimental setup. Computationally, it may be difficult to carry out simulations taking into account the full state of the system if we are treating hundreds of atoms. We study quantum fluctuations in the Dicke model for finite numbers of atoms, usually on the order of tens of atoms, by using the quantum trajectory theory. One advantage of using this theory is computational: the open system dynamics, with losses included, can be described in terms of states instead of density matrices – needed when evolving the system using a

master equation approach. This reduces the number of equations needed to describe the dynamical evolution of the system, as we are dealing with state amplitudes instead of matrix elements. Quantum trajectory theory also provides a way of studying the backaction of measurements, set in different ways, in the system. There has been recent interest in how measurement can preserve or destroy entanglement in quantum-optical systems [20], and in the relationship between measurement and emergence of classical chaos [21, 22].

In summary, we propose a feasible realization of a many body quantum optical system which shows many interesting phenomena and presents a good opportunity to explore a number of quantum optics methods. The outline of the thesis is as follows. Chapter 2 reviews the results of the Dicke model of superradiance applied to the basic systems of quantum optics, explaining the approximations used and their range of validity. Chapter 3 is a review of the Dicke phase transition at non-zero temperature. In Chapter 4 we derive the main Hamiltonian used throughout the remainder of the thesis, and give the corresponding experimental setup. The results of our analysis of the proposed system are given in the following three chapters. In Chapter 5 we first adopt a phase space approach using the Holstein-Primakoff representation to study the system in the thermodynamic limit – where the number of atoms tends to infinity; there we are concerned with entanglement, squeezing, and the behaviour of the fluctuations in the vicinity of the phase transition. In Chapter 6 we introduce the Haken representation for the atoms and use it to repeat the study of the thermodynamic limit. There we show that the Haken representation in its linearized form fails to conserve total angular momentum, but the correct results for field correlation functions are nevertheless obtained. In the same chapter we use the atomic coherent states representation to derive an exact phase space equation for the mesoscopic regime. The results of the thermodynamic limit are compared to the finite number of atoms case in Chapter 7. There we use the quantum trajectory theory to simulate a specific measurement scheme, which we shall use in order to study the dynamical creation of entanglement in the quantum phase transition.

2. Dicke model in the rotating wave approximation

In the theory of quantum radiative emission, the probability that an atom will remain excited decreases exponentially with time [23, 24]. Considering a large number N of (excited) atoms acting *independently* of each other, this would give a continuous radiative emission with the intensity fading exponentially. The radiation emitted is incoherent and proportional to the number of atoms N. This picture is generally valid for large inter-atomic distances (negligible dipole-dipole interactions), and disregards the common field as a mediator of interactions between the atoms. In this chapter we shall show the basic result of the Dicke model for superradiance: that a collection of atoms coupled to, and through, a common field will cooperate to give an intense burst of radiation with maximum intensity proportional to N^2. In doing so, we shall define the Dicke states and collective atomic operators and show their applications within the rotating wave approximation (RWA) – to be explained later. Two regimes are studied within this approximation: weak coupling – where the losses are more important than coupling via the common field and a master equation is used – and the strong coupling regime, where Hamiltonian dynamics plays the main role.

2.1. Dicke states and emission from a collection of atoms

2.1.1. Hamiltonian and collective atomic operators

Consider the Hamiltonian modeling a collection of N two level atoms, each one at a site identified by the index i, interacting with an electromagnetic (EM) field resonant with

the atomic transition:

$$\frac{\hat{H}}{\hbar} = \frac{\omega_0}{2}\sum_i^N \sigma_{zi} + \sum_i^N \mathbf{E}(\mathbf{r}_i)\cdot\mathbf{D}_i. \tag{2.1}$$

Here, $\mathbf{E}(r_i)$ is the electric field at the position $\mathbf{r}_i$, $\mathbf{D}_i$ is the electric dipole moment operator of the atom labeled by the index i, ω_0 is the frequency of the atomic transition, and σ_{zi} is a Pauli matrix for atom i, where the Pauli matrices are defined as

$$\sigma_x = \begin{bmatrix} 0 & 1 \\ 1 & 0 \end{bmatrix}, \sigma_y = \begin{bmatrix} 0 & -i \\ i & 0 \end{bmatrix}, \sigma_z = \begin{bmatrix} 1 & 0 \\ 0 & -1 \end{bmatrix}. \tag{2.2}$$

These matrices have eigenvalues ± 1 and obey the commutation rules

$$[\sigma_x, \sigma_y] = 2i\sigma_z,\ [\sigma_z, \sigma_x] = 2i\sigma_y,\ [\sigma_y, \sigma_z] = 2i\sigma_x. \tag{2.3}$$

The Hamiltonian describing the interaction between atoms and photons can be written in terms of the potential vector. It usually appears in the literature (for a single atom) in the form

$$\hat{H}' = \frac{1}{2\mu}\left(\mathbf{p} - e\mathbf{A}\right)^2 + V(r), \tag{2.4}$$

where μ is the reduced mass of the nucleus-electron system, $\mathbf{A}$ is the potential vector, e is the electron charge, $\mathbf{p}$ is the momentum of the electron, and $V(r)$ is the central (Coulomb) potential depending only on the relative distance r between nucleus and electron. In neglecting the $\mathbf{A}^2$ term, the above Hamiltonian can be shown to be equivalent to (2.1). The term

$$\hat{H}_0 = \frac{\mathbf{p}^2}{2\mu} + V(r), \tag{2.5}$$

gives a discrete set of energy levels as its eigenvalues, from which we choose two, such that their energy difference is resonant with the EM field. This term corresponds to the one proportional to the Pauli matrix σ_z. The atom-field interaction term

$$\hat{W} = \frac{e\mathbf{A}\cdot\mathbf{p}}{\mu}, \tag{2.6}$$

is written in the subspace of the two levels we chose for the transition. We denote the eigenvectors of the non-interacting Hamiltonian, $\hat{H}_0$, by $|\omega_i\rangle, |\omega_j\rangle$, with eigenvalues ω_i

and ω_j. These eigenvectors are used as a basis to write the matrix elements of the atom-field interaction term, $\hat{W}$. With the help of $\left[\mathbf{r}, \hat{H}_0\right] = i\hbar\mathbf{p}/m$ we obtain

$$i\langle\omega_i|e\mathbf{A}\left[\mathbf{r}, \hat{H}_0\right]|\omega_j\rangle = i(\omega_j - \omega_i)\mathbf{A}\cdot\langle\omega_i|e\mathbf{r}|\omega_j\rangle = i\frac{\mathbf{E}}{\omega}(\omega_i - \omega_j)\cdot\mathbf{D}_{ij}, \tag{2.7}$$

where we consider a harmonic field – so the vector potential has the form $\mathbf{E}/\omega$ – and the transition energy is resonant with the field ($\omega_i - \omega_j = \omega$). The dipole moment $\mathbf{D}_{ij}$, to be defined below, has only non-diagonal matrix elements connecting states $|\omega_i\rangle \leftrightarrow |\omega_j\rangle$. This equivalence can be shown as a gauge transformation in the potential vector [25, Complement $\mathsf{A}_{\mathrm{XIII}}$]. The self energy term is neglected compared with the interaction term; their ratio can be written as

$$\frac{e^2A^2/2\mu}{eAp/\mu} = \frac{eAp/2\mu}{p^2/\mu}, \tag{2.8}$$

where we have replaced the operators by their mean-square values. We identify in the last term the ratio between interaction energy and the kinetic energy. For low intensity radiation, this ratio is fairly small and can be neglected [10, Section III.D.1]. In this thesis we opt for writing the interaction Hamiltonian with the term $\mathbf{E}\cdot\mathbf{D}$, which is usually associated with electric dipole energy. The discussion of the potential vector Hamiltonian is of importance to the relevance of the A^2 term to the Dicke phase transition, a topic we take up in Chapter 3.

The electric field $\mathbf{E}$ is to be considered a classical quantity for the moment. The electric dipole of atom i is given by the operator $e\hat{\mathbf{r}}_i$. We define the atomic state space basis as the excited and ground state eigenvectors of the free atomic Hamiltonian denoted, $|+\rangle$ and $|-\rangle$ respectively. In this basis the electric dipole operator of atom i is given, in terms of the Pauli matrices σ_x and σ_y, by

$$\mathbf{D}_i = \mathrm{Re}(\mathbf{d}_{+-})\frac{\sigma_{xi}}{2} + \mathrm{Im}(\mathbf{d}_{+-})\frac{\sigma_{yi}}{2}, \tag{2.9}$$

where $\mathbf{d}_{+-}$ is the dipole matrix element $2e\langle+|\mathbf{r}_i|-\rangle$. Without loss of generality, we are able to find two axes $\mathbf{x}$ and $\mathbf{y}$ in which the matrix elements $\mathbf{d}_x = \langle+|\mathbf{x}|-\rangle$ and $\mathbf{d}_y = \langle+|\mathbf{y}|-\rangle$ are real [26, Complement E_{VI}]. By doing this we can write $\mathbf{d}_{+-} = \mathbf{d}_x + i\mathbf{d}_y$.

This dipole Hamiltonian is a very good approximation provided the electric field has no significant gradient for distances of the order of the atomic size or, equivalently, for an EM wave whose wavelength is bigger than the atomic diameter. This condition is easily satisfied for the usual experimental setups at optical frequencies (wavelengths $\sim 10^{-6}$m versus atomic size of the order of Å). The use of the dipole Hamiltonian corresponds to neglecting the spatial variation of the electric field (i.e. making $\mathbf{E}(\mathbf{r}_i) = \mathbf{E}(0)$), and is referred to as the dipole approximation.

For the situation we are treating here – a collection of atoms interacting with an EM wave – we consider that the atoms are confined to a volume smaller than the wavelength, so all atoms see the same field, and we can replace $\mathbf{E}(\mathbf{r}_i)$ by $\mathbf{E}(0)$ in (2.1). This was justified in the original work of Dicke [3], as the system envisaged was a gas cell excited by microwave radiation, which has wavelength of the order of 10^{-1}m; for that setup the approximation is often referred to as the long wavelength approximation. At optical frequencies, in particular for gases, it is difficult to achieve the configuration envisaged by Dicke. We show in Chapter 4 that with the use of a ring cavity it is possible to overcome this difficulty [27]; this is the sense in which we use the term "long wavelength approximation" in the remainder of this chapter. Under this approximation, the dipole Hamiltonian (2.1) reads

$$\mathbf{E}(0) \cdot \left(\mathbf{d}_x \sum_i^N \frac{\sigma_{xi}}{2} + \mathbf{d}_y \sum_i^N \frac{\sigma_{yi}}{2} \right). \tag{2.10}$$

To calculate the eigenvectors and eigenvalues of the system we introduce the collective operators $\hat{J}_x$, $\hat{J}_y$ and $\hat{J}_z$,

$$\hat{J}_k = \frac{1}{2} \sum_i^N \sigma_{ki}, \tag{2.11}$$

where $k = \{x, y, z\}$. Using this notation we can write the collective electric dipole operator for the atomic system as

$$\hat{\mathbf{D}} = \mathbf{d}_x \hat{J}_x + \mathbf{d}_y \hat{J}_y. \tag{2.12}$$

Let us use as our basis the eigenvectors of the operator σ_z, the states denoted by $|+\rangle$ and $|-\rangle$, which correspond to eigenvalues $+1$ and -1, respectively. The state space for

the full system is given by the tensor product of the states of N atoms; in particular, for all atoms excited, the state vector and eigenvector of $\hat{J}_z$, is

$$|++++\cdots++\rangle, \tag{2.13}$$

corresponding to the non-degenerate eigenvalue $N/2$.

States with one atom in the ground state (e.g. $|+++\cdots+-+\rangle$) belong to an N-fold degenerate set, with $\hat{J}_z$ eigenvalue $N/2-1$. Generally, a similar observation holds for states with n_+ atoms in the excited level and n_- atoms in the ground state. They have degeneracy given by $\frac{N!}{n_+!n_-!}$ and $\hat{J}_z$ eigenvalue $m=(n_+-n_-)/2$. To remove this degeneracy we note that the problem being considered is equivalent to the summation of angular momenta. One observes that, with the definitions (2.11), the operators $\hat{J}_k$ obey the same commutation relations as angular momenta:

$$\left[\hat{J}_x,\hat{J}_y\right]=i\hat{J}_z. \tag{2.14}$$

It is also useful to define the raising and lowering operators $\hat{J}_+=\hat{J}_x+i\hat{J}_y$ and $\hat{J}_-=\hat{J}_x-i\hat{J}_y$, with commutation relations:

$$\left[\hat{J}_+,\hat{J}_-\right]=2\hat{J}_z,\ \left[\hat{J}_\pm,\hat{J}_z\right]=\mp\hat{J}_\pm. \tag{2.15}$$

These relations can be used to derive the effect of the action of the raising and lowering operators on a state with total angular momentum ℓ and $\hat{J}_z$ eigenvalue m [26, Chapter VI]:

$$\hat{J}_\pm|\ell,m\rangle=\sqrt{\ell\,(\ell+1)\pm m\,(m-1)}|\ell,m\pm1\rangle. \tag{2.16}$$

The degeneracy is removed by following the standard procedure of angular momentum addition to generate all collective states of the system. We introduce the operator $\mathbf{J}^2$ which commutes with the operators $\hat{J}_x$, $\hat{J}_y$, $\hat{J}_z$ and $\hat{J}_\pm$, and has eigenvalue $\ell(\ell+1)$, where $0\leq\ell\leq N/2$ [26, Chapter VI]. We then consider the non-degenerate state with highest $\hat{J}_z$ eigenvalue ($m=\ell=N/2$), which is given by (2.13). We apply the operator $\hat{J}_-$ and renormalize the resulting state, whose $\{\mathbf{J}^2,\hat{J}_z\}$ eigenvalues are $\{\ell(\ell+1),m-1\}$. We then repeat the procedure until the state with lowest $\hat{J}_z$ eigenvalue ($m=-\ell$) is reached:

$$|\ell,-\ell\rangle=|---\cdots--\rangle. \tag{2.17}$$

This operation generates all states with $\ell = N/2$ and $-\ell \leq m \leq \ell$, which are denoted by $|\ell, m\rangle = |N/2, M\rangle$.

To generate the states with $\ell = N/2 - 1$ we first note that the state $|\ell, N/2 - 1\rangle$ is a member of an N–fold degenerate set of states, with only 1 state having $\ell = N/2$. The remaining $N - 1$ states have to belong to the subspace $\ell = N/2 - 1$. Requiring that all N states be orthogonal to one another, we are free to choose a state $|N/2 - 1, N/2 - 1\rangle$ orthogonal to $|N/2, N/2 - 1\rangle$, and apply the $\hat{J}_-$ operator to that state to generate all states with $\ell = N/2 - 1$ and $-N/2 + 1 \leq m \leq N/2 - 1$. This procedure can be repeated for $\ell = N/2 - 2$ down to $\ell = 0$. In the case of just two atoms we recover the usual procedure to add angular momenta as described in many textbooks (e.g. [25, Chapter X]).

Notice, however, that Dicke states so created, with total angular momentum ℓ and $\hat{J}_z$ eigenvalue m, have degeneracy given by [28, Equation 6.67]:

$$\frac{N!(2\ell + 1)}{(N/2 + \ell + 1)!(N/2 - \ell)!}. \tag{2.18}$$

We can picture the result as a pyramid shaped graphic as shown in figure 2.1.1. There, each dot represents a state. The quantum number ℓ will be called the "cooperation number" as used by Dicke in his original work [3].

2.1.2. Superradiance

Having defined our state space we turn our attention to the Hamiltonian (2.1). The interesting quantity is the probability (rate) of transition of the atomic ensemble between different states. As known for dipole interactions, the selection rules for (2.1) allow only transitions satisfying $\Delta m = \pm 1$ [25, Complement $\mathsf{A}_{\mathrm{XIII}}$]. Considering only weak interaction (weak oscillatory field $\mathbf{E}(0, t) = \mathbf{E}(0)\sin(\omega t)$), we are able to use first order time dependent perturbation theory. The rate or probability of transition from a state m to $m \pm 1$ will be equal to:

$$\mathcal{P}_{m\to m\pm 1} = |W_{m\to m\pm 1}|^2 = \mathbf{E}(0)^2 \left|\langle \ell, m|\mathbf{d}_x \hat{J}_x + \mathbf{d}_y \hat{J}_y|\ell, m \pm 1\rangle\right|^2. \tag{2.19}$$

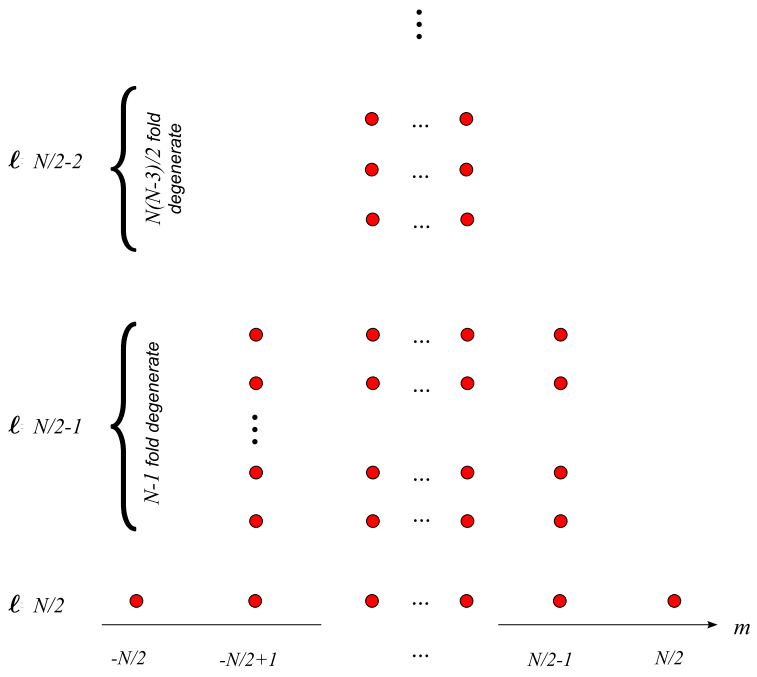

Figure 2.1.: State diagram showing the degeneracies of the Dicke states.

Calculating this expression using the definitions of $\hat{J}_x$ and $\hat{J}_y$ in terms of $\hat{J}_\pm$ we arrive at:

$$|W_{m\to m\pm1}|^2 = \mathbf{E}(0)^2(\mathbf{d}_x^2 + \mathbf{d}_y^2)\,(\ell + m)\,(\ell - m + 1)\,. \tag{2.20}$$

We see that for high cooperation number, $\ell \simeq N/2$, and $m = \ell$, the transition probability, and by consequence the radiated power, is proportional to the number of atoms in the system,

$$|W^{m=\ell}_{m\to m\pm1}|^2 \simeq I_0 N. \tag{2.21}$$

The maximum radiated power will occur when $\ell = N/2$ and $m = 0$, for which the radiation rate is proportional to the square of the number of atoms,

$$|W^{m=0}_{m\to m\pm1}|^2 \simeq I_0 \frac{N^2 + 2N}{4}. \tag{2.22}$$

In this case we say the atoms are in the superradiant regime.

Because Hamiltonian (2.1) commutes with the operator $\mathbf{J}^2$, the state of the system will remain in the subspace with cooperation number ℓ during its evolution. For the average

of the vector **J**, the Heisenberg equations of motion describe an evolution equivalent to that of a magnetic dipole subjected to a magnetic field (E_x, E_y, ω_0). The resulting motion is analogous to the precession of $\langle \mathbf{J} \rangle$ around the "magnetic field".

The burst of superradiant light appearing when the system starts in a fully excited configuration is due to the build up of correlations between the dipoles, in close analogy with a set of classical dipoles oscillating in phase. States with low cooperation number ℓ also show correlations, but corresponding to a classical picture of out-of-phase oscillating dipoles. We can calculate the mean correlation between atoms at different sites as

$$\digamma = \sum_{i \neq j}^{N} \langle \sigma_{i+} \sigma_{j-} \rangle \,, \tag{2.23}$$

where $\sigma_{\pm}$ is the usual raising or lowering Pauli matrix. In a state $|\ell, m\rangle$ (which is symmetric with respect to the permutation of atomic labels) the following relations hold:

$$\langle \hat{J}_+ \hat{J}_- \rangle = \left\langle \sum_i^N \sigma_{i+} \sum_j^N \sigma_{j-} \right\rangle = \digamma + \sum_i^N \langle \sigma_{i+} \sigma_{i-} \rangle = \ell^2 - m^2 + \ell + m, \tag{2.24}$$

and

$$\sum_i^N \langle \sigma_{i+} \sigma_{i-} \rangle = \frac{N}{2} + \langle \hat{J}_z \rangle = \ell + m. \tag{2.25}$$

From these, it follows that $\digamma = (\ell^2 - m^2)$. When the system decays from the fully excited state (2.13) to the superradiant[1] state – that with high ℓ and $m = 0$ – the correlation grows from 0 to ℓ^2 as $m \to 0$, and decreases again as all atoms decay to the ground state $(m \to -\ell)$.

We note also the existence of subradiant states for $\ell < N/2$. In this case the system decays to the final $m = -\ell$ state with a non-zero probability of an atom still being in an excited state (e.g., the singlet state for $N = 2, \ell = 0$). These "dark" states prevent the system from losing any more energy to the field.

[1] The situation where this build up of correlations happens from the initial state $|\ell, \ell\rangle$, as we are considering here, is often referred to as superfluorescence. Here we use the word superradiant in line with the original work of Dicke [3].

A sample of gas can be excited to its upper state (corresponding to $|N/2, N/2\rangle$) by a strong pulse of radiation in order for superradiance to be observed as the system decays to its ground state. Such an experiment shows irreversible losses of energy to the environment. We shall now describe a dynamical model that takes these processes into account.

2.2. Master equation and coherent spontaneous emission – weak coupling regime

In the description above, the EM field was considered a classical quantity, and its state is not altered by the presence of the atoms. In this section we present a more rigorous approach to treat irreversible losses, starting with a quantized field. Dissipative phenomena, like friction or electrical resistance, can be described by the coupling of the system to a reservoir with many degrees of freedom. For the Dicke model, the atoms are coupled to the many modes of the quantized electromagnetic field of free space, which plays the role of the reservoir. We define the quantized electric field operators as

$$\mathbf{E}^{+}(\mathbf{r}) = i\sum_{\mathbf{k}\epsilon} \mathcal{E}_{\mathbf{k}\epsilon}\hat{a}_{\mathbf{k}\epsilon}\mathrm{e}^{i\mathbf{k}\cdot\mathbf{r}}, \qquad \mathbf{E}^{-}(\mathbf{r}) = -i\sum_{\mathbf{k}\epsilon} \mathcal{E}_{\mathbf{k}\epsilon}\hat{a}^{\dagger}_{\mathbf{k}\epsilon}\mathrm{e}^{-i\mathbf{k}\cdot\mathbf{r}}. \tag{2.26}$$

Here $\mathcal{E}_{\mathbf{k}\epsilon}$ is the electric field per photon in a volume $\mathcal{V}$, given by

$$\mathcal{E}_{\mathbf{k}\epsilon} = \sqrt{\frac{\hbar c\,|\mathbf{k}|}{2\varepsilon_0 \mathcal{V}}}\boldsymbol{\epsilon}, \tag{2.27}$$

where $\mathbf{k}$ is the wave vector and $\boldsymbol{\epsilon}$ the polarization vector. The photon creation and annihilation operators, $\hat{a}^{\dagger}_{\mathbf{k}\epsilon}$ and $\hat{a}_{\mathbf{k}\epsilon}$, obey the usual bosonic commutation relations. The Hamiltonian for the atomic system plus the reservoir can be written as

$$\hat{H} = \sum_{\mathbf{k}\epsilon} \hbar\omega_{\mathbf{k}}\hat{a}^{\dagger}_{\mathbf{k}\epsilon}\hat{a}_{\mathbf{k}\epsilon} + \hbar\omega_0\hat{J}_z + \sum_i \left(\mathbf{E}^{+}(\mathbf{r}_i) + \mathbf{E}^{-}(\mathbf{r}_i)\right)\cdot\mathbf{D}_i. \tag{2.28}$$

As in the previous section, we consider that all atoms lie in a small volume so they see the same field. We proceed with the replacement $\mathbf{E}(\mathbf{r}_i) \to \mathbf{E}(0)$. Our aim is to trace out the reservoir and derive an equation for the motion of the atomic system only. Such

a procedure, along with suitable approximations, results in a master equation in the Lindblad form. We shall follow the standard derivation widely know in the literature [4, 28, Chapter 1]. The first step is to write down the Liouville equation of motion for the density matrix of the atom plus field in the interaction picture, denoted by $\tilde{\Lambda}$:

$$i\hbar\frac{\mathrm{d}\tilde{\Lambda}}{\mathrm{d}t} = \left[\hat{H}_{\mathrm{Int}}(t), \tilde{\Lambda}\right]. \tag{2.29}$$

The reduced atomic density operator (in the interaction picture) is defined by

$$\tilde{\rho} = \mathrm{Tr}_{\mathrm{rad}}\tilde{\Lambda}. \tag{2.30}$$

The relationship between the Schrödinger and interaction pictures is given by:

$$\tilde{\Lambda} = \exp\left(\frac{i\hat{\mathcal{H}}_0 t}{\hbar}\right)\Lambda\exp\left(\frac{-i\hat{\mathcal{H}}_0 t}{\hbar}\right), \tag{2.31}$$

$$\tilde{H}_{\mathrm{Int}} = \exp\left(\frac{i\hat{\mathcal{H}}_0 t}{\hbar}\right)\mathbf{E}(0)\cdot\mathbf{D}\exp\left(\frac{-i\hat{\mathcal{H}}_0 t}{\hbar}\right), \tag{2.32}$$

where $\hat{\mathcal{H}}_0$ is the non-interacting field plus atom Hamiltonian, given by

$$\mathcal{H}_0 = \sum_{\mathbf{k}\epsilon}\hbar\omega_{\mathbf{k}}\hat{a}^{\dagger}_{\mathbf{k}\epsilon}\hat{a}_{\mathbf{k}\epsilon} + \hbar\omega_0\hat{J}_z. \tag{2.33}$$

We formally integrate equation (2.29) to obtain an expression for $\tilde{\Lambda}$

$$\tilde{\Lambda}(t) = \frac{1}{i\hbar}\int_0^t\left[\hat{H}_{\mathrm{Int}}, \tilde{\Lambda}(t')\right]\mathrm{d}t'. \tag{2.34}$$

This expression is then inserted on the RHS of the same equation (2.29), and a trace over the reservoir is taken to obtain the equation of motion for the atomic density matrix in the interaction picture in integro-differential form:

$$\frac{\mathrm{d}\tilde{\rho}}{\mathrm{d}t} = -\frac{1}{\hbar^2}\mathrm{Tr}_{\mathrm{rad}}\int_0^t\mathrm{d}t'\left[\hat{H}_{\mathrm{Int}}(t), \left[\hat{H}_{\mathrm{Int}}(t'), \tilde{\Lambda}(t')\right]\right]. \tag{2.35}$$

We suppose that at $t = 0$ the system is uncorrelated with the reservoir, which we consider to be in thermal equilibrium at temperature T:

$$\tilde{\Lambda}(t=0) = \mathcal{R}(T)\otimes\rho_0, \tag{2.36}$$

where the density operator for the reservoir is given by the Bose-Einstein distribution:

$$\mathcal{R}(T) = \prod_{\mathbf{k}\epsilon} \frac{\mathrm{e}^{-\hbar\omega_{\mathbf{k}}\hat{a}_{\mathbf{k}\epsilon}\hat{a}^{\dagger}_{\mathbf{k}\epsilon}/k_B T}}{1-\mathrm{e}^{-\hbar\omega_{\mathbf{k}}/k_B T}}. \tag{2.37}$$

Equation (2.35) is exact. We proceed from here by making approximations. The first approximation we make is to consider that the interaction with the atoms does not change the reservoir state. This corresponds to saying that the correlations between field and atoms are short lived (Born approximation). This is a reasonable assumption considering the reservoir's large number of degrees of freedom. As a result of this approximation we can write $\tilde{\Lambda}(t') = \tilde{\rho}(t') \otimes \mathcal{R}(T)$. The second approximation regards the evolution of the system as Markovian (i.e. future evolution does not depend on past history). This is justified if the reservoir correlation times are much shorter than the characteristic times of evolution of the system. The reservoir, kept in thermal equilibrium, has its past evolution history erased faster than typical atomic evolution times. Looking at the RHS of equation (2.35) we see that $\tilde{\rho}(t)$ depends on all its previous values (the integral in t'). The approximation is made by setting $\tilde{\rho}(t') = \tilde{\rho}(t)$ in equation (2.35). The upper limit of integration goes to infinity as the evolution time of interest is much bigger than the correlation time of the reservoir. Finally, we convert the equations from the interaction picture back to the Schrödinger picture using the relations:

$$\begin{aligned} \mathrm{e}^{i\omega_k \hat{a}^{\dagger}_{\mathbf{k}\epsilon}\hat{a}_{\mathbf{k}\epsilon}t}\hat{a}_{\mathbf{k}\epsilon}\mathrm{e}^{-i\omega_k \hat{a}^{\dagger}_{\mathbf{k}\epsilon}\hat{a}_{\mathbf{k}\epsilon}t} &= \hat{a}_{\mathbf{k}\epsilon}\mathrm{e}^{-i\omega_k t}, \\ \mathrm{e}^{i\omega_0 \hat{J}_z t}\left\{\mathbf{d}_x\hat{J}_x + \mathbf{d}_y\hat{J}_y\right\}\mathrm{e}^{-i\omega_0\hat{J}_z t} &= \mathbf{d}_{+-}\hat{J}_+\mathrm{e}^{i\omega_0 t} + \mathbf{d}^*_{+-}\hat{J}_-\mathrm{e}^{-i\omega_0 t}. \end{aligned} \tag{2.38}$$

On substituting the operators (2.26) into (2.35) the following traces are used:

$$\begin{aligned} &\mathrm{Tr}\big(\mathcal{R}(T)\hat{a}^{\dagger}_{\mathbf{k}\epsilon}\hat{a}^{\dagger}_{\mathbf{k}\epsilon}\big) = 0, \\ &\mathrm{Tr}\big(\mathcal{R}(T)\hat{a}_{\mathbf{k}\epsilon}\hat{a}_{\mathbf{k}\epsilon}\big) = 0, \\ &\mathrm{Tr}\big(\mathcal{R}(T)\hat{a}^{\dagger}_{\mathbf{k}\epsilon}\hat{a}_{\mathbf{k}\epsilon}\big) = \bar{n}(\omega_{\mathbf{k}}, T), \\ &\mathrm{Tr}\big(\mathcal{R}(T)\hat{a}_{\mathbf{k}\epsilon}\hat{a}^{\dagger}_{\mathbf{k}\epsilon}\big) = \bar{n}(\omega_{\mathbf{k}}, T) + 1, \end{aligned} \tag{2.39}$$

where $\bar{n}(\omega_{\mathbf{k}}, T)$ is the mean number of thermal photons of frequency $\omega_{\mathbf{k}}$, given by the Planck black body distribution.

Putting all of these pieces together we have the following equation:

$$\begin{aligned}\frac{\mathrm{d}\rho}{\mathrm{d}t} =& \frac{1}{i\hbar}\left[\hat{H}_0, \rho\right] - \frac{1}{\hbar^2}\sum_{\mathbf{k}\epsilon}\int_0^\infty \mathrm{d}\tau\, |\mathcal{E}_{\mathbf{k}\epsilon}\cdot\mathbf{d}_{\pm}|^2 \Big\{ \big(\hat{J}_+^2 \mathrm{e}^{-i\omega_0\tau} + \hat{J}_-^2 \mathrm{e}^{i\omega_0\tau} \\ &+ \hat{J}_+\hat{J}_- \mathrm{e}^{i\omega_0\tau} + \hat{J}_-\hat{J}_+ \mathrm{e}^{-i\omega_0\tau}\big)\left[(\bar{n}+1)\mathrm{e}^{-i\omega_{\mathbf{k}}\tau} + \bar{n}\mathrm{e}^{i\omega_{\mathbf{k}}\tau}\right]\rho \\ &- \big(\hat{J}_+ + \hat{J}_-\big)\rho\big(\hat{J}_+\mathrm{e}^{-i\omega_0\tau} + \hat{J}_-\mathrm{e}^{i\omega_0\tau}\big)\left[\bar{n}\mathrm{e}^{-i\omega_{\mathbf{k}}\tau} + (\bar{n}+1)\mathrm{e}^{i\omega_{\mathbf{k}}\tau}\right] + \mathrm{h.c.}\Big\}, \end{aligned} \tag{2.40}$$

where $\tau = t - t'$, $H_0 = \hbar\omega_0\hat{J}_z$, and the phase factors from $\mathbf{d}_{+-}$ were absorbed in the $\hat{J}_\pm$ operators (without loss of generality). The variable τ will appear only in exponentials like $\mathrm{e}^{\pm i(\omega_{\mathbf{k}}-\omega_0)\tau}$ and $\mathrm{e}^{\pm i(\omega_{\mathbf{k}}+\omega_0)\tau}$, which can be integrated using the relation:

$$\int_0^\infty \mathrm{d}\tau \mathrm{e}^{-i(\omega\pm\omega_0)\tau} = \pi\delta(\omega\pm\omega_0) + i\mathrm{P}\frac{1}{\omega\pm\omega_0}, \tag{2.41}$$

where P is the Cauchy principal value. The delta-function expresses the requirement for conservation of energy when quanta are exchanged between the system and reservoir (as in Fermi's golden rule). The principal part arises from and accounts for off-resonant interactions; it introduces the Lamb shift and dipole-dipole interactions.

To simplify the right-hand-side of equation (2.40), we transform the sum over $\mathbf{k}$ into an integral over $\mathrm{d}^3\mathbf{k}$. The element of volume in $\mathbf{k}$ space is introduced by taking the limit $\mathcal{V}\to\infty$ and writing

$$\mathrm{d}^3\mathbf{k} = k^2\mathrm{d}k\mathrm{d}\Omega, \tag{2.42}$$

which must be multiplied by the density of states, i.e. the number of states per unit of volume $\mathrm{d}^3\mathbf{k}$, given by [29, Section 4.5]

$$\frac{\mathcal{V}}{(2\pi)^3}. \tag{2.43}$$

The integration over the solid angle Ω accounts for all possible propagation directions (i.e. directions of $\mathbf{k}$). There is still a sum to perform over two polarization directions for each $\mathbf{k}$ direction. We choose one of this polarizations to be perpendicular to the atomic polarization vector $\mathbf{d}_{+-}$. The master equation for the resonant processes only (i.e. proportional to $\delta(\omega_k-\omega_0)$ as the variable $\omega_{\mathbf{k}}$ is by definition positive) is then given

by

$$\left.\frac{\mathrm{d}\rho}{\mathrm{d}t}\right|_{\mathrm{R}} = \frac{1}{i\hbar}\Big[\hat{H}_0,\rho\Big] - \frac{c\,|\mathbf{d}_{\pm}|^2}{16\hbar\varepsilon_0\pi^2}\int_0^\infty k^3\mathrm{d}k\int \mathrm{d}\Omega(\epsilon\cdot\epsilon_a)^2\delta(\omega_{\mathbf{k}}-\omega_0)\Big\{\bar{n}\Big(\hat{J}_+^2\rho + \rho\hat{J}_-^2 + \hat{J}_-\hat{J}_+\rho + \rho\hat{J}_-\hat{J}_+ - 2\hat{J}_+\rho\hat{J}_- - \hat{J}_-\rho\hat{J}_- - \hat{J}_+\rho\hat{J}_+\Big) + \big(\bar{n}+1\big) \times \Big(\hat{J}_-^2\rho + \rho\hat{J}_+^2 + \hat{J}_+\hat{J}_-\rho + \rho\hat{J}_+\hat{J}_- - 2\hat{J}_-\rho\hat{J}_+ - \hat{J}_-\rho\hat{J}_- - \hat{J}_+\rho\hat{J}_+\Big)\Big\}. \tag{2.44}$$

Here ϵ_a is a unit vector parallel to $\mathbf{d}_{+-}$. We carry out the integral in k with the transformation $\omega_{\mathbf{k}} = ck$. Using a coordinate system in which $\epsilon\cdot\epsilon_a = \sin\theta$ (the z axis parallel to the propagation direction $\mathbf{k}$) yields, for the solid angle integral,

$$\int \mathrm{d}\Omega\big(\epsilon\cdot\epsilon_a\big)^2 = \int_0^{2\pi}\mathrm{d}\phi\int_0^\pi \sin^3\theta = \frac{8\pi}{3}. \tag{2.45}$$

The result is the master equation for spontaneous emission from a collection of atoms coupled to a common reservoir [30]:

$$\begin{aligned}\left.\frac{\mathrm{d}\rho}{\mathrm{d}t}\right|_{R} &= \frac{1}{i\hbar}\Big[\hat{H}_0,\rho\Big] + \big(\bar{n}+1\big)\frac{\Gamma}{2}\Big(\hat{J}_-\rho\hat{J}_+ + \hat{J}_-\rho\hat{J}_- - \hat{J}_-^2\rho - \hat{J}_+\hat{J}_-\rho + \mathrm{h.c}\Big)\\ &\quad + \frac{\bar{n}\Gamma}{2}\Big(\hat{J}_+\rho\hat{J}_- + \hat{J}_+\rho\hat{J}_+ - \hat{J}_-\hat{J}_+\rho - \hat{J}_+^2\rho + \mathrm{h.c}\Big),\end{aligned} \tag{2.46}$$

where

$$\Gamma = \frac{\omega_0^3\,|\mathbf{d}_{\pm}|^2}{3\hbar\varepsilon_0\pi c^3}, \tag{2.47}$$

is the Einstein A coefficient for spontaneous emission, as obtained from Fermi's golden rule in standard time-dependent perturbation theory.

Using data for the hydrogen atom we get a value of $\Gamma \approx 2\times 10^8\mathrm{s}^{-1}$ for the Lyman series ($\omega_0 \approx 10^{15}s^{-1}$). A search in the appropriate database [31] shows that the ratio $\Gamma/\omega_0 \sim 10^{-7}$ for most atomic transitions in the optical regime (100-1000 nm). In this case a simple calculation shows that the counter rotating terms, like $\hat{J}_{\pm}^2\rho$, will make a first order contribution of Γ/ω_0, so they can be neglected in equation (2.46). For regimes where $\Gamma/\omega_0 \sim 1$, like microwave radiation [32], the Markov approximation does not hold, and the dynamics shall be described by the strong coupling model we introduce below. At room temperature and optical frequencies, the mean number of thermal photons $\bar{n}$ is negligible, whereas for infra-red and microwave radiation $\bar{n}$ may be significant.

We can use equation (2.46) to derive the equations of motion for the quantum means of the operators: $\langle \hat{J}_z \rangle = \mathrm{Tr}(\hat{J}_z \rho)$ and $\langle \hat{J}_\pm \rangle = \mathrm{Tr}(\hat{J}_\pm \rho)$. The density matrix representing the mixed state of the system is written as the linear combination

$$\rho = \sum_{i=-\ell}^{\ell} \sum_{j=-\ell}^{\ell} c_{ij} |\ell, i\rangle\langle \ell, j|. \tag{2.48}$$

The evolution of the state of the system is obtained by solving the equations of motion for each coefficient c_{ij}. This will give N equations to be solved, which can be simulated in a computer. In figure 2.2 we show $\langle \hat{J}_+ \hat{J}_- \rangle$, which is proportional to the rate of photon emission [4], and the mean atomic inversion $\langle \hat{J}_z \rangle$ versus time. The system starts with all atoms in the excited state $|N/2, N/2\rangle$ and loses all its energy to the field to reach the state $|N/2, -N/2\rangle$. For one atom the system relaxes exponentially, for five atoms the system shows a superradiant peak, which becomes more prominent for nine atoms.

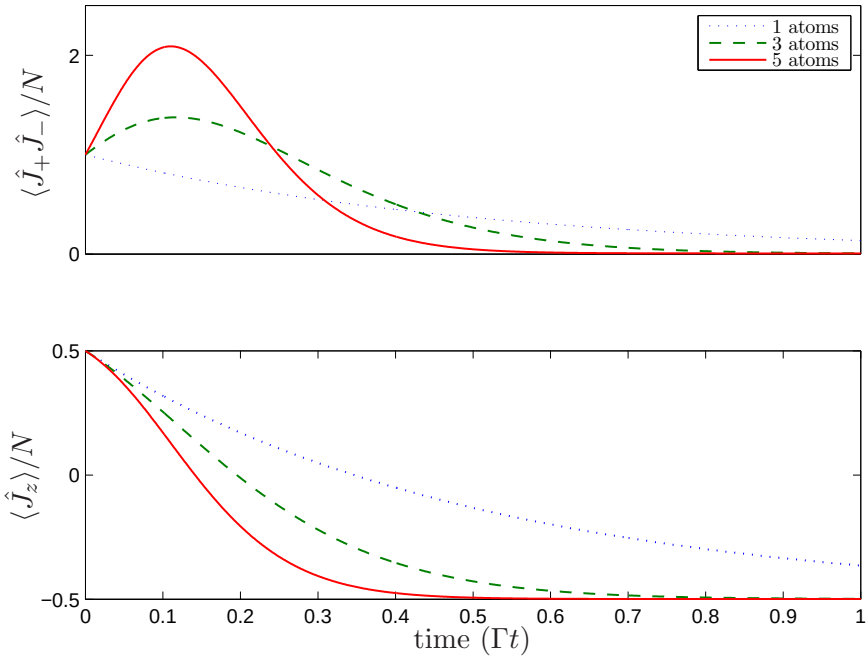

Figure 2.2.: Radiated power and atomic inversion for different numbers of atoms.

The imaginary part of (2.41), containing the Cauchy principal value, is neglected

when applied to equation (2.40). The off-resonant interactions arising from the principal value of (2.40) depend upon wavelengths different from those resonant with the atomic transition. With their inclusion, the approximation that all atoms see the same field is not valid. On relaxing this approximation, they give rise to diffraction and Van der Waals dephasing terms, which depend on the inter-atomic distances.

By placing the atoms in a cavity with resonance frequency ω_0 we are able to neglect diffraction terms by considering that all atoms see the same field, as well as providing a common mode coupling to all atoms. Such a cavity creates a spectral profile with a peak at $\omega = \omega_0$, which must be taken into account when deriving equation (2.40). For sufficiently large cavity linewidth, the decay term Γ will be enhanced by a factor proportional to the cavity finesse, while the principal part of the product of the spectrum and $1/(\omega \pm \omega_0)$, representing off-resonant interactions, will be depleted [32, Section G].

The cavity also creates high intensity electric fields, allowing low density atomic clouds to couple strongly with the light field. This is required to rule out Van der Waals dephasing interactions[2], included by adding the terms $\sum_{i>j} \Omega_{ij} \left[\sigma_{\pm i}, \sigma_{\pm_j}\right]$ to the Hamiltonian part of the master equation, where Ω_{ij} is the dipole-dipole interaction strength, which depends on the atomic separation $\mathbf{r}_{ij}$. Interactions depending on inter-atomic distances are non-symmetrical and do not conserve the total angular momentum ℓ. Using the dipole moment for the Lyman series shown above ($\Gamma \approx 10^8$ Hz) as an example, we have a dipole-dipole energy interaction (according [4]) on the order of 2×10^6 Hz for atomic separation just the size of the wavelength of the radiation ($\approx$ 100 nm). A complete picture of Van der Waals interaction in large gas samples is given in [4].

The same rationale applies to the Lamb shift, which comes from considering terms like $\sigma_{\pm i}\sigma_{\pm i}$ in (2.40). The complete Lamb shift is due to both vacuum fluctuations (terms not proportional to $\bar{n}$) and the ac Stark shift (terms proportional to $\bar{n}$). Both contributions may be incorporated as small shifts of the energy levels in $\bar{H}_0$.

[2]This process bears the name of Van der Waals as $\Omega_{ij} \propto r_{ij}^{-3} - r_{ij}^{-5}$, but this description does not give an account of electrostatic inter-atomic interactions as they have to be added in $\hat{H}$.

2.3. Dicke model in a cavity – strong coupling regime

In the previous section we considered the atoms radiating spontaneously, as their collective state decays from $|\ell, \ell\rangle$ to $|\ell, -\ell\rangle$, and ignored the dynamical mechanism pumping the system to its excited state. We mentioned that an optical resonator will enhance the interaction of the atoms with the EM field, of frequency ω_0, allowing low density ensembles to be strongly coupled to a single light mode, thus enabling Van der Waals interactions to be neglected.

The corresponding experimental setup is that of an atomic cloud placed in a cavity interacting with a laser pulse, which pumps all atoms to the excited state. One may observe directly the intensity of the light emitted by the cavity, which shows a peak as in Figure 2.2. Such an experiment has been done in the past for both microwave [33] and visible light [34][3]. It is implicit in the account given in the previous section that the cavity decay rate, κ, has to satisfy $\kappa > \Gamma$, so that the cavity field is not significantly modified when the system emits a quantum of radiation; the photons are expelled from the cavity before interacting again with the atoms.

Improvements in the experimental art has lead to high finesse cavities, widely available today. These cavities can generate strong electric fields, making the interaction between the cavity mode and the atoms more important than spontaneous emission and cavity losses. Going back to equation (2.28), we must have $\hbar\kappa \ll \mathbf{E}\cdot\mathbf{D}$ (for a good account see [2, p. 208]). We have to consider the field dynamics of this mode. This scenario corresponds to the *strong coupling* regime. High quality optical cavities provide a necessary (but not sufficient) condition to reach this regime.

We start with equation (2.28), but consider only the cavity mode with wave vector $\mathbf{k}_{cav}$. We shall be concerned with how the atoms change the field. We assumed in past

[3] The microwave experiments make use of Rydberg atoms; atoms are pumped by the laser to a highly excited state, while the cavity is tuned to transitions between two such highly excited levels (with transition frequency ω_0). In the experiment for optical frequencies, the intensity of the emission is measured for different vapor pressures, thus changing the gas density and enabling one to verify that the intensity $\propto N^2$.

sections the field to be classical – a c-number in Section 2.1 – or a multi mode quantized field which was eliminated in the Born-Markov approximation. In the master equation approach, the important quantum effect of the light field comes from the +1 in the term $\bar{n}+1$, giving rise to spontaneous emission (due to vacuum fluctuations) and from the Lamb shift which was incorporated into $\hat{H}_0$. Now we are interested to learn about how the state of the field is changed by the presence of the atoms. We introduce, in Hamiltonian (2.1), quantized field operators (here $\hbar=1$) such that

$$\hat{H}=\omega\hat{a}^\dagger\hat{a}+\omega_0\hat{J}_z+\mathcal{E}_\omega\left|\mathbf{d}_{+-}\right|\left(\hat{a}+\hat{a}^\dagger\right)\left(\hat{J}_++\hat{J}_-\right). \tag{2.49}$$

The Hamiltonian above is considered to be in the long wavelength approximation, in the sense defined in Section 2.1.1 (i.e., all atoms couple to a single field mode). Usually, experiments with atoms in a cavity are carried out with coupling constants on the order of a few MHz [6], to be compared with optical frequencies on the order of PHz (10^{15} Hz) for ω and ω_0. Under this condition we can make the rotating wave approximation as follows. We write Hamiltonian (2.49) in the interaction picture as

$$\hat{H}_{\mathrm{Int}}=\left|\mathbf{d}_{+-}\right|\mathcal{E}_\omega\left(\hat{a}\hat{J}_++\hat{a}^\dagger\hat{J}_-+\mathrm{e}^{i(\omega+\omega_0)t}\hat{a}^\dagger\hat{J}_++\mathrm{e}^{-i(\omega+\omega_0)t}\hat{a}\hat{J}_-\right). \tag{2.50}$$

The Schrödinger equation determining the evolution of the state $|\tilde{\psi}(t)\rangle$ in the interaction picture is integrated to give

$$|\tilde{\psi}(t)\rangle=|\tilde{\psi}(0)\rangle+\frac{\left|\mathbf{d}_{+-}\right|\mathcal{E}_\omega}{i}\int_0^t\mathrm{d}t'\left(\hat{a}\hat{J}_++\hat{a}^\dagger\hat{J}_-+\mathrm{e}^{i(\omega+\omega_0)t}\hat{a}^\dagger\hat{J}_++\mathrm{e}^{-i(\omega+\omega_0)t}\hat{a}\hat{J}_-\right)|\tilde{\psi}(t')\rangle. \tag{2.51}$$

This expression can be substituted on the right-hand side of the Schrödinger equation and the procedure iterated to give the Dyson series [35, Section 5.6]. The integration of the time dependent terms $\mathrm{e}^{\pm i(\omega+\omega_0)t}$ results in terms proportional to

$$\pm\frac{\left|\mathbf{d}_{+-}\right|\mathcal{E}_\omega}{(\omega+\omega_0)}. \tag{2.52}$$

In the regime we mentioned ($\mathcal{E}_\omega\left|\mathbf{d}_{+-}\right|\ll\omega,\omega_0$), these terms, which are proportional to $\hat{a}^\dagger\hat{J}_+$ and $\hat{a}\hat{J}_-$, can be neglected. We finally have the Hamiltonian (normalized to $\hbar$):

$$\hat{H}=\omega\hat{a}^\dagger\hat{a}+\omega_0\hat{J}_z+\frac{\lambda}{\sqrt{N}}\left(\hat{a}\hat{J}_++\hat{a}^\dagger\hat{J}_-\right), \tag{2.53}$$

where the coupling constant λ is defined in terms of the density $\aleph = N/\mathcal{V}$ as

$$\lambda = \frac{\sqrt{\omega\aleph}\,|\mathbf{d}|_{\pm}}{\sqrt{2\hbar\varepsilon_0}}. \tag{2.54}$$

In table 1 we summarize typical experimental values for λ and the related parameters described in Section 2.2. These values are based on a cavity with mirror separation of 50 μm:

parameter	**value**
ω	2×10^{15} Hz
Γ	$10^8 \sim 10^7$ Hz
$\lvert\mathbf{d}_{+-}\rvert$	10^{-28} Cm
Dipole-dipole (Max)	2×10^6 Hz
λ	1.3×10^{11} Hz
$\lambda/\sqrt{N}$	3×10^8 Hz
$\bar{n}(T = 273K)$	10^{-25} photons

Table 2.1.: Typical experimental parameters for cavity QED

The operator corresponding to the total number of energy quanta, $\hat{a}^\dagger\hat{a} + \hat{J}_z + \ell$, commutes with $\hat{H}$, therefore it is a conserved quantity and can be simultaneously diagonalized with the $\hat{\mathbf{J}}^2$ operator. The state space will be denoted by $|\ell, m, n\rangle$, where n is the eigenvalue of the $\hat{a}^\dagger\hat{a}$ operator, and m, $-\ell < m < \ell$, is the eigenvalue of $\hat{J}_z$. An exact solution [5] can be obtained as a linear combination of states $|\ell, m, n\rangle$ such that $m + n$ is constant. The eigenvalues of Hamiltonian (2.53), at zero coupling ($\lambda = 0$) and at resonance ($\omega = \omega_0$), are given by $(m + n)\omega$. These eigenvalues have degeneracy of order $2\ell + 1$ if $m + n > 2\ell + 1$, and $m + \ell + 1$ otherwise. As the interaction is turned on, the degeneracy is lifted, as can be seen in Figure 2.3, which displays the eigenvalues calculated numerically from the matrix expression of Hamiltonian (2.53) in a (truncated) Fock space. In the figure, the eigenvalues of $\hat{H}$ are plotted with respect the number of energy quanta $m + n$ for different λ. The system is at resonance and the

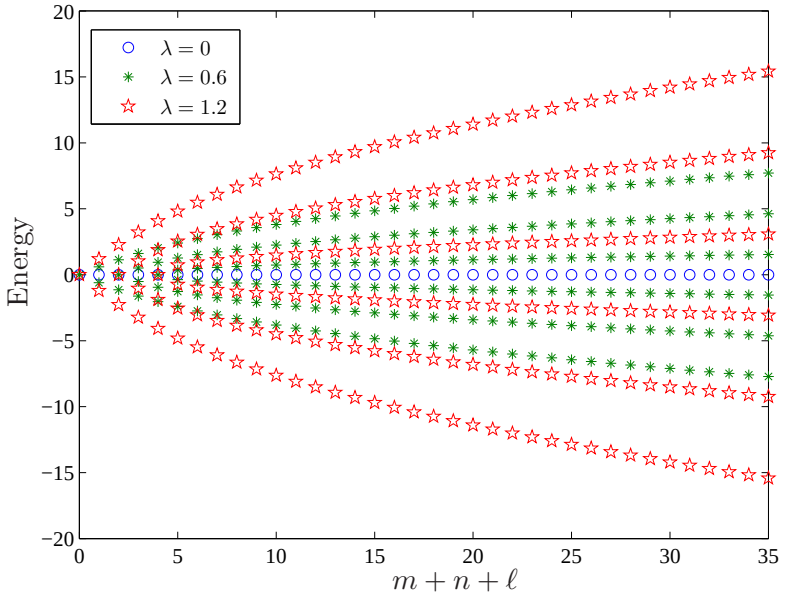

Figure 2.3.: Eigenvalues of the N-atom generalization of the Jaynes Cummings Hamiltonian for $N = 5$ atoms and $\omega = \omega_0 = 1$.

solutions are shown for the interaction picture (thus the value of zero for the energy in the non-interacting case). The degenerate states, which are eigenvectors of $\omega(\hat{a}^\dagger\hat{a} + \hat{J}_z)$, are indicated by the blue circles. As the interaction strengthens, the splitting between the eigenvalues with a determined number of quanta increases. This is the N-atom generalization of the Jaynes-Cummings model, whose eigenvalue asymptotic behaviour is given by $\lambda\sqrt{n+1}$. Here the eigenvalues are proportional to $\ell\sqrt{n+m}$ in the limit of a large number of quanta [5, Table I], with a different branch for each m.

The evolution of the system shows Rabi oscillations: energy quanta are emitted and reabsorbed by the atoms into and from the cavity. Generalizing the dressed states formalism, the system shows many frequencies of oscillation that depend also on $\sqrt{m}$. The evolution of the probabilities can show beats and revivals as in the one atom case [36, Section 10.4].

Finally, we can take cavity losses into consideration for this model by using the master

equation [28, Chapter 1]

$$\frac{\mathrm{d}\rho}{\mathrm{d}t} = \frac{1}{i}\left[\hat{H}, \rho\right] + \kappa\left(2\hat{a}\rho\hat{a}^\dagger - \rho\hat{a}^\dagger\hat{a} - \hat{a}^\dagger\hat{a}\rho\right). \tag{2.55}$$

In this case the system is damped and eventually loses all its energy, ending up in the state $|\ell, -\ell, 0\rangle$.

3. Dicke model in the thermodynamic limit I

In this chapter, once we have established the model and justified the choice of the parameters, we show how a phase transition arises in the model for non-zero temperatures. The approach here is different from what will be done further on, where we treat a quantum phase transition at zero temperature. In this chapter we consider the interplay between the common electric field, which introduces order in the system, and the thermal fluctuations of the environment, which tends to disorganize the system. The result is similar to a phase transition in a magnetic system as described by the Ising model (see [37] for example): for low temperatures the system of radiating atoms is able to self-organize, and shows a superradiant phase, while above a critical temperature the thermal fluctuations destroy the order in the system. We also discuss the role played by the $\mathbf{A}^2$ term in the Dicke phase transition.

3.1. Phase transition at finite T

We present here the results of Hepp and Lieb [9], as developed by Wang and Hioe [38], whose work is more familiar to the quantum optics audience. In the following chapters we show how the phase transition also occurs at zero temperature, by making a semiclassical analysis. For the moment we are concerned with thermal fluctuations and how they introduce disorder into the system. We will not restrict our attention to the Dicke states with $\ell = N/2$, or deal with damping in the system, as we do in the chapters to come. We include the counter rotating terms $\hat{a}^\dagger\sigma_+$ and $\hat{a}\sigma_-$ [39, 40, 41], and use the full

Dicke Hamiltonian

$$\hat{H} = \omega \hat{a}^\dagger \hat{a} + \frac{\omega_0}{2} \sum_i \sigma_{zi} + \sum_i \frac{\lambda}{\sqrt{N}} \left(\hat{a}^\dagger + \hat{a} \right) (\sigma_{+i} + \sigma_{-i}) \,. \tag{3.1}$$

The thermodynamic analysis is carried out by considering the partition function for this Hamiltonian [42] (where $\beta = (k_b T)^{-1}$),

$$\mathscr{Z} = \mathrm{Tr} \left[\mathrm{e}^{-\beta \hat{H}} \right] . \tag{3.2}$$

We carry out the trace using the coherent states of the radiation field $|\alpha\rangle$ [43] and the atomic state space

$$\prod_i^N |\varepsilon_i\rangle, \tag{3.3}$$

where $|\varepsilon_i\rangle$ is an eigenvector of the Pauli matrix σ_z for atom i (eigenvalues $\varepsilon_i = \pm 1$). The partition function is written as

$$\mathscr{Z} = \sum_{\{\varepsilon_i = \pm 1\}} \int \frac{\mathrm{d}^2 \alpha}{\pi} \prod_i^N \langle \varepsilon_i | \langle \alpha | \mathrm{e}^{-\beta \hat{H}} | \alpha \rangle \prod_i^N | \varepsilon_i \rangle. \tag{3.4}$$

For the noninteracting case $\hat{H} = \omega \hat{a}^\dagger \hat{a} + \sum_i \omega_0 \sigma_{zi}/2$, and we can easily calculate the partition function knowing that $\hat{a}|\alpha\rangle = \alpha|\alpha\rangle$. It is given by

$$\mathscr{Z}_{\lambda=0} = \frac{1}{\omega\beta} \left(2 \cosh(\frac{1}{2} \omega_0 \beta) \right)^N . \tag{3.5}$$

Using this result, the free energy per particle can be calculated to be

$$f = -\beta \ln (\mathscr{Z}) = -k_b T \ln \cosh \left(\frac{1}{2} \omega_0 \beta \right) . \tag{3.6}$$

Turning now to the interacting case, we rewrite the exponential $\mathrm{e}^{-\beta \hat{H}}$ in normal order, with all $\hat{a}^\dagger$ operators to the left. The expansion of the exponential (3.2) will have terms $\hat{H}^n$ of all powers n. If we introduce the operators

$$\hat{a}_N^\dagger = \frac{\hat{a}^\dagger}{\sqrt{N}}, \quad \hat{a}_N = \frac{\hat{a}}{\sqrt{N}}, \tag{3.7}$$

the commutator of the renormalized operators is equal to $1/N$, and we can safely argue that for large N the operators $\hat{a}_N^\dagger$ and $\hat{a}_N$ commute. The Hamiltonian can be rewritten as

$$\hat{H} = \sum_i^N \left[\omega \hat{a}_N^\dagger \hat{a}_N + \omega_0 \frac{\sigma_{zi}}{2} + \lambda \left(\hat{a}_N^\dagger + \hat{a}_N \right) (\sigma_{i+} + \sigma_{i-}) \right]. \tag{3.8}$$

This expression is substituted into (3.2). We arrange the power expansion of the exponential in normal order using the commutation relations. In general, the expansion has terms like

$$\cdots \hat{a}_N \hat{a}_N \hat{a}_N^\dagger \cdots . \tag{3.9}$$

Each $\hat{a}_N^\dagger$ operator is passed to the left of the $\hat{a}$ operators using the commutation relations; the general result of this operation is

$$\cdots \hat{a}_N \hat{a}_N^\dagger \hat{a}_N \cdots + \frac{1}{N} \hat{a}_N \cdots . \tag{3.10}$$

Each such operation introduces a N^{-1} term in the expansion, which vanishes in the limit $N \to \infty$. Provided that $\hat{a}^\dagger/\sqrt{N}$ exists in this limit, it can be shown that only normally ordered terms will survive in the expansion of $\mathrm{e}^{-\beta \hat{H}}$. We can therefore make the replacement $\hat{a} \to \alpha$ and $\hat{a}^\dagger \to \alpha^*$ in (3.8). The resulting integral reads

$$\mathscr{Z} = \prod_i^N \sum_{\varepsilon_i = \pm 1} \int \frac{\mathrm{d}^2\alpha}{\pi} \mathrm{e}^{-\beta\omega|\alpha|^2} \langle \varepsilon_i | \exp \left[-\beta \left(\frac{\omega_0}{2} \sigma_{zi} + \frac{2\lambda\chi}{\sqrt{N}} \left(\sigma_{i+} + \sigma_{i-} \right) \right) \right] | \varepsilon_i \rangle, \tag{3.11}$$

where $\chi = \mathrm{Re}\alpha$. To evaluate the trace of the exponential operator, we need to find the eigenvalues of the operator in the square brackets. This operator is represented by the transfer matrix in the Ising model,

$$\begin{pmatrix} \omega_0/2 & 2\lambda\chi/\sqrt{N} \\ 2\lambda\chi/\sqrt{N} & -\omega_0/2 \end{pmatrix}, \tag{3.12}$$

with eigenvalues

$$\mathscr{G}_\pm = \pm \frac{1}{2} \sqrt{\omega_0^2 + 16\lambda^2\chi^2/N}. \tag{3.13}$$

The product of expectation values in expression (3.11) becomes

$$\left(2 \cosh \left[\beta \mathscr{G}_+ \right] \right)^N . \tag{3.14}$$

We may then perform the integral over the complex plane with respect to $\mathrm{d}^2\alpha = \mathrm{d}\chi \mathrm{dIm}(\alpha)$, where the integral over the imaginary part of α can be performed immediately. Defining

$$\vartheta = -\beta\omega u^2 + \ln \left[2 \cosh \beta \mathscr{G}_+ \right], \tag{3.15}$$

where $u^2 = \chi^2/N$, the expression for the partition function (3.11) becomes

$$\mathscr{Z} = 2\sqrt{\frac{N}{\pi\omega\beta}} \int \mathrm{d}u \exp[N\vartheta(u)]. \tag{3.16}$$

We now use the method of steepest descent (also known as Laplace's method) [44, Section 7.4] to carry out the remaining integration. If the function ϑ has a maximum and $N \to \infty$, the integral is approximated by the exponential of $\vartheta(u_0)$,

$$\mathscr{Z} = 2\sqrt{\frac{N}{\pi\omega\beta}} \exp[N\vartheta(u_0)], \tag{3.17}$$

where u_0 is the point that maximizes ϑ. The equation to be solved for u is

$$\vartheta' = -2\omega\beta u + \frac{8\beta\lambda^2 u}{2\mathscr{G}_+} \tanh\left[\beta\mathscr{G}_+\right] = 0, \tag{3.18}$$

which has two possible solutions, a trivial one, $u = 0$, and a second solution satisfying

$$\frac{\omega\omega_0}{4\lambda^2}\left(1 + \frac{16\lambda^2 u^2}{\omega_0^2}\right)^{1/2} = \tanh\left[\frac{\beta}{2}\mathscr{G}_+\right]. \tag{3.19}$$

Note now that the function $\tanh(x)$ is smaller than one, so, for $4\lambda^2 < \omega\omega_0$, there is only the trivial solution. In this case the free energy per particle, f, is the same as that calculated for the noninteracting case, (3.6). For $4\lambda^2 > \omega\omega_0$, the solution depends on the parameter β. We define the critical temperature for a given coupling λ, β_c, as the solution of the equation

$$\frac{\omega\omega_0}{4\lambda^2} = \tanh(\beta_c\frac{\omega_0}{2}); \tag{3.20}$$

if $\beta < \beta_c$, the solution is $u = 0$, and the free energy is still given by Eq. (3.6) while for $\beta > \beta_c$, we must solve Eq. (3.19) for u, and the free energy per particle is given by

$$-\beta f = \ln\left[2\cosh(\beta\lambda^2 u_0)\right] - \beta\left(4\lambda^2 u_0^2 + \frac{\omega_0}{16\omega\lambda^2}\right). \tag{3.21}$$

Now, *for a fixed temperature* such that $\beta > \beta_c$, the system changes its behaviour as the coupling λ becomes bigger than a critical value, λ_c, given by

$$\lambda_c = \sqrt{\frac{\omega\omega_0}{4\tanh(\beta\frac{\omega_0}{2})}}. \tag{3.22}$$

The free energy has a point of non-analyticity at $\lambda = \sqrt{\omega\omega_0}/2$, which characterizes a phase transition.

Having now identified the existence of the critical values β and λ_c, we calculate the mean photon number of the atom plus field system in order to show that the system enters a superradiant regime for $\beta > \beta_c$ and $\lambda > \lambda_c$. The calculation proceeds as follows: first we define the mean number of photons per number of atoms,

$$\frac{\langle \hat{a}^\dagger \hat{a} \rangle}{N} = \frac{1}{N} \frac{\mathrm{Tr}\left[\hat{a}^\dagger \hat{a} \mathrm{e}^{\beta \hat{H}}\right]}{\mathrm{Tr}\left[\mathrm{e}^{\beta \hat{H}}\right]}. \tag{3.23}$$

We then follow the same procedure as for the calculation of the free energy. We evaluate the trace as an integral over the coherent state amplitude α and use the eigenvalues of matrix (3.12) to obtain

$$\frac{\langle \hat{a}^\dagger \hat{a} \rangle}{N} = \frac{1}{N\mathscr{Z}} \int_{-\infty}^{\infty} \mathrm{d}^2\alpha \, |\alpha|^2 \, \mathrm{e}^{-\omega\beta} \, (2\cosh[\mathscr{G}_+]). \tag{3.24}$$

Performing the integration over the imaginary part of α, we get

$$\frac{\langle \hat{a}^\dagger \hat{a} \rangle}{N} = \frac{\int_0^\infty \mathrm{d}u u^2 \exp[N\vartheta(u)]}{\int_0^\infty \mathrm{d}u \exp[N\vartheta(u)]} + \frac{1}{N} \frac{k_B T}{\omega}, \tag{3.25}$$

and the method of steepest descent yields

$$\frac{\langle \hat{a}^\dagger \hat{a} \rangle}{N} = \begin{cases} \frac{k_B T}{2\omega} & \text{if } \beta < \beta_c \text{ or } \lambda < \lambda_c \\ u_0^2 + \frac{k_b T}{2\omega} & \text{if } \beta > \beta_c \text{ and } \lambda > \lambda_c. \end{cases} \tag{3.26}$$

For the Dicke model in the RWA, with Hamiltonian

$$\hat{H} = \omega \hat{a}^\dagger \hat{a} + \frac{1}{2} \sum_i \sigma_{zi} + \sum_i \frac{\lambda}{\sqrt{N}} \left(\hat{a}^\dagger \sigma_{-i} + \hat{a} \sigma_{+i} \right), \tag{3.27}$$

a similar calculation gives

$$\frac{\langle \hat{a}^\dagger \hat{a} \rangle}{N} = \begin{cases} 0 & \text{if } \beta < \beta_c \\ \frac{u_0^2}{4} & \text{if } \beta > \beta_c \end{cases}. \tag{3.28}$$

The zero mean photon number below threshold in this case arises from the lack of any term in Hamiltonian 3.27 with a net transfer of energy from atoms to the field. Both

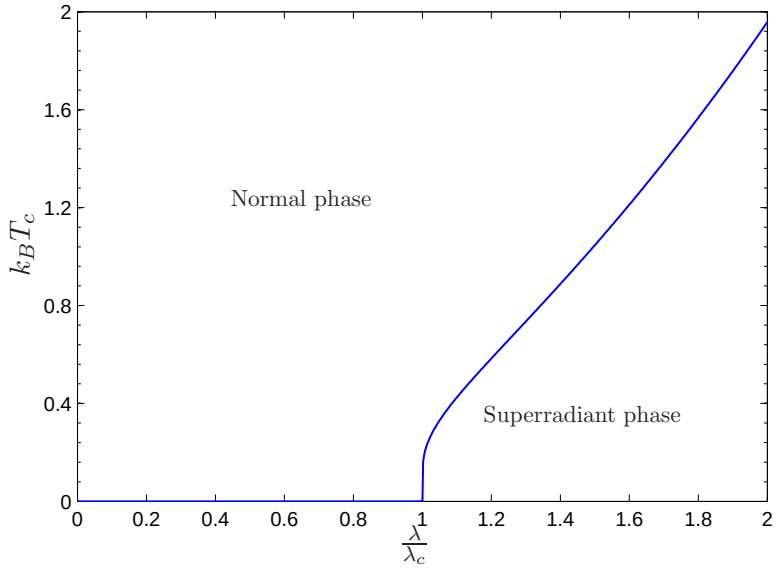

Figure 3.1.: Phase diagram at finite temperature

cases, with and without the RWA, however, show a phase transition analogous to the ordering in a magnetic system: in the uncoupled regime ($\lambda = 0$) the system shows no net magnetic alignment; the ordered state $|+++\cdots\rangle$ has low statistical weight; once the coupling is turned on the system does not organize itself until the coupling constant reaches a temperature-dependent critical value, at which the system undergoes a phase transition. We show in Figure 3.1 the corresponding phase diagram for the Dicke system without the RWA given by Eq. (3.20). It must be stressed that, in contrast of what was discussed in Chapter 1 (and will be seen in more detail in Chapter 4), here we are dealing with a *closed system*. Thus, in contrast to what 3.28 might imply, we do not have a source of field drawn from a thermal bath at temperature T. This equation simply describes the statistics of a field-atom system in *equilibrium*. In order to perform useful work (e.g. extract a net output flux of photons) this system should be coupled to another system at a *lower* temperature.

3.2. Dicke phase transition and A^2 term

It was noted by Rzazewski et. al. [14] that the phase transition, as presented in the previous section, arises because of the absence of the $\mathbf{A}^2$ term. This term appears when the field-atom interaction Hamiltonian is written as

$$\hat{H} = \sum_i^N \left[\frac{1}{2\mu} \left(\mathbf{p}_i - e\mathbf{A}(\mathbf{r}_i) \right)^2 + V(r_i) \right] + \hbar\omega \hat{a}^\dagger \hat{a}, \tag{3.29}$$

where $\mathbf{p}_i$ is the momentum operator of the electron indexed by i, μ is the reduced mass of the nucleus plus electron system, and the vector potential at the position of an atom $\mathbf{r}_i$, $\mathbf{A}(\mathbf{r}_i)$, is given in terms of the quantized field operators $\hat{a}$ and $\hat{a}^\dagger$ by [36, Section 2.1] (for interaction with a single light mode)

$$\mathbf{A}(\mathbf{r}_i, t) = \frac{\mathcal{E}_{\mathbf{k}\epsilon}}{\omega_{\mathbf{k}}} \left(\hat{a} \mathrm{e}^{i(\mathbf{k}\cdot\mathbf{r}_i - \omega t)} + \hat{a}^\dagger \mathrm{e}^{-i(\mathbf{k}\cdot\mathbf{r}_i - \omega t)} \right), \tag{3.30}$$

where the relation $c\,|\mathbf{k}| = \omega_{\mathbf{k}}$ holds, and $\mathcal{E}_{\mathbf{k}\epsilon}$ is the electric field per photon given by (2.27), i.e.,

$$\mathcal{E}_{\mathbf{k}\epsilon} = \sqrt{\frac{\hbar c\,|\mathbf{k}|}{2\varepsilon_0 \mathcal{V}}}\epsilon. \tag{3.31}$$

The atom-field coupling λ of Hamiltonian (3.1) is given in this picture, according to (2.7), by

$$\lambda = \omega_0 \frac{\mathcal{E}_{\mathbf{k}\epsilon} \cdot \mathbf{D}}{\omega_{\mathbf{k}}} \sqrt{N}, \tag{3.32}$$

where $\mathbf{D}$ is the electric dipole moment given by $\mathbf{D} = \langle + |\mathbf{r}| - \rangle$. All atoms are considered to couple to the same field, as justified in Section 2.1.1 for microwave radiation (long wavelength approximation), and at optical frequencies as shown in Section 4.2; thus we replace $\mathbf{A}(\mathbf{r}_i)$ by $\mathbf{A}(0) = \mathbf{A}$. It was shown in Section 2.1.1 that the usual dipole Hamiltonian is obtained by neglecting the terms proportional to $\mathbf{A}^2$. We write them explicitly as

$$\sum_i^N \frac{e^2 \mathbf{A}^2}{2\mu} = \frac{N e^2 \mathcal{E}_{\mathbf{k}\epsilon}^2}{2\mu\omega_{\mathbf{k}}^2} (\hat{a}^{\dagger 2} + \hat{a}^2 + 2\hat{a}^\dagger \hat{a} + 1). \tag{3.33}$$

Using the data for experimental cavity volumes [6] we get, for the constant multiplying the operator, a number of the order 10^{-6} MHz per atom (normalized to $\hbar$), which is to

be compared with an atom-field coupling per atom of the order 10 MHz, making this term negligible in the context of current cavity QED experiments.

However, we include the $\mathbf{A}^2$ term above in the Hamiltonian (3.1) and follow the same procedure used to calculate the partition function. The method of steepest descent will modify equation (3.19), which becomes [14]

$$\frac{\omega\omega_0}{4\lambda^2}\left(1+\frac{2Ne^2\mathcal{E}^2_{\mathbf{k}\epsilon}}{\mu\omega^3_{\mathbf{k}}}\right)\left(1+\frac{16\lambda^2u^2}{\omega_0^2}\right)^{1/2}=\tanh\left[\frac{\beta}{2}\mathscr{G}_+\right]. \tag{3.34}$$

The difference from equation (3.19) is the extra term multiplying the LHS in equation (3.34). The existence of a phase transition depends upon the requirement that the term

$$\frac{\omega\omega_0}{4\lambda^2}\left(1+\frac{2Ne^2\mathcal{E}^2_{\mathbf{k}\epsilon}}{\mu\omega^3_{\mathbf{k}}}\right)=\frac{\omega^2_{\mathbf{k}}\epsilon_0}{2\omega_0\hbar\left|\mathbf{D}\right|^2N/\mathcal{V}}\left(1+\frac{e^2\hbar}{\mu\omega^2_{\mathbf{k}}\epsilon_0}\frac{N}{\mathcal{V}}\right) \tag{3.35}$$

be smaller than unity, which yields the condition

$$\left|\mathbf{D}\right|^2\omega_0>\frac{e^2}{2\mu}. \tag{3.36}$$

The values of ω_0 and $|\mathbf{D}|^2$ are not arbitrary. They are restricted by the Thomas-Reiche-Kuhn sum rule (as argued in [14] and references therein), and in fact, from this rule, we may deduce that

$$\left|\mathbf{D}\right|^2\omega_0<\frac{e^2}{2\mu}. \tag{3.37}$$

We conclude from this calculation that the phase transition, as presented by Hepp and Lieb [9], does not exist for a system of atoms interacting with a cavity mode. In the following chapter we show how this difficulty is overcome by writing an effective Hamiltonian where the frequency ω_0 and the atomic dipole $\mathbf{D}$ are effective couplings which can be, in principle, experimentally controlled. Such a situation is possible for an open system where the system has an external source of energy and the equilibrium analysis, based upon the partition function, is no longer appropriate.

4. Proposed realisation of the non-RWA Dicke model

In the previous chapter we presented the Dicke model of superradiance for a collection of atoms. All the situations shown have assumed the coupling between the field and atoms, through a dipole interaction, to be small compared with the field frequency. This leads to the rotating-wave approximation typically made in the Jaynes-Cummings Hamiltonian. In this chapter we present a proposed realization of the Dicke model where the RWA is not valid, enabling new phenomena, in particular, a quantum phase transition, to be studied.

4.1. Introduction

We discussed the Jaynes-Cummings model using Hamiltonian (2.49), a regime where $\mathcal{E}_\omega \left|\mathbf{d}_\pm\right| / \hbar \ll \{\omega, \omega_0\}$ and the rotating wave approximation (RWA) applies, as seen in Eq. (2.53). Under this condition we also neglect the self energy terms of the dipole interaction, as we noted in Section 2.1, or equivalently, we neglect the vector potential term $\mathbf{A}^2$ in a $(\mathcal{P} - q\mathbf{A})^2$-type Hamiltonian [10]. The counter rotating terms, $\hat{a}^\dagger \hat{J}_+$ and $\hat{a}\hat{J}_-$, neglected in the RWA, do not conserve energy, and account for virtual processes happening at a frequency $\omega + \omega_0$.

The RWA makes the system integrable. Remembering the discussion in Section 2.3, and looking into the references for the analytical solutions [5], we see that each eigenvector remains in a finite subspace of vectors $|\ell, m, n\rangle$ with constant $m + n$. This is not the case if we consider a Hamiltonian retaining the counter rotating terms, for which

the eigenvectors have to be expressed as a combination of an infinite number of states and for which the corresponding semi-classical equations of motion can show chaotic behaviour [45].

As seen in Chapter 3, the Dicke model is associated with a phase transition, whose existence depends on the self energy term $\mathbf{A}^2$ being neglected. We are particularly interested in the quantum phase transition appearing at zero temperature. This phase transition only occurs if the counter rotating terms are present, i.e. in a regime where the Hamiltonian

$$\hat{H} = \omega_0 \hat{J}_z + \omega \hat{a}^\dagger \hat{a} + \frac{\lambda}{\sqrt{N}} \left(\hat{a} + \hat{a}^\dagger\right) \left(\hat{J}_+ + \hat{J}_-\right) \tag{4.1}$$

has parameters $\omega, \omega_0 \approx \lambda$. For such a regime to be reached at optical frequencies, the system must have a high electric field per photon. In reference [6], the usual coupling per atom, λ, is given to be of the order of MHz, while optical frequencies commonly used are of the order of 10^7MHz. In order to reach such an intense electric field (see Eq. (2.27)) the volume of the cavity has to be reduced by a factor of 10^{-14}, i.e., a length reduction of 10^{-4}. Cavity mirror separation would have to drop from μm to Å (the order of the atomic diameter!).

Even if such an apparatus were possible with actual technology, the intense electric field would make the self energy term $\mathbf{A}^2$ important and it could not be neglected as seen in Section 2.1.1. As a result this would destroy the phase transition we are interested in (Section 3.2).

We present in this Chapter an *effective* Hamiltonian which is equivalent to (4.1) with $\omega, \omega_0 \approx \lambda$, and where the self energy term $\mathbf{A}^2$ can be consistently neglected. To achieve this goal we propose an experimental scheme yielding a Hamiltonian in which the coupling λ and the frequencies ω and ω_0 do not have the same meaning as in the Jaynes-Cummings model, but are effective parameters, which can, in principle, be easily changed in an experimental setup. The inclusion of the counter rotating terms and the apparent lack of energy conservation is justified in our model as we are dealing with a non-equilibrium system, with a continuous flow of energy through it.

4.2. Proposed realization of the full Dicke model

One possible experimental realization of Dicke superradiance makes use of Rydberg atoms [32] and microwave cavities with superconducting mirrors. In these experiments the atom is raised to a high excited state, and the superradiant emission occurs between two levels tuned to a cavity.

A simpler realization uses a three level structure to induce a Raman transition by a cavity ([4] and references therein). In this situation the Hamiltonian has terms $\hat{a}^\dagger \hat{J}_-$ and $\hat{a}\hat{J}_+$, responsible for the creation of a photon in the cavity and the destruction of an excitation in the atomic system, and vice-versa.

The counter rotating terms $\hat{a}^\dagger \hat{J}_+$ and $\hat{a}\hat{J}_-$ account for adding a photon in the cavity and raising an atom to its excited state and vice-versa. These processes do not conserve energy, and are usually neglected as they happen on a very fast timescale. To make them relevant in our system we use a four level atom and stimulate two Raman transitions through different paths to produce the rotating and counter rotating terms.

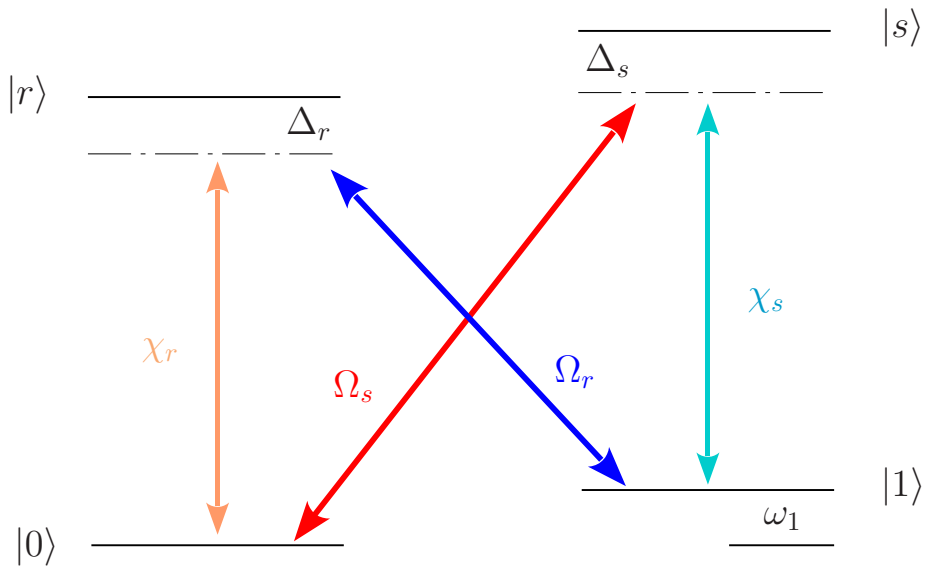

Figure 4.1.: Transition scheme

Figure 4.1 shows two Raman transitions mediated by the cavity field, with dipole

coupling constants to the cavity mode χ_r and χ_s, and two lasers with Rabi frequencies Ω_r and Ω_s. The target states are $|0\rangle$ and $|1\rangle$, separated by an energy ω_1. The path taking the atom from state $|0\rangle$ to state $|1\rangle$, following the red arrow, will deliver one photon to the cavity while promoting the atom to its upper level, thus realising the counter rotating term $\hat{a}^\dagger \hat{J}_+$; the inverse path represents the absorption of a photon from the cavity as the atom returns to its lower energy level, corresponding to the term $\hat{a}\hat{J}_-$. The usual Jaynes-Cummings terms correspond to transitions $|0\rangle \rightarrow |1\rangle$ and $|1\rangle \rightarrow |0\rangle$ through the orange and green arrows ($\hat{a}\hat{J}_+$ and $\hat{a}^\dagger \hat{J}_-$ respectively). The lasers are far detuned from the atomic transition frequencies, so that the dynamics of the transitions $|0\rangle \rightarrow |s\rangle$ and $|1\rangle \rightarrow |r\rangle$ occur on a fast time scale and the states $|r\rangle$ and $|s\rangle$ can be adiabatically eliminated.

We develop the detailed description of the single atom system as follows. First we introduce the Hamiltonian of the cavity mode, with frequency ω_c,

$$\hat{H}_{\mathrm{c}} = \omega_{\mathrm{c}} \hat{a}^\dagger \hat{a}, \tag{4.2}$$

and of the atom, with zero of energy set at the energy of state $|0\rangle$,

$$\hat{H}_{\mathrm{A}} = \omega_r |r\rangle\langle r| + \omega_s |s\rangle\langle s| + \omega_1 |1\rangle\langle 1|. \tag{4.3}$$

The interaction between the atom and the lasers is modeled, in the Schrödinger picture, by the Hamiltonian

$$\hat{H}_{AL}(t) = \Omega_s \left[|s\rangle\langle 0| \mathrm{e}^{-i\omega_{ls}t} \mathrm{e}^{i\mathbf{k}_s \cdot \mathbf{x}_i} + \mathrm{h.c.} \right] + \Omega_r \left[|r\rangle\langle 1| \mathrm{e}^{-i\omega_{lr}t} \mathrm{e}^{i\mathbf{k}_r \cdot \mathbf{x}_i} + \mathrm{h.c.} \right], \tag{4.4}$$

where ω_{ls} and ω_{lr} are the frequencies of the laser fields represented by the red and blue arrows in Figure 4.1, respectively, $\mathbf{k}_r$ and $\mathbf{k}_s$ are the wave vectors of the laser fields, and $\mathbf{x}_i$ is the position of the atom indexed by i. We finally include the interaction between the atoms and the cavity,

$$\hat{H}_{Ac} = \left[\chi_s |s\rangle\langle 1| \hat{a} + \chi_r |r\rangle\langle 0| \hat{a} \right] \mathrm{e}^{i\mathbf{k}\cdot\mathbf{x}_i} + \mathrm{h.c.}. \tag{4.5}$$

Note that the rotating wave approximation was made in (4.4) and (4.5).

We shall consider all fields to be copropagating, in order that the phases introduced by the terms $e^{i\mathbf{k}\cdot\mathbf{x}}$ are the same ($\mathbf{k}_r \simeq \mathbf{k}_s \simeq \mathbf{k}$). With this configuration the effective Hamiltonian we shall derive will be independent of the location of atom in the cavity. Also, the recoil the atom gains by absorbing a photon from the laser field is essentially canceled by emitting a photon in the same direction. The choice of mode function $e^{i\mathbf{k}\cdot\mathbf{x}_i}$ for the cavity field means that the corresponding experimental setup is that of a ring cavity (see Sec. 4.3).

We follow the derivation of the effective Dicke Hamiltonian by transforming the system Hamiltonian,

$$\hat{H} = \hat{H}_c + \hat{H}_A + \hat{H}_{AL} + \hat{H}_{Ac}, \tag{4.6}$$

to a rotating frame in order to eliminate the time dependent exponentials in $\hat{H}_{AL}$. Using the transformation $e^{i\hat{H}_0 t}\hat{H}e^{-i\hat{H}_0 t}$, with

$$\hat{H}_0 = \frac{1}{2}(\omega_{lr} + \omega_{ls})\left(\hat{a}^\dagger\hat{a} + |r\rangle\langle r|\right) + \frac{1}{2}\left(\omega_{ls} - \omega_{lr}\right)|1\rangle\langle 1| + \omega_{ls}|s\rangle\langle s|, \tag{4.7}$$

the evolution of the system is given by the Hamiltonian

$$\tilde{\hat{H}} = \Delta_c\hat{a}^\dagger\hat{a} + \Delta_r|r\rangle\langle r| + \Delta_s|s\rangle\langle s| + \Delta_1|1\rangle\langle 1| + \hat{H}_{AL}(0) + \hat{H}_{Ac}. \tag{4.8}$$

Noting that $\omega_{ls} - \omega_{lr} \approx 2\omega_1$, we can defined the detunings, according to Figure 4.1:

$$\Delta_s = \omega_s - \omega_{ls}, \tag{4.9}$$

$$\Delta_c = \omega_c - \frac{\omega_{lr} + \omega_{ls}}{2}, \tag{4.10}$$

$$\Delta_r = \omega_r - \frac{\omega_{lr} + \omega_{ls}}{2}, \tag{4.11}$$

$$\Delta_1 = \omega_1 - \frac{\omega_{lr} - \omega_{ls}}{2}. \tag{4.12}$$

We then use the Schrödinger equation to determine the evolution of the state written as

$$|\Psi(t)\rangle = \sum_{m=0}^{\infty}\left[(c_r^m|r\rangle + c_s^m|s\rangle + c_1^m|1\rangle + c_0^m|0\rangle)\otimes|m\rangle\right], \tag{4.13}$$

where the coefficients c_i are time dependent, and $|m\rangle$ is the state of the cavity mode with number of photons m. We then calculate the equations governing the evolution of

the coefficients in the atomic space using the Schrödinger equation

$$i\frac{\mathrm{d}|\Psi(t)\rangle}{\mathrm{d}t} = \hat{H}|\Psi\rangle. \tag{4.14}$$

The term $\Delta_c \hat{a}^\dagger \hat{a}$ in Hamiltonian (4.8) is neglected when deriving the equations of motion for the coefficients c_i:

$$i\dot{c}_r^m = \Delta_r c_r^m + \mathrm{e}^{i\mathbf{k}\cdot\mathbf{x}}\left(\Omega_r c_1^m + \chi_r c_0^{m+1}\sqrt{m+1}\right), \tag{4.15}$$

$$i\dot{c}_s^m = \Delta_s c_s^m + \mathrm{e}^{i\mathbf{k}\cdot\mathbf{x}}\left(\Omega_s c_0^m + \chi_s c_1^{m+1}\sqrt{m+1}\right), \tag{4.16}$$

$$i\dot{c}_1^m = \Delta_1 c_1^m + \mathrm{e}^{-i\mathbf{k}\cdot\mathbf{x}}\left(\Omega_r c_r^m + \chi_s c_s^{m-1}\sqrt{m}\right), \tag{4.17}$$

$$i\dot{c}_0^m = \mathrm{e}^{-i\mathbf{k}\cdot\mathbf{x}}\left(\Omega_s c_s^m + \chi_r c_r^{m-1}\sqrt{m}\right). \tag{4.18}$$

If the detunings Δ_r and Δ_s are much bigger than the couplings $\Omega_{\{r,s\}}$ and $\chi_{\{r,s\}}$, the states $|r\rangle$ and $|s\rangle$ will follow adiabatically states $|1\rangle$ and $|0\rangle$. On long timescales, the time derivatives of c_r^m and c_s^m are effectively zero. This yields, for these coefficients,

$$c_s^m = -\frac{\mathrm{e}^{i\mathbf{k}\cdot\mathbf{x}_i}}{\Delta_s}\left(\Omega_s c_0^m + \chi_s c_1^{m+1}\sqrt{m+1}\right), \tag{4.19}$$

$$c_r^m = -\frac{\mathrm{e}^{i\mathbf{k}\cdot\mathbf{x}_i}}{\Delta_r}\left(\Omega_r c_1^m + \chi_r c_0^{m+1}\sqrt{m+1}\right). \tag{4.20}$$

The coefficients c_r^m and c_s^m so calculated are replaced in Eqs. (4.17) and (4.18) to obtain the equations governing the evolution of c_1^m and c_0^m

$$i\dot{c}_1^m = \left(\Delta_1 - \frac{\Omega_r^2}{\Delta_r}\right)c_1^m - \frac{\Omega_r\chi_r}{\Delta_r}\sqrt{m+1}c_0^{m+1} - \frac{\chi_s\Omega_s}{\Delta_s}\sqrt{m}c_0^{m-1} - \frac{\chi_s^2}{\Delta_s}c_1^m m \tag{4.21}$$

$$i\dot{c}_0^m = -\frac{\Omega_s^2}{\Delta_s}c_0^m - \frac{\Omega_s\chi_s}{\Delta_s}\sqrt{m+1}c_1^{m+1} - \frac{\chi_r\Omega_r}{\Delta_r}\sqrt{m}c_1^{m-1} - \frac{\chi_r^2}{\Delta_r}c_0^m m. \tag{4.22}$$

The above equations can be obtained from an effective Hamiltonian involving only the states $|0\rangle$ and $|1\rangle$ given by

$$\begin{aligned}\hat{H}_{\text{eff}} = &\left(\Delta_1 - \frac{\Omega_r^2}{\Delta_r}\right)|1\rangle\langle 1| - \frac{\Omega_r\chi_r}{\Delta_r}\left(\sigma_+\hat{a} + \sigma_-\hat{a}^\dagger\right) - \frac{\Omega_s\chi_s}{\Delta_s}\left(\sigma_-\hat{a} + \sigma_+\hat{a}^\dagger\right)\\ &- \frac{\Omega_s^2}{\Delta_s}|0\rangle\langle 0| - \frac{\chi_s^2}{\Delta_s}\hat{a}^\dagger\hat{a}|1\rangle\langle 1| - \frac{\chi_r^2}{\Delta_r}\hat{a}^\dagger\hat{a}|0\rangle\langle 0|\end{aligned} \tag{4.23}$$

where we defined

$$\sigma_+ = |1\rangle\langle 0|, \tag{4.24}$$

$$\sigma_- = |0\rangle\langle 1|. \tag{4.25}$$

We can also rewrite the diagonal terms $|0\rangle\langle 0|$ and $|1\rangle\langle 1|$ with the help of the definitions for σ_z and $\mathbb{1}$,

$$|1\rangle\langle 1| = \frac{\mathbb{1}+\sigma_z}{2}, \tag{4.26}$$

$$|0\rangle\langle 0| = \frac{\mathbb{1}-\sigma_z}{2}. \tag{4.27}$$

We ignore the constant terms, which arrive from the multiplications by $\mathbb{1}$, to write the effective Hamiltonian. From (4.8) we have

$$\hat{H}_{\text{eff}} = \omega\hat{a}^\dagger\hat{a} + \omega_0\frac{\sigma_z}{2} + \daleth\hat{a}^\dagger\hat{a}\frac{\sigma_z}{2} + \lambda_r\left(\hat{a}^\dagger\sigma_- + \hat{a}\sigma_+\right) + \lambda_s\left(\hat{a}^\dagger\sigma_+ + \hat{a}\sigma_-\right), \tag{4.28}$$

where the constants are defined as follows:

$$\lambda_r = -\frac{\chi_r\Omega_r}{\Delta_r}, \tag{4.29}$$

$$\lambda_s = -\frac{\chi_s\Omega_s}{\Delta_s}, \tag{4.30}$$

$$\daleth = \frac{\chi_r^2}{\Delta_r} - \frac{\chi_s^2}{\Delta_s}, \tag{4.31}$$

$$\omega_0 = \frac{\Omega_s^2}{\Delta_s} - \frac{\Omega_r^2}{\Delta_s} + \Delta_1, \tag{4.32}$$

$$\omega = \Delta_c - \left(\frac{\chi_r^2}{\Delta_r} + \frac{\chi_s^2}{\Delta_s}\right). \tag{4.33}$$

As the constants Ω and Δ can be varied experimentally, we assume (for simplicity) that we may set

$$\frac{\chi_r^2}{\Delta_r} = \frac{\chi_s^2}{\Delta_s}, \tag{4.34}$$

$$\frac{\Omega_r^2}{\Delta_r} = \frac{\Omega_s^2}{\Delta_s}. \tag{4.35}$$

in order that $\daleth = 0$ and $\lambda_r = \lambda_s = \lambda$. We arrive at an effective Hamiltonian having counter rotating terms, and where the constants ω, ω_0, and λ can be changed by a convenient choice of the detunings Δ_s and Δ_r, and the laser intensities Ω_r and Ω_s.

For an ensemble of atoms, the extension of this derivation is straightforward. We consider the inter-atomic distance to be big enough to neglect dipole-dipole interactions and Van der Waals dephasing. By doing this we just have to add an index to each $\sigma_{\pm i}$

and perform the sum. We also have to take care that, in adding the $\mathbb{1}$'s from each atomic subspace, the number of particles N will appear in the definition of ω. Redefining λ in terms of the density (the cavity coupling has a $\mathcal{V}^{-1/2}$ term) we arrive at the Hamiltonian for the Dicke model:

$$\boxed{\hat{H} = \omega \hat{a}^\dagger \hat{a} + \omega_0 \hat{J}_z + \frac{\lambda}{\sqrt{N}} \left(\hat{a}^\dagger + \hat{a}\right) \left(\hat{J}_+ + \hat{J}_-\right)}, \tag{4.36}$$

where the constants ω and λ are redefined as

$$\lambda = \frac{\sqrt{N}\Omega_s \chi_s}{\Delta_s}, \tag{4.37}$$

$$\omega = \Delta_c - N\left(\frac{\chi_r^2}{\Delta_r} + \frac{\chi_s^2}{\Delta_s}\right). \tag{4.38}$$

A final observation must be made before following on. We notice that even when the counter rotating terms are added to the Jaynes-Cummings Hamiltonian, the resulting equation, shown in (4.36), is Hermitian and, obviously, commutes with itself; as a consequence energy is conserved, since any Hamiltonian eigenstate is a stationary state of the system. In what sense then do we claim that the counter rotating terms $\hat{a}\hat{J}_-$ and $\hat{a}^\dagger \hat{J}_+$ do not conserve energy? These counter rotating terms represent processes where the net number of quanta in the system is increased or decreased — increased when the field gains a photon and the atoms receive an energy quantum via the term $\hat{a}^\dagger \hat{J}_+$, or decreased when the atoms loose an energy quantum and a photon is lost from the field through $\hat{a}\hat{J}_-$). Thus, when using the eigenvectors of the *non-interacting* Hamiltonian ($\lambda = 0$) to write the probability amplitudes of transition in first order perturbation theory these terms are energy non-conserving. On the other hand, for the usual rotating terms, the probabilities of transition are proportional to $\langle n_i m_i | \hat{J}_+ \hat{a} | n_f m_f \rangle$; the states to which transitions are allowed are such that the total number of energy quanta is conserved—i.e., $n_i + m_i = n_f + m_f$.

4.2.1. Phase transition and the effective model

This effective Hamiltonian (4.36) has the counter-rotating terms and negligible self energy, $\mathbf{A}^2$. We note that there is a continuous flux of energy into the system through the

lasers inducing the transitions $|0\rangle \rightarrow |s\rangle$ and $|1\rangle \rightarrow |s\rangle$ in Figure 4.1. As a consequence the steady state of such a system, *when including cavity dissipation*, may show a non-zero output flux of photons. In a closed system in thermal equilibrium, as discussed in Chapter 3, such output of energy is not allowed. In our model, it accounts for the fact we are dealing with a non-equilibrium system.

The existence of a non-zero output flux of photons will depend on the strenght of the couplings λ_r and λ_s – considering we are in the regime $\lambda \approx \omega$ so the counter rotating terms are not negligible. For a system in thermal equilibrium, where the Hamiltonian may express a "true" interaction energy, the regime where the RWA does not hold may be achieved by applying a strong electric field. In such a situation, as seen in Section 2.1.1, the self energy term proportional to $\mathbf{A}^2$ must be taken into account, and we have a situation where the phase transition does not exist, as described in Section 3.2. The couplings λ_r and λ_s in our system depend on the laser intensities, and can be varied.

4.3. Experimental Realization

The system described above can be experimentally realised by an atomic cloud inside an optical cavity. In order that the cavity field seen by the atoms has a $e^{i\mathbf{k}\cdot\mathbf{x}}$ profile – instead of $\cos(2\mathbf{k}\cdot\mathbf{x})$ – a ring cavity can be used. This can be achieved with the pump lasers co-propagating with the cavity mode through the atomic cloud [27] as shown in Figure 4.2. The transition scheme shown in Figure 4.1 can be obtained for the transition $\mathscr{F} = 1 \leftrightarrow \mathscr{F}' = 1$, as present in Rubidium atoms. In this case a static magnetic field, perpendicular to the lasers' polarization, is applied to achieve a Zeeman splitting of the ground levels $m_{\mathscr{F}} = \{+1, -1\}$ of $\mathscr{F} = 1$. The cavity mode needs to be linearly polarized along an axis perpendicular to the magnetic field direction. In this case ω_1 will depend on the strength of the magnetic field. Typical values for the coupling constants found in the literature [46, 47], are $\chi_r \approx 50$ KHz, $N = 10^6$ atoms. For large detunings, we have an effective coupling $\Omega_s/\Delta_s \approx 10^{-3}$. With these parameters the coupling λ can be on the order of a few hundreds of kHz, while, with suitable detunings, it is possible to make $\omega \sim \omega_0 \sim \lambda$. It can also be shown that, in this regime, the losses due to spontaneous

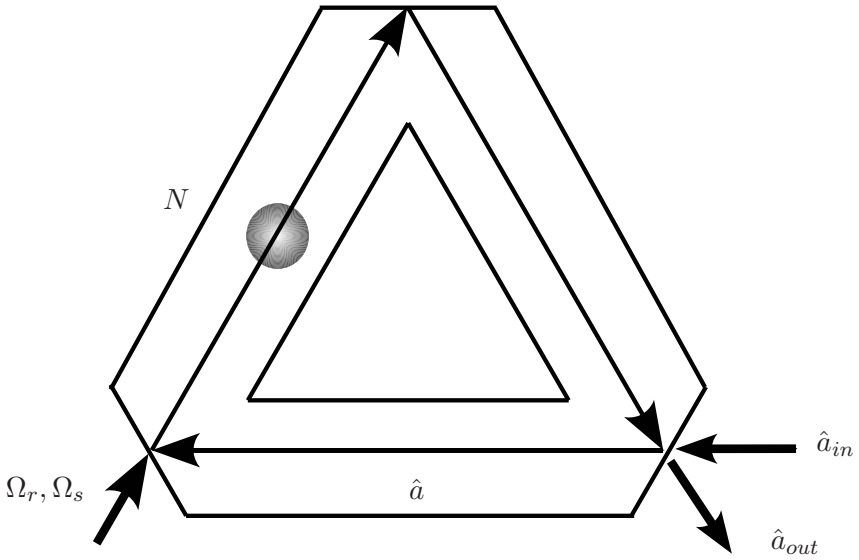

Figure 4.2.: Experimental setup

emission are of the order of a few Hz, while the cavity losses are around 10 kHz. With these values we can assume that our system is in the strong coupling regime.

For the remaining of this work, unless otherwise stated, we shall assume the normalized frequencies $\omega = 1$ and $\omega_0 = 1$.

5. Dicke model in the thermodynamic limit II

In Chapter 3 we showed how the phase transition occurs in the Dicke model for finite temperatures. There we considered how mixed states self-organize when the interaction becomes sufficiently strong, and the system enters the superradiant phase. Now we look at the phase transition occurring at zero temperature. However, as the model has no closed solution, we have to use an approximation method, and in this chapter we employ the Holstein-Primakoff representation.

5.1. Holstein-Primakoff representation – Non-dissipative case

Hamiltonian (4.36) has no analytical expression for its eigenvalues. As we noticed in Section 2.3, in the RWA the total number of quanta is a conserved quantity. The eigenvectors, in that case, have an expansion with a finite number of terms, all with constant total number of quanta $m+n$. The inclusion of the counter rotating terms, however, introduces non-integrability into the system: the solution is now an infinite sum of states. We are interested in the limit $N \to \infty$, with $N/\mathcal{V}$ constant. In this situation we can use an approximation method, a linearization, assuming the ratio between mean values and fluctuations scales like $\sqrt{N}$. There is a whole plethora of methods one can explore. Here we make the linearization using the Holstein-Primakoff (HP) representation. It has the advantage, as we shall see later in Section 6.2, of giving rise to equations that intrinsically conserve the total angular momenta, which fails in the linearized Haken representation.

The HP representation utilizes a relationship between the angular momentum operators $\hat{J}_\pm$ and the bosonic operators [16]; in particular, the angular momentum operators can be expressed in terms of bosonic operators $\hat{b}^\dagger$ and $\hat{b}$ (with $[\hat{b}, \hat{b}^\dagger] = 1$) as

$$\hat{J}_z = \hat{b}^\dagger \hat{b} - \frac{N}{2}, \tag{5.1a}$$

$$\hat{J}_+ = \hat{b}^\dagger \sqrt{N} \sqrt{1 - \frac{\hat{b}^\dagger \hat{b}}{N}}, \tag{5.1b}$$

$$\hat{J}_- = \sqrt{N} \sqrt{1 - \frac{\hat{b}^\dagger \hat{b}}{N}}\ \hat{b}. \tag{5.1c}$$

(Note that the operators so defined obey the usual commutation relations for angular momentum operators (2.15)). We substitute these expressions in (4.36) to give

$$\hat{H} = \omega \hat{a}^\dagger \hat{a} + \omega_0 \hat{b}^\dagger \hat{b} + \lambda \left(\hat{a}^\dagger + \hat{a}\right) \left(\hat{b}^\dagger \sqrt{1 - \hat{b}^\dagger \hat{b}/N} + \sqrt{1 - \hat{b}^\dagger \hat{b}/N} \hat{b}\right) - \frac{N\omega_0}{2}. \tag{5.2}$$

We then linearize the bosonic operators around their mean values using

$$\hat{b}^\dagger = N^{1/2} \langle \bar{b}^\dagger \rangle + \hat{\beta}^\dagger, \tag{5.3a}$$

$$\hat{a}^\dagger = N^{1/2} \langle \bar{a}^\dagger \rangle + \hat{\alpha}^\dagger, \tag{5.3b}$$

where the Greek symbols represent fluctuation operators, and the bar denotes that the operators are normalized by $N^{-1/2}$.

Based on the behaviour of the semiclassical equations, to be seen later, we can set, for $\lambda < \lambda_c$,

$$\langle \hat{a} \rangle = \langle \hat{a}^\dagger \rangle = 0, \tag{5.4}$$

$$\langle \hat{b} \rangle = \langle \hat{b}^\dagger \rangle = 0, \tag{5.5}$$

where λ_c is a critical coupling constant to be determined. By making these substitutions into (5.3) and (5.2), and taking the limit $N \to \infty$, we end up with the Hamiltonian for the *normal phase* of the Dicke model, $\hat{H}_N$,

$$\hat{H}_N = \omega \hat{\alpha}^\dagger \hat{\alpha} + \omega_0 \hat{\beta}^\dagger \hat{\beta} + \lambda \left(\hat{\alpha}^\dagger + \hat{\alpha}\right) \left(\hat{\beta}^\dagger + \hat{\beta}\right) - \frac{N\omega_0}{2}. \tag{5.6}$$

This is the Hamiltonian for two coupled harmonic oscillators, which can be diagonalized with a suitable basis transformation [26]. We present the derivation of the full result in Appendix A [48]:

$$\hat{H}_N = \varepsilon_- \hat{c}_1^\dagger \hat{c}_1 + \varepsilon_+ \hat{c}_2^\dagger \hat{c}_2 - \frac{1}{2}\left(\omega + \omega_0 - \varepsilon_+ - \varepsilon_-\right) - \frac{N\omega_0}{2}, \tag{5.7}$$

where $\hat{c}_1$ and $\hat{c}_2$ are the operators for the two independent modes of excitation. At zero coupling, $\lambda = 0$, the operator $\hat{c}_1$ depends only on $\hat{\alpha}$ and $\hat{c}_2$ only on $\hat{\beta}$; for this reason we call ε_- the photonic eigenvalue, and ε_+ the atomic eigenvalue; more generally (i.e., for $\lambda > 0$), each one of these normal mode operators depends on both $\hat{a}$ and $\hat{b}$. The fundamental energies of the normal modes are given by

$$\varepsilon_\pm = \sqrt{\frac{1}{2}\left(\omega^2 + \omega_0^2 \pm \sqrt{\left(\omega_0^2 - \omega^2\right)^2 + 16\lambda^2\omega\omega_0}\right)}. \tag{5.8}$$

We note that, for ε_- to be real, the condition

$$\lambda < \frac{\sqrt{\omega\omega_0}}{2} = \lambda_c$$

must be satisfied.

For the *superradiant* phase, we assume the means $\langle\hat{b}\rangle$ and $\langle\hat{a}\rangle$ have non-zero values. We make the substitution (5.3) into (5.2), and do a series expansion of the fluctuation operators around 0, retaining only terms of order $O(N)$ in $\hat{\alpha}$ and $\hat{\beta}$. For consistency, we have $\langle\hat{\alpha}\rangle = 0$ and $\langle\hat{\beta}\rangle = 0$, implying a Hamiltonian without linear terms in $\hat{\alpha}$ and $\hat{\beta}$; we use this condition to determine $\langle\bar{b}\rangle$ and $\langle\bar{a}\rangle$:

$$\langle\bar{a}\rangle = \langle\bar{a}^\dagger\rangle = \pm\frac{2\lambda}{\omega}\sqrt{\frac{1-\mu^2}{2}}, \tag{5.9a}$$

$$\langle\bar{b}\rangle = \langle\bar{b}^\dagger\rangle = \mp\sqrt{\frac{1-\mu}{2}}, \tag{5.9b}$$

where $\mu = \lambda_c^2/\lambda^2$. The Hamiltonian for this superradiant phase reads,

$$\begin{aligned}\hat{H}_N = {} & \omega\hat{\alpha}^\dagger\hat{\alpha} + \omega_0'\hat{\beta}^\dagger\hat{\beta} + \omega_0''\left(\hat{\beta}^\dagger + \hat{\beta}\right)^2 + \lambda'\left(\hat{\alpha}^\dagger + \hat{\alpha}\right)\left(\hat{\beta}^\dagger + \hat{\beta}\right) \\ & - \frac{N}{2}\left\{\frac{2\lambda^2}{\omega} + \frac{\omega_0^2\omega}{8\lambda^2}\right\} - \frac{\lambda^2}{\omega}\left(1-\mu\right)\end{aligned} \tag{5.10}$$

with constants defined as

$$\omega_0' = \frac{\omega_0}{2\mu}(1+\mu), \tag{5.11a}$$

$$\omega_0'' = \frac{\omega_0(1-\mu)(3+\mu)}{8\mu(1+\mu)}, \tag{5.11b}$$

$$\lambda' = \lambda\mu\sqrt{\frac{2}{1+\mu}}. \tag{5.11c}$$

This Hamiltonian can be diagonalized in the same way as $\hat{H}_N$. The diagonalized operators, however, are different from $\hat{c}_1$ and $\hat{c}_2$:

$$\hat{H}_S = \varepsilon_-'\hat{e}_1^\dagger\hat{e}_1 + \varepsilon_+'\hat{e}_2^\dagger\hat{e}_2 - \frac{N}{2}\left\{\frac{2\lambda^2}{\omega} + \frac{\omega_0^2\omega}{8\lambda^2}\right\} + \left(\varepsilon_+' + \varepsilon_-' - \frac{\omega_0}{2\mu}(1+\mu) - \omega - \frac{2\lambda^2}{\omega}(1-\mu)\right) \tag{5.12}$$

where the eigenvalues are

$$\varepsilon_\pm' = \sqrt{\frac{\omega_0^2}{\mu^2} + \omega^2 \pm \sqrt{\left(\frac{\omega_0}{\mu^2} - \omega^2\right)^2 + 4\omega^2\omega_0^2}}. \tag{5.13}$$

The condition for the eigenvalue ε_- to be real is

$$\lambda > \lambda_c.$$

As seen above, the macroscopic means of the operators $\hat{a}$ and $\hat{b}$ have two possible values; therefore, the corresponding set of eigenvalues is doubly degenerate for $\lambda > \lambda_c$. The change in the symmetry undergone by the normal mode operators of the system, from $\hat{c}_1$ and $\hat{c}_2$ to $\hat{e}_1$ and $\hat{e}_2$, at λ_c, corresponds to the phase transition. We explain the role played by the symmetry in Appendix A.

5.2. Dissipative Dicke model in phase space

5.2.1. Spectra and variance

We turn now to the study of the quantum fluctuations of the Dicke model across the phase transition. As seen above, with the Holstein-Primakoff representation we are able

to calculate the means of the operators $\langle\hat{a}\rangle$ and $\langle\hat{b}\rangle$ in the thermodynamic limit. By using (5.3a) and (5.9b) in (5.1), we have, for the means of the angular momentum operators,

$$\frac{\langle\hat{J}_z\rangle}{N} = \langle\bar{J}_z\rangle = -\frac{\mu}{2}, \tag{5.14}$$

$$\frac{\langle\hat{J}_+\rangle}{N} = \langle\bar{J}_+\rangle = \langle\bar{J}_-\rangle = \mp\frac{1}{2}\sqrt{1-\mu^2}. \tag{5.15}$$

We are also interested in the fluctuations and correlations of the field and atomic variables, for example

$$\langle\bar{J}_\pm, \bar{a}\rangle = \langle\bar{J}_\pm\bar{a}\rangle - \langle\bar{J}_\pm\rangle\langle\bar{a}\rangle, \tag{5.16}$$

$$\langle\bar{a}^\dagger, \bar{a}\rangle = \langle\bar{a}^\dagger\bar{a}\rangle - \langle\bar{a}^\dagger\rangle\langle\bar{a}\rangle, \tag{5.17}$$

$$\langle\bar{J}_\pm, \bar{J}_\pm\rangle = \langle\bar{J}_\pm\bar{J}_\pm\rangle - \langle\bar{J}_\pm\rangle\langle\bar{J}_\pm\rangle. \tag{5.18}$$

These quantities depend on the dispersion in the Holstein Primakoff variables and can be calculated using (5.3); knowing that $\langle\hat{\beta}\rangle = 0$ we have, for example,

$$\langle\hat{b}, \hat{b}\rangle = \langle\hat{\beta}^2\rangle.$$

We are also interested in the power spectrum of the light emitted by the cavity mode, given by the Fourier transform of the field correlation function,

$$\mathcal{S}(\nu) = \frac{1}{\pi}\int_{-\infty}^{\infty} \mathrm{d}\tau\langle\hat{a}^\dagger(\tau)\hat{a}\rangle \mathrm{e}^{i\nu\tau}, \tag{5.19}$$

where the operator $\hat{a}^\dagger(\tau)$ is given, in the Heisenberg picture, by $\hat{a}^\dagger(\tau) = \mathrm{e}^{i\hat{H}\tau}\hat{a}^\dagger\mathrm{e}^{-i\hat{H}\tau}$. Neglecting dissipation for the moment, we can interpret the spectrum straightforwardly by writing the operators $\hat{a}$ and $\hat{a}^\dagger$ in a basis of eigenvectors of the Hamiltonian $\hat{H}$, denoted by $\{|\omega_i\rangle\}$; that is, writing

$$\hat{a} = \sum_{i,j} C_{ij}|\omega_i\rangle\langle\omega_j|.$$

We assume the eigenvectors are non-degenerate for the moment. The correlation function, in this basis, is given by

$$\langle\hat{a}^\dagger(\tau)\hat{a}\rangle = \sum_{j,k} |C_{kj}|^2 \mathrm{e}^{i(\omega_j-\omega_k)\tau}, \tag{5.20}$$

where, using an expansion of $\hat{a}$ in terms of the number states,

$$C_{ij} = \sum_n \sqrt{n} \langle \omega_i | n-1 \rangle \langle n | \omega_j \rangle. \tag{5.21}$$

Hence, the spectrum possesses δ-functions at the frequencies $\nu = \omega_j - \omega_k$ for which single-photon transitions between eigenstates of the system are allowed.

In a more realistic description that includes dissipation, we must use the master equation to describe the evolution of the density matrix,

$$\frac{\mathrm{d}\rho}{\mathrm{d}t} = \mathcal{L}\rho. \tag{5.22}$$

Here $\mathcal{L}$ is the Liouvillian superoperator, defined as

$$\mathcal{L}\rho = \frac{1}{i}\left[\hat{H}, \rho\right] + \kappa\left(2\hat{a}\rho\hat{a}^\dagger - \rho\hat{a}^\dagger\hat{a} - \hat{a}^\dagger\hat{a}\rho\right). \tag{5.23}$$

By expanding any operator, say $\hat{a}^\dagger$, in a basis of eigenvectors of $\mathcal{L}$, we end up with a similar result for the spectrum, but the eigenvalues of $\mathcal{L}$ may also have a real part, responsible for damping; as a consequence, the peaks at $\omega_j - \omega_k$ broaden and their (finite) heights are proportional to the mean number of photons emitted with frequency $\omega_j - \omega_k$.

5.2.2. Phase space representation

To calculate the variances and the spectra for this system, in the damped case, we use a phase space formalism. In particular, we derive a Fokker-Planck equation in the Glauber-Sudarshan P-representation [49, 50] to express the quantum state of the system in terms of coherent states $|\alpha\rangle$ and $|\beta\rangle$. Treatments of quantum systems in phase space were first done by [51]. For the properties of coherent states see, for example, [29, 52]. For a general description of phase space methods and coherent states in quantum optics, see, for example, [36] or [28].

The inclusion of damping in the system changes the displacements $\langle\bar{b}\rangle$ and $\langle\bar{a}\rangle$ as given by (5.9). In the next chapter, we show how they are calculated from the mean of the angular momenta operators in the steady state. We could, however, calculate the new values of $\langle\bar{b}\rangle$ and $\langle\bar{a}\rangle$ from their equations of motion derived from the master equation.

A similar procedure will be presented with the atomic coherent state representation in Chapter 6. Such calculations give results of the same form as in Section 5.1, but with a new critical λ given by:

$$\lambda_c = \frac{1}{2}\sqrt{\frac{\omega_0\left(\omega^2+\kappa^2\right)}{\omega}}. \tag{5.24}$$

In this approach we introduce classical analogues, α and β, of the fluctuation operators. First we define the characteristic function

$$\chi(x,y) = \mathrm{Tr}\left[\mathrm{e}^{ix^*\hat{\alpha}^\dagger}\mathrm{e}^{ix\hat{\alpha}}\mathrm{e}^{iy^*\hat{\beta}^\dagger}\mathrm{e}^{iy\hat{\beta}}\rho\right], \tag{5.25}$$

where x and y are complex variables. The function so defined allows the calculation of any mean in normal order through the relation

$$\langle\hat{\alpha}^\dagger{}^m\hat{\alpha}^n\hat{\beta}^\dagger{}^p\hat{\beta}^q\rangle = i^{-(m+n+p+q)}\frac{\partial^{m+n+p+q}\chi(x,y)}{\partial x^{*m}\partial x^n\partial y^{*p}\partial y^q}\bigg|_{\{x,y\}=0}. \tag{5.26}$$

Under the Fourier transformation, $\chi(x,y)\rightarrow\mathcal{P}(\alpha,\beta)$, the derivative becomes a multiplication and the averages read

$$\langle\hat{\alpha}^\dagger{}^m\hat{\alpha}^n\hat{\beta}^\dagger{}^p\hat{\beta}^q\rangle = \int\mathcal{P}(\alpha,\beta)\alpha^{*m}\alpha^n\beta^{*p}\beta^q\mathrm{d}^2\alpha\mathrm{d}^2\beta,$$

where $\mathrm{d}^2\alpha = \mathrm{dRe}(\alpha)\mathrm{dIm}(\alpha)$. The function $\mathcal{P}$ has the properties of a probability distribution, with the variables α and β corresponding to their operator counterparts $\hat{\alpha}$ and $\hat{\beta}$. We calculate the equation of motion for the characteristic function by using (5.22):

$$\frac{\mathrm{d}\chi}{\mathrm{d}t} = \mathrm{Tr}\left[\mathrm{e}^{ix^*\hat{a}^\dagger}\mathrm{e}^{ix\hat{a}}\mathrm{e}^{iy^*\hat{b}^\dagger}\mathrm{e}^{iy\hat{b}}\mathcal{L}\rho\right]. \tag{5.27}$$

Using the Dicke Hamiltonian for each phase, (5.10) and (5.6), we encounter terms like $\mathrm{e}^{ix\hat{a}}\hat{a}^\dagger$, which can be placed in normal order using the relation

$$\mathrm{e}^{ix^*\hat{a}^\dagger}\hat{a} = \left(ix^*+\hat{a}\right)\mathrm{e}^{ix^*\hat{a}^\dagger}. \tag{5.28}$$

The multiplication by an $\hat{a}$ operator on the right side of the characteristic function can be achieved by applying the operator $i\partial_x$ on the characteristic function. A Fourier transform and integration by parts follow in order to the obtain an equation in the distribution $\mathcal{P}$. We show in Section 6.1.2 the detailed procedure of such a derivation;

here we present the result, which is a *linear* Fokker-Planck equation of motion for the pseudo-probability distribution $\mathcal{P}$,

$$\frac{\partial \mathcal{P}}{\partial t} = \frac{\partial}{\partial \boldsymbol{\zeta}^\intercal}\mathbf{A}\boldsymbol{\zeta}\mathcal{P} + \frac{1}{2}\frac{\partial}{\partial \boldsymbol{\zeta}^\intercal}\mathbf{D}\frac{\partial}{\partial \boldsymbol{\zeta}}\mathcal{P}, \tag{5.29}$$

where $\boldsymbol{\zeta} = (\alpha, \alpha^*, \beta, \beta^*)^\intercal$, and $\partial_{\boldsymbol{\zeta}} = (\partial_\alpha, \partial_{\alpha^*}, \partial_\beta, \partial_{\beta^*})^\intercal$; $\mathbf{A}$ is a 4×4 matrix giving the deterministic motion of the means of $\boldsymbol{\zeta}$, and $\mathbf{D}$ is the diffusion matrix, giving the evolution of the broadening of $\mathcal{P}$. This equation has the corresponding *Ito stochastic differential equation*,

$$\mathrm{d}\boldsymbol{\zeta} = -\mathbf{A}\boldsymbol{\zeta}\mathrm{d}t + \mathbf{B}^\intercal d\mathbf{W}(t), \tag{5.30}$$

where $\mathbf{B}\mathbf{B}^\intercal = \mathbf{D}$ and $d\mathbf{W}(t) = (dw_1(t), dw_2(t), dw_3(t), dw_4(t))^\intercal - w_i$ is a Wiener process, with properties: $\langle w_i(t) w_j(t')\rangle = \mathrm{d}t\delta(t-t')\delta_{ij}$, and $\langle w_i\rangle = 0$. Matrices $\mathbf{A}$ and $\mathbf{D}$ are constants, so this equation describes an Ornstein-Uhlenbeck process [53]. The drift matrix, $\mathbf{A}$, can also be derived from the equations of motion obtained from (5.22); for example,

$$\frac{\mathrm{d}\langle\hat{\alpha}\rangle}{\mathrm{d}t} = \mathrm{Tr}\left[\hat{\alpha}\mathcal{L}\rho\right] = \sum_j A_{1j}\langle\zeta_j\rangle. \tag{5.31}$$

The eigenvalues of $\mathbf{A}$ give the frequencies and linewidths of the normal modes of the Dicke model. The drift matrix we obtain is:

$$\mathbf{A} = \begin{cases} \begin{pmatrix} \kappa + i\omega & 0 & i\lambda & i\lambda \\ 0 & \kappa - i\omega & -i\lambda & -i\lambda \\ i\lambda & i\lambda & i\omega_0 & 0 \\ -i\lambda & -i\lambda & 0 & -i\omega_0 \end{pmatrix} & \text{if } \lambda < \lambda_c \\ \begin{pmatrix} \kappa + i\omega & 0 & i\lambda' & i\lambda' \\ 0 & \kappa - i\omega & -i\lambda' & -i\lambda' \\ i\lambda' & i\lambda' & i\left(\omega_0' + 2\omega_0''\right) & 2i\omega_0'' \\ -i\lambda' & -i\lambda' & -2i\omega_0'' & -i\left(\omega_0 + 2\omega_0''\right) \end{pmatrix} & \text{if } \lambda > \lambda_c. \end{cases} \tag{5.32}$$

The constants ω', ω'' and λ' are defined in (5.11), with λ_c given by (5.24).

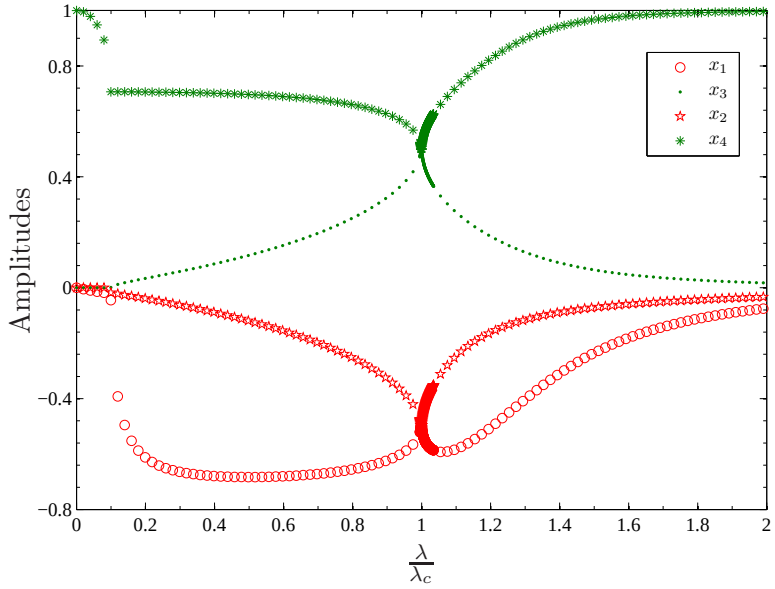

Figure 5.1.: Real part of an eigenvector of $\mathbf{A}$ associated with the atomic eigenvalue ε_+ ($\omega = \omega_0 = 1$ and $\kappa = 0.1$)

The eigenvectors, following the analysis of [48], show how the normal mode operators, $\hat{c}_{1(2)}$ or $\hat{e}_{1(2)}$, are composed in terms of the atomic and photonic operators, $\hat{a}$ and $\hat{b}$. We write the eigenvectors as (x_1, x_2, x_3, x_4), where x_1, x_2 are the amplitudes of the photonic operators $\hat{a}$ and $\hat{a}^\dagger$, and x_3, x_4 the amplitudes for the atomic operators $\hat{b}$ and $\hat{b}^\dagger$. Figure 5.1 shows these amplitudes for one eigenvector, associated with the ε_+ eigenvalue as λ is varied. At zero coupling the eigenvector is composed exclusively of atomic operators; the normal mode operator becomes a linear combination of operators $\hat{a}^\dagger$, $\hat{a}$, $\hat{b}$ and $\hat{b}^\dagger$ as the coupling grows. At critical coupling ($\lambda = \lambda_c$), the nature of the fundamental excitation changes and its symmetry is broken. This can be seen as x_1 and x_3 in Figure 5.1 follow independent curves above λ_c.

The imaginary parts of the eigenvalues of $\mathbf{A}$, for the normal and superradiant phases, are given, when $\kappa = 0$, by equations (5.8) and (5.13) respectively. With dissipation, the eigenvalues acquire a real part corresponding to the damping; the eigenvalues are plotted in Figures 5.2 and 5.3. The imaginary parts of the eigenvalues of $\mathbf{A}$ give the

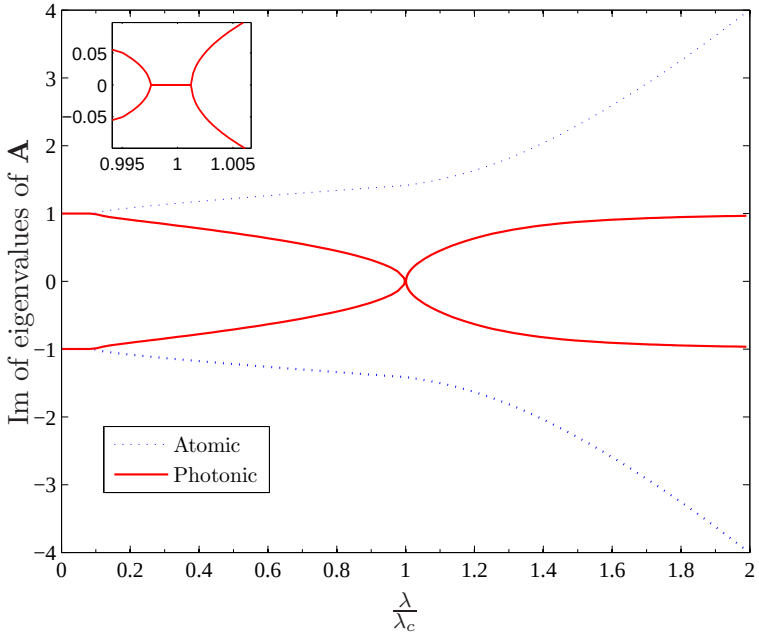

Figure 5.2.: Imaginary parts of the eigenvalues of -**A** for $\omega = \omega_0 = 1$ and $\kappa = 0.1$. The inset shows a magnified view of the region around $\lambda/\lambda_c = 1$

energy of excitation of the normal modes of the system. The atomic branch has a non analyticity at $\lambda = \lambda_c$, corresponding to the break in the symmetry.

The real parts of the eigenvalues correspond to the damping of the normal modes of the system. At λ_c, the real part of one of the photonic eigenvalues vanishes, and the fluctuations of this mode diverge, a characteristic signature of the phase transition.

We define the covariance matrix, $\mathbf{C} = \langle \boldsymbol{\zeta}\boldsymbol{\zeta}^\intercal \rangle$. The steady state covariance matrix can be calculated using

$$\mathbf{A}\mathbf{C} + \mathbf{C}\mathbf{A}^\intercal = -\mathbf{D}. \tag{5.33}$$

This equation can also be obtained from the equations of motion for second order moments of the noise operators, $\langle \hat{a}^\dagger \hat{a} \rangle, \langle \hat{a}^\dagger \hat{b} \rangle, \cdots$, derived from master equation (5.22). Matrix **D** is, by definition, the stationary value of $\langle \dot{\mathbf{C}} \rangle$ [53]. This set of linear equations can be solved; as matrix **C** is symmetric we have to solve for 10 variables instead of 16. The

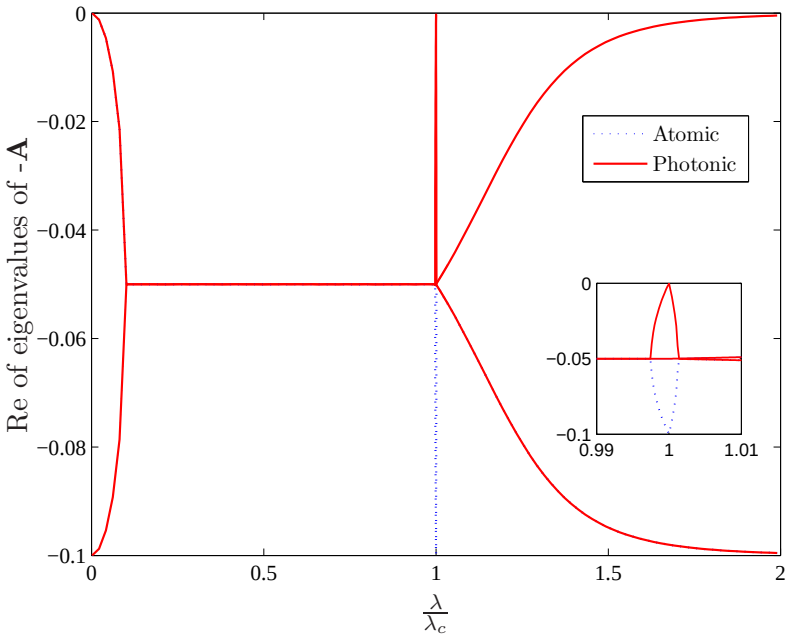

Figure 5.3.: Real part of the eigenvalues of **A**. The inset shows a magnified view of the region around $\lambda/\lambda_c = 1$

diffusion matrix for the Fokker-Planck equation of motion for $\mathcal{P}$ is given by

$$\mathbf{D} = \begin{cases} i\lambda \begin{pmatrix} 0 & 0 & -1 & 0 \\ 0 & 0 & 0 & 1 \\ -1 & 0 & 0 & 0 \\ 0 & 1 & 0 & 0 \end{pmatrix} & \text{if } \lambda < \lambda_c \\ \begin{pmatrix} 0 & 0 & -i\lambda' & 0 \\ 0 & 0 & 0 & i\lambda' \\ -i\lambda' & 0 & -2i\omega_0'' & 0 \\ 0 & i\lambda' & 0 & 2i\omega_0'' \end{pmatrix} & \text{if } \lambda > \lambda_c. \end{cases} \tag{5.34}$$

5.2.3. Results – entanglement, spectra, and squeezing

We present here the solutions for some of the covariances:

$$\langle\alpha^2\rangle = \begin{cases} \frac{(i\kappa+\omega)^2}{8(\mu-1)\omega^2} & \text{if } \lambda < \lambda_c \\ \\ \frac{\mu^2(\kappa-i\omega)^2}{8(\mu^2-1)\omega^2} & \text{if } \lambda > \lambda_c \end{cases} \tag{5.35}$$

$$\langle\alpha\alpha^*\rangle = \begin{cases} \frac{\kappa^2+\omega^2}{8(\mu-1)\omega^2} & \text{if } \lambda < \lambda_c \\ \\ \frac{\mu^2\left(\kappa^2+\omega^2\right)}{8(1-\mu^2)\omega^2} & \text{if } \lambda > \lambda_c \end{cases} \tag{5.36}$$

$$\langle\beta\beta^*\rangle = \begin{cases} \frac{1}{8}\left(\frac{(2\mu-1)\left(\kappa^2+\omega^2\right)}{(\mu-1)\omega\omega_0} + \frac{2\omega_0}{\omega}\right) & \text{if } \lambda < \lambda_c \\ \\ \frac{1}{16}\left(\frac{\mu(3\mu-5)\left(\kappa^2+\omega^2\right)}{(\mu^2-1)\omega\omega_0} + \frac{\left(5+2\mu+\mu^2\right)\omega_0}{(\mu+\mu^2)\omega} - 8\right) & \text{if } \lambda > \lambda_c \end{cases} \tag{5.37}$$

$$\langle\beta\alpha\rangle = \begin{cases} \frac{\sqrt{\kappa^2+\omega^2}}{(i\kappa\mu^4+\omega_0-\mu^4(\omega+\omega_0))} 8\mu^2(-1+\mu^4)\omega_0\omega^{3/2} & \text{if } \lambda < \lambda_c \\ \\ \frac{\sqrt{\left(\kappa^2+\omega^2\right)\omega_0}\left(i\kappa-\omega+2\left(\mu^2-1\right)\omega_0\right)}{8\sqrt{2}\left(\mu^2-1\right)\left(\mu^2+1\right)^{1/2}\omega^{3/2}} & \text{if } \lambda > \lambda_c \end{cases} \tag{5.38}$$

In Figure 5.4, we plot the covariance matrix. The peaks show clearly how the fluctuations diverge at the critical point, related to the vanishing real part of one of the eigenvalues of the drift matrix.

Entanglement

We can use these moments to obtain information about the entanglement between atoms and field. We define the quadrature operators by

$$\hat{X}_{\hat{a}}^{\theta} = \frac{1}{2}\left(\hat{a}\mathrm{e}^{i\theta} + \hat{a}^{\dagger}\mathrm{e}^{-i\theta}\right), \tag{5.39}$$

$$\hat{X}_{\hat{b}}^{\phi} = \frac{1}{2}\left(\hat{b}\mathrm{e}^{i\phi} + \hat{b}^{\dagger}\mathrm{e}^{-i\phi}\right), \tag{5.40}$$

and the EPR operators by

$$\begin{aligned} \hat{u} &= \hat{X}_{\hat{a}}^{\theta} + \hat{X}_{\hat{b}}^{\phi}, \\ \hat{v} &= \hat{X}_{\hat{a}}^{\theta+\frac{\pi}{2}} + \hat{X}_{\hat{b}}^{\phi+\frac{\pi}{2}}. \end{aligned}$$

With these definitions a sufficient condition for entanglement between atoms and field is given by [54, 55]

$$\langle(\Delta\hat{u})^2\rangle + \langle(\Delta\hat{v})^2\rangle < 1.$$

These variances can be calculated from the normally ordered means of the operators $\hat{a}$ and $\hat{b}$. We use the commutation relations to rearrange the product of the operators $\hat{a}\hat{a}^\dagger$ and $\hat{b}\hat{b}^\dagger$ to normal order; this makes the criterion

$$\langle :(\Delta\hat{u})^2: \rangle + \langle :(\Delta\hat{v})^2: \rangle < 0,$$

where the colon denotes normal ordering. The required means are given by the elements of the covariance matrix: $\langle\hat{a}^2\rangle = C_{11}$, $\langle\hat{a}^\dagger\hat{b}^\dagger\rangle = C_{24}$, and so on. For the normal phase, with $\omega_0 = \omega$ and $\phi = 0$, we have

$$\langle(\Delta\hat{u})^2\rangle + \langle(\Delta\hat{v})^2\rangle = \frac{\mu^2(\kappa^2\mu^4+\omega^2) + \sqrt{\kappa^2+\omega^2}(\omega(1-2\mu^4)\cos[\theta] - \kappa\mu^4\sin[\theta])}{4\mu^2(\mu^4-1)\omega^2}. \quad (5.41)$$

The singularities at $\lambda = \lambda_c$ are removed by choosing $\cos[\theta] = \omega/\sqrt{\omega^2+\kappa^2}$ – this is the angle which maximizes the squeezing as seen below. We can see in Figure 5.5 that the entanglement between atoms and photons has its maximum at λ_c.

Power spectrum

We calculate the power spectrum as defined in (5.19). In particular, we can use the solution of (5.30) [53] to derive that

$$\mathbf{S}(\nu) = \frac{1}{2\pi}\left(\mathbf{A} + \nu i\mathbb{1}\right)^{-1}\mathbf{D}\left(\mathbf{A} - \nu i\mathbb{1}\right)^{-1}. \quad (5.42)$$

This generates a 4×4 matrix giving the Fourier transform of all possible correlations $\langle\hat{\alpha}(\tau)\hat{\alpha}\rangle, \langle\hat{\alpha}(\tau)\hat{\alpha}^\dagger\rangle, \langle\hat{\alpha}(\tau)\hat{\beta}\rangle$ and so on. The power spectrum is given by the element $S_{12} = \mathcal{S}(\nu)$. At resonance, $\omega = \omega_0$, it is given by

$$\mathcal{S}(\nu) = \frac{1}{2\pi}\left|\frac{2\sqrt{2\kappa}\omega\lambda^2\tilde{\mu}}{(\kappa - i(\nu-\omega))(\kappa - i(\nu+\omega))\left(\nu^2 - \frac{\omega^2}{\tilde{\mu}^2}\right) + 4\omega^2\lambda^2\tilde{\mu}}\right|^2, \quad (5.43)$$

where $\tilde{\mu} = 1$ if $\lambda < \lambda_c$, and $\tilde{\mu} = \lambda_c^2/\lambda^2$ otherwise.

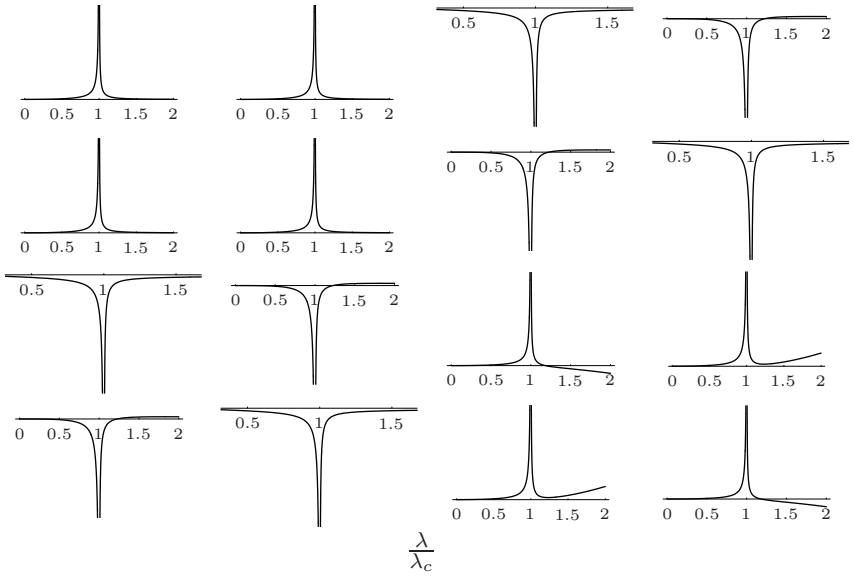

Figure 5.4.: Graphical representation of the covariance matrix vs. λ/λ_c ($\omega = \omega_0 = 1, \kappa = 0.1$). All elements are plotted on the same vertical scale

Spectra are shown in Figure 5.6 for different values of λ. The locations of the peaks are given by the eigenvalues of $\mathbf{A}$; the outer and inner peaks give the field intensities of the atomic and photonic modes in the steady state, respectively. The singularity at $\lambda = \lambda_c$ comes from the amplification of fluctuations associated with the phase transition.

Probe transmission spectrum

We can study the effect of a probe field using linear response theory; we introduce a weak field of frequency ν, and, by treating it as a small perturbation, we are able to calculate the intensity of the transmitted probe field as a function of the frequency (see for example [10]), given by

$$\mathcal{T}(\nu) = \left| \int_0^\infty \mathrm{d}\tau \mathrm{e}^{i\nu\tau} \left\langle \left[\hat{a}(\tau), \hat{a}^\dagger \right] \right\rangle \right|^2 . \tag{5.44}$$

In order to calculate this quantity we would have to compute the moments in anti-normal order; we can not simply use the commutation relations to make the required rearrangements from the normal order expressions, as we are dealing with operators at different times. We derive a Fokker-Planck equation using a $\mathcal{Q}$ phase space representation

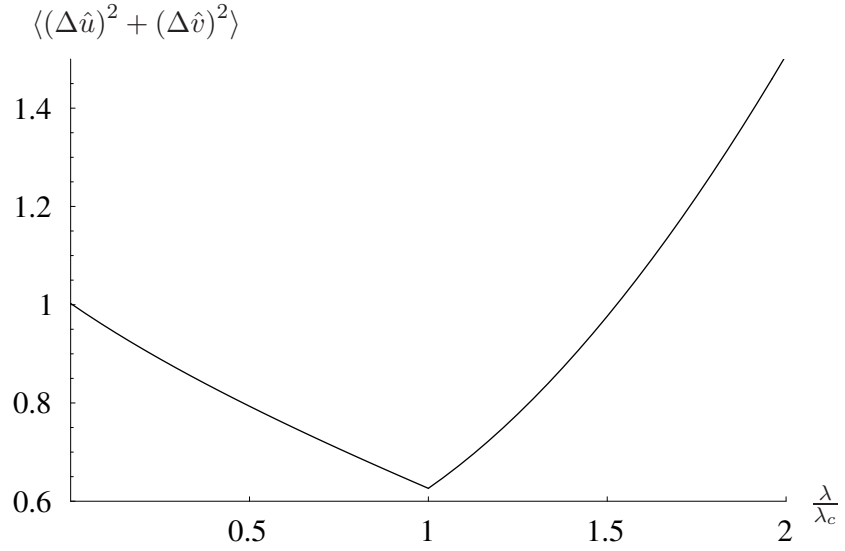

Figure 5.5.: Entanglement vs. λ/λ_c for $\kappa = 0.1$ and $\omega = \omega_0 = 1$.

[29]. This corresponds to perform the same calculations of Section 5.2.2 but using the following (antinormally ordered) characteristic function

$$\chi_{AN} = \mathrm{Tr}\left(\mathrm{e}^{ix\hat{\alpha}}\mathrm{e}^{ix^*\hat{\alpha}^\dagger}\mathrm{e}^{ix^*\hat{\alpha}^\dagger}\mathrm{e}^{ix\hat{\alpha}}\rho\right). \tag{5.45}$$

Following the same steps of Section 5.2.2 we obtain the following drift and diffusion matrices for the antinormally ordered Fokker-Planck equation

$$\mathbf{D}_{AN} = \begin{cases} i\lambda \begin{pmatrix} 0 & \frac{2\kappa}{i\lambda} & 0 & -1 \\ \frac{2\kappa}{i\lambda} & 0 & 1 & 0 \\ 0 & 1 & 0 & 0 \\ -1 & 0 & 0 & 0 \end{pmatrix} & \text{if } \lambda < \lambda_c \\ \begin{pmatrix} 0 & 2\kappa & 0 & -i\lambda' \\ 2\kappa & 0 & i\lambda' & 0 \\ 0 & -i\lambda' & -2i\omega_0'' & 0 \\ -i\lambda' & 0 & 0 & 2i\omega_0'' \end{pmatrix} & \text{if } \lambda > \lambda_c. \end{cases} \tag{5.46}$$

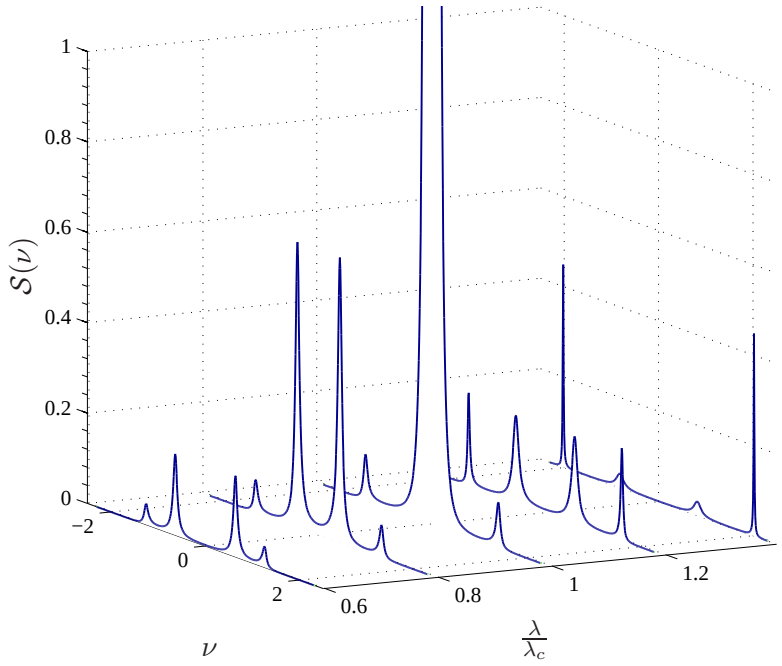

Figure 5.6.: Power spectra

This is consistent with the fact that antinormally-ordered detection schemes introduce vacuum fluctuations – represented by the 2κ terms. Once this is done we can use equations (5.33) and (5.42), and by combining antinormally-ordered and normally-ordered spectra, we can calculate $\mathcal{T}(\nu)$. In Figure 5.7 we plot transmission spectra for different λ. At zero interaction the spectrum simply exhibits the cavity resonance (photonic mode) at $\nu = 1$ (not shown in the Figure). For $\lambda < \lambda_c$, this peak splits as the probe excitation is distributed between the atomic and photonic modes; this last one is favoured, and diverges at λ_c, where the damping of this mode vanishes. Above the critical point the atomic mode is favoured; this is due to the change in the symmetry of the normal modes occurring at λ_c. The small peaks for negative frequencies represent photo absorption occurring in both modes, which is more significant above the critical, favouring the atomic mode at higher coupling.

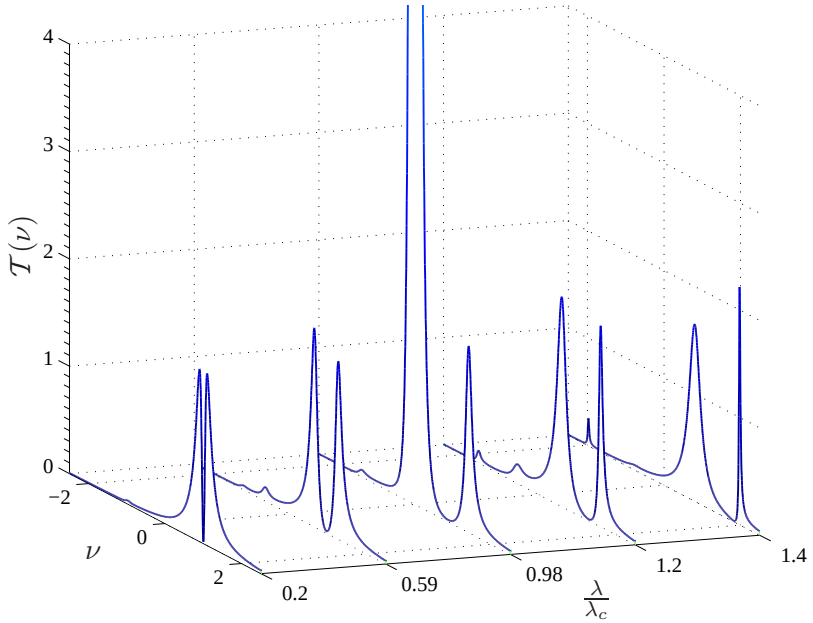

Figure 5.7.: Probe transmission spectra ($\omega = \omega_0 = 1$ and $\kappa = 0.1$)

.

Squeezing spectrum

We can also show that the light emitted by cavity is squeezed by using the definition for the quadrature of the light field, given by (5.39), to define the squeezing spectrum as the Fourier transform of the quadrature correlation function [56],

$$\mathcal{S}_\theta(\nu) = \int_{-\infty}^{\infty} \mathrm{d}\tau \mathrm{e}^{i\nu\tau} \langle : \hat{X}_{\hat{a}}^{\theta}(\tau) \hat{X}_{\hat{a}}^{\theta} : \rangle.$$

We can compute this directly from the spectrum matrix $\mathbf{S}$ by adding the appropriate elements. The normal ordering places the quantum vacuum level at $\mathcal{S}_\theta(\nu) = 0$; negative values indicate squeezing, and $-1/2$ corresponds to perfect squeezing. We can see in the spectra in Figure 5.8 that squeezing appears in the atomic mode in the X quadrature ($\theta = 0$), while it appears in the photonic mode in the Y quadrature ($\theta = \pi/2$). In Figure 5.9 we consider the variance around $\nu = 0$ and plot the smallest value of the squeezing parameter and the angle at which it occurs. We see that close to λ_c the optimal angle

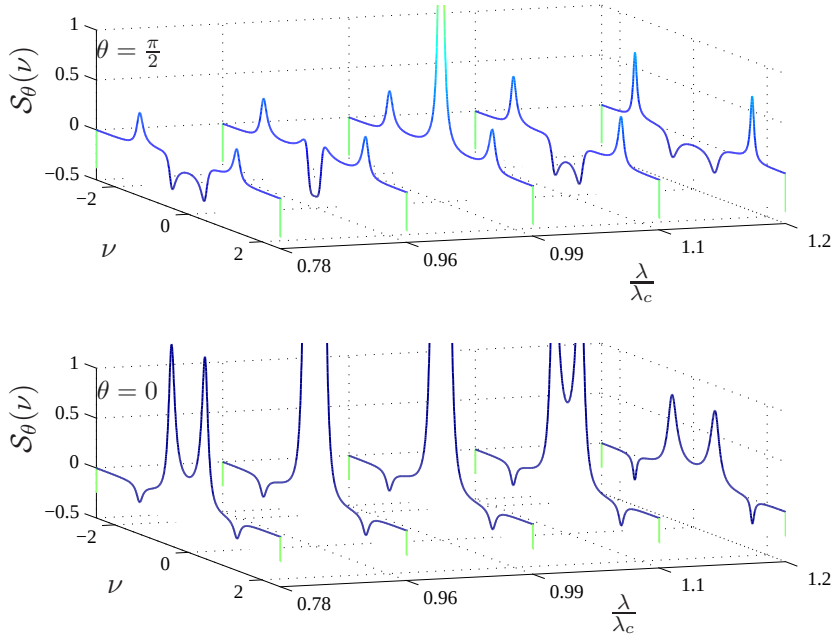

Figure 5.8.: Quadrature noise spectra for $\omega = \omega_0 = 1$ and $\kappa = 0.1$.

becomes close to $\theta_{opt} = \arctan[\kappa/\omega] + \pi/2$ (for the parameters chosen, $\kappa = 0.1$ and $\omega = 1$, $\theta_{opt}/\pi \approx 5.3$ degrees). As we shall see later, this is the angle of rotation of the macroscopic field amplitudes above the phase transition, as seen in the Wigner function, and is related to the maximum entanglement angle derived above.

5.3. Input/output formalism

5.3.1. Introduction

The phase space techniques used here are equivalent to the input/output formalism [57], as used in [58] to obtain most of the results presented here. In this approach the effect of the reservoir is included in the equations of motion as sources of noise: we obtain quantum Langevin equations. This contrasts with the approach of Section 2.2, where the reservoir is traced out and there is no direct reference to the reservoir variables.

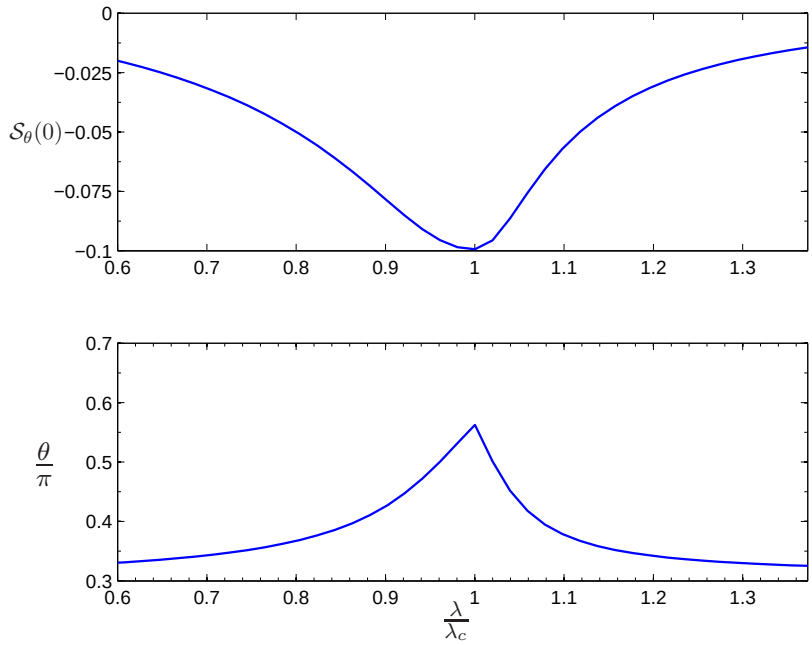

Figure 5.9.: Minimum squeezing around $\mathcal{S}_\theta(0)$ for $\omega = \omega_0$ and $\kappa = 0.1$.

We write the system plus reservoir Hamiltonian of Section 2.2, with the interaction part shown explicitly, as

$$\hat{H} = \hat{H}_{sys} + \hat{H}_{res} + 2\pi \int_{-\infty}^{\infty} \mathrm{d}\nu K(\nu) \left(\hat{a}\hat{\mathcal{B}}^{\dagger}(\nu) - \hat{a}^{\dagger}\hat{\mathcal{B}}(\nu) \right), \tag{5.47}$$

where $\hat{H}_{sys}$ is the system Hamiltonian, in our case the Dicke Hamiltonian, $\hat{H}_{res}$ is the free Hamiltonian for the reservoir, $\hat{\mathcal{B}}$ is the reservoir bosonic annihilation operator, and $\kappa(\nu)$ is the coupling between reservoir and the system, which we consider to be constant over a range around the characteristic system frequency. This corresponds to $K = \sqrt{\kappa/\pi}$, in a derivation similar to what was done in section 2.2 with the cavity cutoff, so the integration limits are extended from $-\infty$ to ∞. The Heisenberg equation of motion for $\hat{\mathcal{B}}$ reads

$$\frac{\mathrm{d}\hat{\mathcal{B}}(\nu)}{\mathrm{d}t} = -i\nu\hat{\mathcal{B}}(\nu) + K\hat{a}. \tag{5.48}$$

This equation can be formally integrated as follows

$$\hat{\mathcal{B}} = \begin{cases} \mathrm{e}^{-i\nu(t-t_0)}\hat{\mathcal{B}}_0 + K\int_{t_0}^{t} \mathrm{e}^{-i\nu(t-t')}\hat{a}(t')\mathrm{d}t' & \text{if } t_0 < t \\ \\ \mathrm{e}^{-i\nu(t-t_1)}\hat{\mathcal{B}}_1 - K\int_{t}^{t_1} \mathrm{e}^{-i\nu(t-t')}\hat{a}(t')\mathrm{d}t' & \text{if } t_1 < t, \end{cases} \tag{5.49}$$

where $\hat{\mathcal{B}}_{1(0)}$ is the value of $\hat{\mathcal{B}}(\nu)$ at $t = t_{1(0)}$. These equations should be used whether we have the initial ($\hat{\mathcal{B}}_0$) or final ($\hat{\mathcal{B}}_1$) condition. The equations of motion for the intracavity field can be obtained in a similar way

$$\frac{\mathrm{d}\hat{a}}{\mathrm{d}t} = -i\left[\hat{a}, \hat{H}_{sys}\right] - K\int_{-\infty}^{\infty} \mathrm{d}\nu\hat{\mathcal{B}}(\nu). \tag{5.50}$$

We use equations (5.49) to write the external field operator $\hat{\mathcal{B}}$ in terms of its initial value $\hat{\mathcal{B}}_0$,

$$\frac{\mathrm{d}\hat{a}}{\mathrm{d}t} = -i\left[\hat{a}, \hat{H}_{sys}\right] - K\int_{-\infty}^{\infty} \mathrm{d}\nu \mathrm{e}^{i\nu(t-t_0)}\hat{\mathcal{B}}_0(\nu) - K^2\int_{-\infty}^{\infty} \mathrm{d}\nu \int_{t_0}^{t} \mathrm{e}^{i\nu(t-t')}\hat{a}(t')\mathrm{d}t. \tag{5.51}$$

The second term is the Fourier transform of the reservoir field operator; they are the source of noise in the Langevin equations, we can define

$$\hat{a}_{in} = -\frac{1}{\sqrt{2\pi}}\int_{-\infty}^{\infty} \mathrm{d}\nu \mathrm{e}^{i\nu(t-t_0)}\hat{\mathcal{B}}_0(\nu). \tag{5.52}$$

The term proportional to K^2 can be integrated using

$$\int_{-\infty}^{\infty} \mathrm{d}\nu \mathrm{e}^{i\nu(t-t')} = 2\pi\delta(t-t') \tag{5.53a}$$

and

$$\int_{t_0}^{t} \hat{a}(t')\delta(t-t')\mathrm{d}t' = \frac{\hat{a}(t)}{2} \quad (t_0 < t < t_1). \tag{5.53b}$$

The equation of motion for the field operators become

$$\frac{\mathrm{d}\hat{a}}{\mathrm{d}t} = -i\left[\hat{a}, \hat{H}_{sys}\right] + \sqrt{2\kappa}\hat{a}_{in} - \kappa\hat{a}(t')\hat{a}. \tag{5.54}$$

We can derive a similar equation in terms of the final conditions of the external field operators $\hat{\mathcal{B}}_1$. We define the output field

$$\hat{a}_{out} = \frac{1}{\sqrt{2\pi}} \int_{-\infty}^{\infty} \mathrm{d}\nu \mathrm{e}^{i\nu(t-t_1)} \hat{\mathcal{B}}_1(\nu). \tag{5.55}$$

The procedure shown above will give the following equation for the intracavity field

$$\frac{\mathrm{d}\hat{a}}{\mathrm{d}t} = -i\left[\hat{a}, \hat{H}_{sys}\right] - \sqrt{2\kappa}\hat{a}_{in} + \kappa\hat{a}(t')\hat{a}. \tag{5.56}$$

We subtract (5.56) from (5.54) to obtain the relationship between the input and output fields

$$\hat{a}_{in} + \hat{a}_{out} = \sqrt{2\kappa}\hat{a} \tag{5.57}$$

The noises $\hat{a}_{in}$ and $\hat{a}_{out}$ are Markovian: $\left[\hat{a}_{in}(t), \hat{a}_{in}^{\dagger}(t')\right] = \delta(t-t')$.

5.3.2. Application to the Dicke Hamiltonian

We can apply this formalism to the Dicke Hamiltonian with the Holstein-Primakoff approach. The Heisenberg equations of motion are linear and we recover all results of Section 5.2. We define the vector $\hat{\mathbf{a}} = (\hat{a}, \hat{a}^{\dagger}, \hat{b}, \hat{b}^{\dagger})^{\intercal}$, and the input noise $\hat{\mathbf{a}}_{in} = (\hat{a}_{in}, \hat{a}_{in}^{\dagger}, 0, 0)^{\intercal}$. We write the equation of motion by noticing the drift matrix of Section 5.2 can be obtained from the Heisenberg equations of motion (minus the damping terms proportional to κ):

$$\frac{\mathrm{d}\hat{\mathbf{a}}}{\mathrm{d}t} = \mathbf{A}\hat{\mathbf{a}}(t) + \sqrt{2\kappa}\hat{\mathbf{a}}_{in}(t). \tag{5.58}$$

In the equation in terms of $\hat{a}_{out}$ we have to account the change in sign of κ, so in this case we have to replace $\kappa \to -\kappa$ and denote the "drift" matrix by $\mathbf{A}_{out}$.

We can calculate the power spectrum by solving this equation in the frequency space. We perform a Fourier transform

$$\hat{\mathbf{a}}(t) = \int_{-\infty}^{\infty} \mathrm{e}^{i\nu(t-t_0)} \hat{\mathbf{a}}(\nu). \tag{5.59}$$

The equation in frequency space becomes

$$i\nu\hat{\mathbf{a}}(\nu) = \mathbf{A}\hat{\mathbf{a}}(\nu) + \sqrt{2\kappa}\hat{\mathbf{a}}_{in}(\nu). \tag{5.60}$$

We use relation (5.57) to eliminate the intracavity field, obtaining

$$\hat{\mathbf{a}}_{out}(\nu) = -\left\{\mathbf{A}_{out} + i\nu\mathbb{1}\right\}\left\{\mathbf{A} + i\nu\mathbb{1}\right\}^{-1}\hat{\mathbf{a}}_{in} \tag{5.61}$$

The input field satisfies $\langle \hat{a}_{in}(\nu)\hat{a}^{\dagger}_{in}(\nu')\rangle = \delta(\nu - \nu')$, with all other input correlation zero. Using this, we are able to derive all results presented so far, e.g., the power spectrum is given by

$$\delta(\nu - \nu')\mathcal{S}_{\theta}(\nu) = \langle \hat{a}^{\dagger}_{out}(\nu)\hat{a}_{out}(\nu')\rangle. \tag{5.62}$$

6. Dicke model in the thermodynamic limit III

In this chapter we extend the treatment of chapter 5 by exploring different representations in phase space. First we introduce an extended version of the Haken representation for two level atoms. The equations in this representation describe the evolution of the fluctuations of the atomic operators without further transformations, as in the Holstein-Primakoff model. Both representations, Haken and Holstein-Primakoff, should return the same results, but it is shown that the former, in its linearized version, fails to conserve the total angular momentum $\mathbf{J}^2$. Despite this disagreement, we find out that the optical spectrum still agrees with those derived with the Holstein-Primakoff formalism, while the spectra involving the atomic variables do not agree. We present also the atomic coherent state representation, which intrinsically conserves angular momentum, so we do expect it to give different results from the ones obtained in Chapter 5. It has the additional advantage, however, of yielding an exact Fokker-Planck equation (in the Positive-P interpretation) for finite number of atoms, albeit with non-linear drift and diffusion coefficients, which we shall use to generate stochastic differential equations.

6.1. Haken representation

Before introducing the Haken representation, we analyse the motion of the mean values of the operators. We assume that the means of operator products can be factorized in the equations of motion for the means, following a similar treatment given by [59]. We obtain the steady states, which are to be used for the linearization, and show that the

semiclassical equations give rise to chaos, as mentioned in Section 4.1, and as discussed by [60].

6.1.1. Semi-classical analysis

We consider, at zero temperature, that the light field is damped through cavity losses κ and the atomic state space (or angular momentum state space) is one with $\ell = N/2$. We use the master equation

$$\frac{\mathrm{d}\rho}{\mathrm{d}t} = \frac{1}{i}\left[\hat{H}, \rho\right] + \kappa\left(2\hat{a}\rho\hat{a}^\dagger - \rho\hat{a}^\dagger\hat{a} - \hat{a}^\dagger\hat{a}\rho\right), \tag{6.1}$$

where the Hamiltonian is given by Eq. (4.36),

$$\hat{H} = \omega\hat{a}^\dagger\hat{a} + \omega_0\hat{J}_z + \frac{\lambda}{\sqrt{N}}\left(\hat{a}^\dagger + \hat{a}\right)\left(\hat{J}_+ + \hat{J}_-\right). \tag{6.2}$$

Further we consider the thermodynamic limit by taking the limit $N \to \infty$. The reasoning is similar to that in Section 2.3, where we consider that, for large system size, the quantum fluctuations will be of the order of the interaction energy of a single quantum. We can write the operators as a mean plus a fluctuation, which, in the limit $N \to \infty$, will be negligible compared to the mean; we follow the standard procedure of Van Kampen, [61], writing for the operators:

$$\hat{a} = N^{1/2}\langle\bar{a}\rangle + \hat{\alpha}, \tag{6.3a}$$

$$\hat{a}^\dagger = N^{1/2}\langle\bar{a}^\dagger\rangle + \hat{\alpha}^*, \tag{6.3b}$$

$$\hat{J}_- = N\langle\bar{J}_-\rangle + N^{1/2}\hat{\nu}, \tag{6.3c}$$

$$\hat{J}_+ = N\langle\bar{J}_+\rangle + N^{1/2}\hat{\nu}^*, \tag{6.3d}$$

$$\hat{J}_z = N\langle\bar{J}_z\rangle + N^{1/2}\hat{\varsigma}, \tag{6.3e}$$

where the bar over the operators indicates $\bar{J}_z = \hat{J}_z/N$, etc, and the Greek letters represent noise operators, with $\langle\hat{\alpha}\rangle = 0$; note that the mean-values-to-noise ratio vanishes as $N \to \infty$. We derive equations for the operator means from (6.1) and substitute equations (6.3) into them. Retaining only terms of order N gives the following factorized

equations of motion:

$$\frac{\mathrm{d}\langle\bar{\hat{a}}\rangle}{\mathrm{d}t} = -\left(i\omega+\kappa\right)\langle\bar{a}\rangle - i\lambda\left(\langle\bar{J}_+\rangle + \langle\bar{J}_-\rangle\right), \tag{6.4a}$$

$$\frac{\mathrm{d}\langle\bar{J}_+\rangle}{\mathrm{d}t} = -i\omega_0\langle\bar{J}_+\rangle + 2i\lambda\left(\langle\bar{a}\rangle + \langle\bar{a}\rangle^*\right)\langle\bar{J}_z\rangle, \tag{6.4b}$$

$$\frac{\mathrm{d}\langle\bar{J}_z\rangle}{\mathrm{d}t} = i\lambda\left(\langle\bar{a}\rangle + \langle\bar{a}\rangle^*\right)\left(\langle\bar{J}_+\rangle - \langle\bar{J}_-\rangle\right). \tag{6.4c}$$

In Fig. 6.1 we present the numerical integration of these equations to illustrate the dynamics of the system without damping ($\kappa = 0$), as studied by Milonni *et. al.* [45]. In Figure 6.1 we show the trajectory of the vector $\langle\hat{\mathbf{J}}\rangle$. Note that its motion is constrained to lie on a sphere – a consequence of the conservation of the total angular momentum. Below

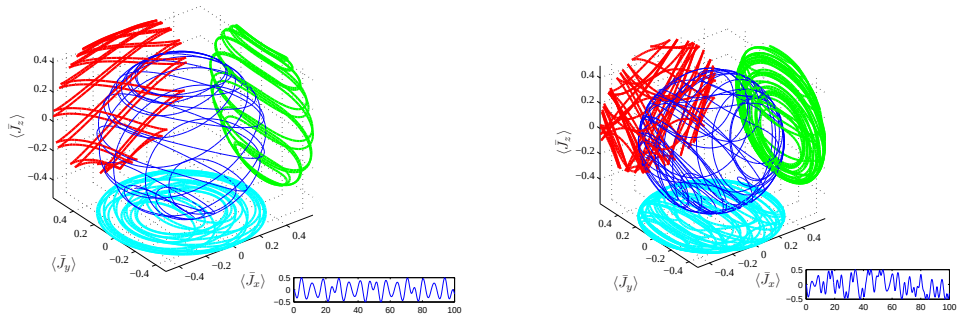

Figure 6.1.: Chaos in the Dicke model: $\lambda = 0.4\lambda_c$ (left), $\lambda = 1.2\lambda_c$ (right)

the critical point the system shows quasi-periodic behaviour, while above it becomes chaotic.

We can use the damped equations of motion to determine the mean values of the operators in the steady state. We define quadratures variables,

$$X = \frac{\langle\bar{a}\rangle + \langle\bar{a}\rangle^*}{2}, \tag{6.5}$$

$$Y = \frac{\langle\bar{a}\rangle - \langle\bar{a}\rangle^*}{2i}, \tag{6.6}$$

$$V = \frac{\langle\bar{J}_+\rangle + \langle\bar{J}_-\rangle}{2}, \tag{6.7}$$

$$W = \frac{\langle\bar{J}_+\rangle - \langle\bar{J}_-\rangle}{2i}, \tag{6.8}$$

and setting

$$Z = \langle \bar{J}_z \rangle \tag{6.9}$$

we have,

$$\dot{X} = \omega Y - \kappa X, \tag{6.10a}$$

$$\dot{Y} = -\omega X - \kappa Y - 2\lambda V, \tag{6.10b}$$

$$\dot{V} = \omega_0 W, \tag{6.10c}$$

$$\dot{W} = -\omega_0 V + 4\lambda X Z, \tag{6.10d}$$

$$\dot{Z} = -4\lambda X W. \tag{6.10e}$$

Then, on setting the time derivatives to zero, the resulting equations are not fully determined; we must also note that

$$\frac{\mathrm{d}}{\mathrm{d}t}\left(V^2 + W^2 + Z^2\right) = 0, \tag{6.11}$$

where the conserved quantity is the total angular momentum. This conservation law is a consequence of the commutation of the Hamiltonian with the operator $\mathbf{J}^2$. In terms of the normalized quantities, V, W, and Z, we have:

$$V^2 + W^2 + Z^2 = \frac{\ell\,(\ell+1)}{N^2} = \frac{1}{4} + \frac{1}{2N} \overset{N\to\infty}{\approx} \frac{1}{4}.$$

From equations (6.10) and the conservation law, there are two sets of steady state solutions: a trivial solution, with $Z = 1/2$ and $\{V, W, X, Y\} = 0$, and a non-trivial one,

$$X_{ss} = \mp\frac{\omega_0}{4\lambda}\sqrt{\frac{\lambda^4}{\lambda_c^4} - 1}, \tag{6.12}$$

$$Y_{ss} = \mp\frac{\kappa\omega_0}{4\lambda\omega}\sqrt{\frac{\lambda^4}{\lambda_c^4} - 1}, \tag{6.13}$$

$$V_{ss} = \pm\frac{1}{2}\sqrt{1 - \frac{\lambda_c^4}{\lambda^4}}, \tag{6.14}$$

$$W_{ss} = 0, \tag{6.15}$$

$$Z_{ss} = -\frac{1}{2}\frac{\lambda_c^2}{\lambda^2}, \tag{6.16}$$

valid only when $\lambda > \lambda_c$, with

$$\lambda_c = \frac{1}{2}\sqrt{\frac{\omega_0}{\omega}(\omega^2 + \kappa^2)}.$$

The trivial solution becomes unstable for $\lambda > \lambda_c$, so the full stable solution is

$$\{X_{ss}, Y_{ss}, V_{ss}, W_{ss}\} = \begin{cases} 0 & \text{if } \lambda < \lambda_c, \\ \text{Eq. (6.12) – (6.15)} & \text{if } \lambda > \lambda_c, \end{cases} \tag{6.17a}$$

$$Z_{ss} = \begin{cases} -\frac{1}{2} & \text{if } \lambda < \lambda_c, \\ \text{Eq. (6.16)} & \text{if } \lambda > \lambda_c \end{cases} \tag{6.17b}$$

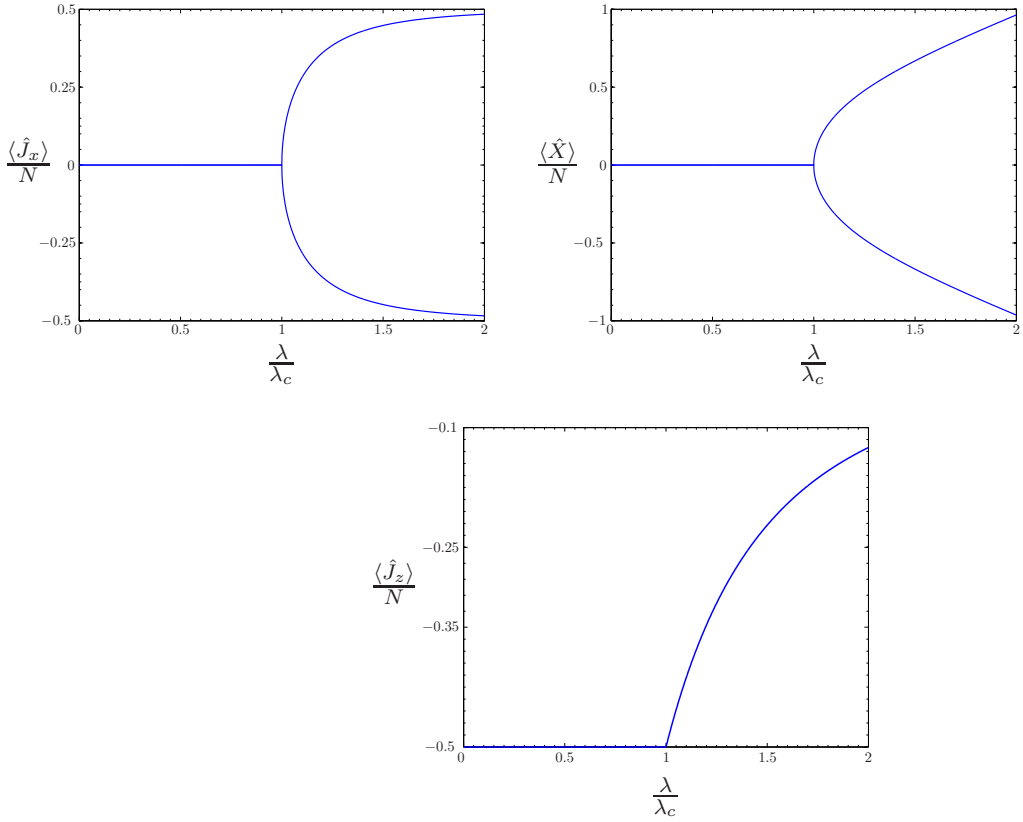

Figure 6.2.: Steady state solutions for $\langle \hat{J}_x \rangle / N$, X_{ss} and $\langle \hat{J}_z \rangle / N$ plotted as function of λ/λ_c for $\omega = \omega_0 = 1$ and $\kappa = 0.1$.

The solutions for X_{ss} and V_{ss} from (6.17) are plotted in figure 6.2. The bifurcation is a consequence of the degeneracy of the eigenstates of the Hamiltonian at $\lambda = \lambda_c$.

6.1.2. Phase space representation

Our aim in this section is to derive an equation of motion for the quasiprobability density, $\mathcal{P}(\alpha, \xi, \mu)$, which yields the correct mean values of atomic operator moments written in normal order, such as,

$$\langle \hat{a}^{\dagger m} \hat{a}^n \hat{J}_+^p \hat{J}_z^q \hat{J}_-^r \rangle = \int \mathcal{P}(\alpha, \xi, \mu) \alpha^{*m} \alpha^n \xi^{*p} \mu^q \xi^r \mathrm{d}^2\alpha \mathrm{d}^2\xi \mathrm{d}\mu. \tag{6.18}$$

We follow the work of Haken [17] by defining, as we did in Section 5.2.2, the characteristic function

$$\chi(x, v, w) = \mathrm{Tr}\left[\mathrm{e}^{ix^*\hat{a}^\dagger} \mathrm{e}^{ix\hat{a}} \mathrm{e}^{iv^*\hat{J}_+} \mathrm{e}^{iw\hat{J}_z} \mathrm{e}^{iv\hat{J}_-} \rho \right]. \tag{6.19}$$

This characteristic function has the same property given by equation (5.26), i.e.,

$$\langle \hat{a}^{\dagger m} \hat{a}^n \hat{J}_+^p \hat{J}_z^q \hat{J}_-^r \rangle = i^{-(m+n+p+q+r)} \frac{\partial^{m+n+p+q+r} \chi(x, v, w)}{\partial x^{*m} \partial x^n \partial v^{*p} \partial w^q \partial v^r} \bigg|_{\{x,v,w\}=0}. \tag{6.20}$$

From now on we omit the operators $\hat{a}^\dagger$ and $\hat{a}$, as they commute with the angular momentum operators and we can add them later. We must find a way of making the connection between Eq. (6.20) and (6.18) to be able to write an equation of motion for $\mathcal{P}$. This is done as follows: we write the equation of motion for χ as

$$\frac{\mathrm{d}\chi}{\mathrm{d}t} = \mathrm{Tr}\left[\mathrm{e}^{iv^*\hat{J}_+} \mathrm{e}^{iw\hat{J}_z} \mathrm{e}^{iv\hat{J}_-} \mathcal{L}\rho \right], \tag{6.21}$$

where the Liouvillian superoperator is given by (6.1), i.e.,

$$\mathcal{L}\rho = \frac{1}{i}\left[\hat{H}, \rho\right] + \kappa\left(2\hat{a}\rho\hat{a}^\dagger - \rho\hat{a}^\dagger\hat{a} - \hat{a}^\dagger\hat{a}\rho\right).$$

By writing out the equations of motion in full, we find the following terms, which are not yet in the prescribed order:

$$\mathrm{e}^{iv^*\hat{J}_+} \mathrm{e}^{iw\hat{J}_z} \mathrm{e}^{iv\hat{J}_-} \hat{J}_+ \rho,$$
$$\mathrm{e}^{iv^*\hat{J}_+} \mathrm{e}^{iw\hat{J}_z} \mathrm{e}^{iv\hat{J}_-} \hat{J}_z \rho,$$
$$\mathrm{e}^{iv^*\hat{J}_+} \mathrm{e}^{iw\hat{J}_z} \mathrm{e}^{iv\hat{J}_-} \rho \hat{J}_-,$$
$$\mathrm{e}^{iv^*\hat{J}_+} \mathrm{e}^{iw\hat{J}_z} \mathrm{e}^{iv\hat{J}_-} \rho \hat{J}_z.$$

We rearrange them using the relations

$$\mathrm{e}^{iv\hat{J}_-}\hat{J}_+ = \left\{\hat{J}_+ - 2iv\hat{J}_z - (iv)^2\hat{J}_-\right\}\mathrm{e}^{iv\hat{J}_-}, \tag{6.22}$$

$$\mathrm{e}^{iv\hat{J}_-}\hat{J}_z = \left\{\hat{J}_z + iv\hat{J}_-\right\}\mathrm{e}^{iv\hat{J}_-}, \tag{6.23}$$

$$\mathrm{e}^{iw\hat{J}_z}\hat{J}_+ = \hat{J}_+\mathrm{e}^{iw}. \tag{6.24}$$

Using the above equations plus the property given by (6.19), on expanding the right hand side of (6.21), we find

$$\begin{aligned}
\hat{J}_+\rho &\leftrightarrow \left\{\mathrm{e}^{iw}\frac{\partial}{\partial(iv^*)} - 2(iv)\frac{\partial}{\partial(iw)} - (iv)^2\frac{\partial}{\partial(iv)}\right\}\chi,\\
\hat{J}_z\rho &\leftrightarrow \left\{\frac{\partial}{\partial(iw)} + (iv)\frac{\partial}{\partial(iv)}\right\}\chi,\\
\hat{J}_-\rho &\leftrightarrow \frac{\partial}{\partial(iv)}\chi,\\
\rho\hat{J}_+ &\leftrightarrow \frac{\partial}{\partial(iv^*)}\chi,\\
\rho\hat{J}_z &\leftrightarrow \left\{\frac{\partial}{\partial(iw)} + (iv^*)\frac{\partial}{\partial(iv^*)}\right\}\chi,\\
\rho\hat{J}_- &\leftrightarrow \left\{\mathrm{e}^{iw}\frac{\partial}{\partial(iv)} - 2(iv^*)\frac{\partial}{\partial(iw)} - (iv^*)^2\frac{\partial}{\partial(iv^*)}\right\}\chi.
\end{aligned}$$

We then use similar reasoning to write the following relations for the photonic operators:

$$\hat{a}^\dagger\rho \leftrightarrow \left\{ix + \frac{\partial}{\partial(ix^*)}\right\}\chi, \tag{6.25a}$$

$$\hat{a}\rho \leftrightarrow \left\{\frac{\partial}{\partial ix}\right\}\chi, \tag{6.25b}$$

$$\rho\hat{a}^\dagger \leftrightarrow \left\{\frac{\partial}{\partial ix^*}\right\}\chi, \tag{6.25c}$$

$$\rho\hat{a} \leftrightarrow \left\{ix^* + \frac{\partial}{\partial(ix)}\right\}\chi. \tag{6.25d}$$

We now assume that χ has the following expansion on $\mathcal{P}$

$$\chi(x,v,w) = \int \mathrm{e}^{ix\alpha}\mathrm{e}^{ix^*\alpha^*}\mathrm{e}^{iv\xi}\mathrm{e}^{iv^*\xi^*}\mathrm{e}^{iw\mu}\mathcal{P}(\alpha,\xi,\mu)\mathrm{d}^2x\mathrm{d}^2v\mathrm{d}w, \tag{6.26}$$

and by performing an integration by parts transfer the effects of the operators to $\mathcal{P}$, as for example

$$\begin{aligned} ix\chi &\leftrightarrow -\frac{\partial}{\partial\alpha}\mathcal{P}, \\ \frac{\partial}{\partial ix}\chi &\leftrightarrow \alpha\mathcal{P}, \\ &\vdots \end{aligned}$$

When carrying out the integration by parts we assume that the surface terms of the integral vanish. We also have to assume the existence of (6.26); if starred variables are complex conjugates of each other this means we assume the existence of the Fourier transform of χ. We shall see that these equations give non-positive definite diffusion matrices, a problem we overcome by interpreting this representation as a *positive*-P representation [19], where the variables α and α^*, for example, are independent complex variables instead of conjugates. Using these assumptions we can write the final relations between the Haken representation and the operators as:

$$\hat{J}_+\rho \leftrightarrow \left\{ \mathrm{e}^{-\frac{\partial}{\partial\mu}}\xi^* + 2\mu\frac{\partial}{\partial\xi} - \frac{\partial^2}{\partial\xi^2}\xi \right\}\mathcal{P}, \tag{6.27a}$$

$$\hat{J}_z\rho \leftrightarrow \left\{ \mu - \frac{\partial}{\partial\xi}\xi \right\}\mathcal{P}, \tag{6.27b}$$

$$\hat{J}_-\rho \leftrightarrow \xi\mathcal{P}, \tag{6.27c}$$

$$\rho\hat{J}_+ \leftrightarrow \xi^*\mathcal{P}, \tag{6.27d}$$

$$\rho\hat{J}_z \leftrightarrow \left\{ \mu - \frac{\partial}{\partial\xi^*}\xi^* \right\}\mathcal{P}, \tag{6.27e}$$

$$\rho\hat{J}_- \leftrightarrow \left\{ \mathrm{e}^{-\frac{\partial}{\partial\mu}}\xi + 2\mu\frac{\partial}{\partial\xi^*} - \frac{\partial^2}{\partial\xi^{*2}}\xi^* \right\}\mathcal{P}, \tag{6.27f}$$

while for the photonic operators we have that

$$\hat{a}^\dagger\rho \leftrightarrow \left\{ \alpha^* - \frac{\partial}{\partial\alpha} \right\}\mathcal{P}, \tag{6.28a}$$

$$\hat{a}\rho \leftrightarrow \alpha\mathcal{P}, \tag{6.28b}$$

$$\rho\hat{a}^\dagger \leftrightarrow \alpha^*\mathcal{P}, \tag{6.28c}$$

$$\rho\hat{a} \leftrightarrow \left\{ \alpha - \frac{\partial}{\partial\alpha^*} \right\}\mathcal{P}. \tag{6.28d}$$

With these correspondence relations we can readily arrive at the equation of motion for $\mathcal{P}$,

$$\begin{aligned}\frac{\partial \mathcal{P}}{\partial t} =& -i\omega\left(\frac{\partial}{\partial\alpha^*}\alpha^* - \frac{\partial}{\partial\alpha}\alpha\right)\mathcal{P} - i\omega_0\left(\frac{\partial}{\partial\xi^*}\xi^* - \frac{\partial}{\partial\xi}\xi\right)\mathcal{P} \\ &- i\frac{\lambda}{\sqrt{N}}\Bigg\{[\alpha+\alpha^*]\left[(\xi-\xi^*)\left(1-e^{-\frac{\partial}{\partial\mu}}\right)+2\mu\left(\frac{\partial}{\partial\xi}-\frac{\partial}{\partial\xi^*}\right)-\left(\frac{\partial^2}{\partial\xi^2}\xi-\frac{\partial^2}{\partial\xi^{*2}}\xi^*\right)\right] \\ &+\frac{\partial}{\partial\alpha^*}\left(\xi^*+e^{-\frac{\partial}{\partial\mu}}\xi+2\mu\frac{\partial}{\partial\xi^*}-\frac{\partial^2}{\partial\xi^{*2}}\xi^*\right)-\frac{\partial}{\partial\alpha}\left(\xi+e^{-\frac{\partial}{\partial\mu}}\xi^*+2\mu\frac{\partial}{\partial\xi}-\frac{\partial^2}{\partial\xi^2}\xi\right)\Bigg\}\mathcal{P}.\end{aligned} \tag{6.29}$$

Note that the terms $\mathrm{e}^{\frac{\partial}{\partial\mu}}$ are displacement operators, i.e., $\mathrm{e}^{-\frac{\partial}{\partial\mu}}\mathcal{P}(\mu) = \mathcal{P}(\mu+1)$. Therefore, for a finite number of atoms, $\ell = N/2$, Eq. (6.29) corresponds to a set of $N+1$ coupled partial differential equations, indexed as $\mathcal{P}(\mu=-N/2),\cdots,\mathcal{P}(\mu=N/2)$. We also note the existence of third order derivatives, $\frac{\partial^3}{\partial\alpha\partial\xi^2}$, and non-linearities, so we cannot expect to solve this system of equations without some approximation method. Our choice is to linearize the variables α,ξ and μ about the steady state, in order to obtain a Fokker-Planck equation that is valid in the thermodynamic limit (see Chapter 5). First, we expand the operator $\mathrm{e}^{\frac{\partial}{\partial\mu}}$ to second order:

$$e^{-\frac{\partial}{\partial\mu}} = 1 - \frac{\partial}{\partial\mu} + \frac{1}{2}\frac{\partial^2}{\partial\mu^2}.$$

This approximation corresponds to assuming μ very large, so a Taylor expansion can be made. The linearization also makes third order derivatives of order N^{-1}, so we omit these from now on and write the Fokker-Planck equation in the Haken representation as

$$\frac{\partial\mathcal{P}}{\partial t} = \frac{\partial}{\partial\boldsymbol{\zeta}^\intercal}\mathcal{A}\mathcal{P} + \frac{1}{2}\frac{\partial}{\partial\boldsymbol{\zeta}^\intercal}\mathbf{D}\frac{\partial}{\partial\boldsymbol{\zeta}}\mathcal{P},$$

where

$$\boldsymbol{\zeta} = (\alpha,\alpha^*,\xi,\xi^*,\mu)^\intercal,$$

and

$$\frac{\partial}{\partial\boldsymbol{\zeta}} = (\partial_\alpha,\partial_{\alpha^*},\frac{1}{\sqrt{N}}\frac{\partial}{\partial\xi},\frac{1}{\sqrt{N}}\frac{\partial}{\partial\xi^*},\frac{1}{\sqrt{N}}\frac{\partial}{\partial\mu})^\intercal,$$

but $\mathcal{A}$, in this case, is a column vector given by

$$\mathcal{A}(\boldsymbol{\zeta}) = \begin{pmatrix} (i\omega+\kappa)\alpha + i\lambda N^{-1/2}(\xi+\xi^*) \\ (-i\omega+\kappa)\alpha^* - i\lambda N^{-1/2}(\xi+\xi^*) \\ i\omega_0\xi - 2i\lambda N^{-1/2}(\alpha+\alpha^*)\,\mu \\ -i\omega_0\xi^* + 2i\lambda N^{-1/2}(\alpha+\alpha^*)\,\mu \\ i\lambda N^{-1/2}(\xi^*-\xi)(\alpha+\alpha^*) \end{pmatrix}, \tag{6.30}$$

and $\mathbf{D}$ is a 5×5 matrix given by

$$\mathbf{D}(\boldsymbol{\zeta}) = \frac{i}{\sqrt{N}} \begin{pmatrix} 0 & 0 & 2\mu & 0 & -\xi^* \\ 0 & 0 & 0 & -2\mu & \xi \\ 2\mu & 0 & 2\xi(\alpha+\alpha^*) & 0 & 0 \\ 0 & -2\mu & 0 & -2\xi^*(\alpha+\alpha^*) & 0 \\ -\xi^* & \xi & 0 & 0 & 2(\xi-\xi^*)(\alpha+\alpha^*) \end{pmatrix}. \tag{6.31}$$

We linearize this equation around the mean values:

$$\boldsymbol{\zeta}_0 = (N^{1/2}\langle\bar{a}\rangle, N^{1/2}\langle\bar{a}^\dagger\rangle, N\langle\bar{J}_+\rangle, N\langle\bar{J}_-\rangle, N\langle\bar{J}_z\rangle)^\intercal.$$

Thus, expanding the matrices $\mathcal{A}$ and $\mathbf{D}$ in a Taylor series, and keeping only terms of order $N^{1/2}$ and N^0,

$$\frac{\partial\mathcal{P}}{\partial\boldsymbol{\zeta}^\intercal}\frac{\mathrm{d}\boldsymbol{\zeta_0}}{\mathrm{d}t} + \frac{\partial\mathcal{P}}{\partial t} = \frac{\partial}{\partial\boldsymbol{\zeta}^\intercal}\left(\mathcal{A}(\boldsymbol{\zeta}_0) + \mathbf{A}\right)\boldsymbol{\zeta}\mathcal{P} + \frac{1}{2}\frac{\partial}{\partial\boldsymbol{\zeta}}\mathbf{D}(\boldsymbol{\zeta_0})\frac{\partial}{\partial\boldsymbol{\zeta}^\intercal}\mathcal{P} \tag{6.32}$$

where $\mathbf{A}$ is the constant drift matrix given by the derivative of $\mathcal{A}$ evaluated at $\boldsymbol{\zeta}_0$ as

$$\mathbf{A} = \frac{\partial}{\partial\boldsymbol{\zeta}^\intercal}\mathcal{A}^\intercal(\boldsymbol{\zeta}_0). \tag{6.33}$$

Clearly we have terms of order $N^{1/2}$, which give the evolution of the means, and of order N^0 which define fluctuations around the means. In order to identify the role played by each term, we redefine the vectors $\boldsymbol{\zeta}$, $\boldsymbol{\zeta}_0$ and $\partial_{\boldsymbol{\zeta}}$:

$$\boldsymbol{\zeta} \to (\alpha, \alpha^*, \xi, \xi^*, \mu)^\intercal, \tag{6.34}$$

$$\boldsymbol{\zeta}_0 \to (\langle\bar{a}\rangle, \langle\bar{a}^\dagger\rangle, \langle\bar{J}_+\rangle, \langle\bar{J}_-\rangle, \langle\bar{J}_z\rangle)^\intercal, \tag{6.35}$$

$$\frac{\partial}{\partial\boldsymbol{\zeta}} \to (\partial_\alpha, \partial_{\alpha^*}, \frac{\partial}{\partial\xi}, \frac{\partial}{\partial\xi^*}, \frac{\partial}{\partial\mu})^\intercal. \tag{6.36}$$

The equations of motion become

$$\frac{\partial \mathcal{P}}{\partial t} = N^{1/2}\left(\frac{\partial}{\partial \boldsymbol{\zeta}^{\intercal}}\mathcal{A}(\boldsymbol{\zeta}_0)\mathcal{P} - \frac{\partial \mathcal{P}}{\partial \boldsymbol{\zeta}^{\intercal}}\frac{\mathrm{d}\boldsymbol{\zeta_0}}{\mathrm{d}t}\right) + \frac{\partial}{\partial \boldsymbol{\zeta}^{\intercal}}\left(\frac{\partial \mathcal{A}}{\partial \boldsymbol{\zeta}^{\intercal}}\right)_{\boldsymbol{\zeta}=\boldsymbol{\zeta}_0}\boldsymbol{\zeta}\mathcal{P} + \frac{1}{2}\frac{\partial^2 \mathbf{D}(\boldsymbol{\zeta}_0)\mathcal{P}}{\partial \boldsymbol{\zeta}^{\intercal}\partial \boldsymbol{\zeta}}. \tag{6.37}$$

We set the terms multiplied by $N^{1/2}$ to zero, this gives equations of motion for the means, corresponding to equation (6.4), with solutions given by (6.16). The terms of order N^0 give the linear Fokker-Planck equation for the fluctuations about the means, with drift and diffusion matrices:

$$\left(\frac{\partial \mathcal{A}}{\partial \boldsymbol{\zeta}^{\intercal}}\right)_{\boldsymbol{\zeta}=\boldsymbol{\zeta}_0} = \mathbf{A} = \begin{pmatrix} i\omega+\kappa & 0 & i\lambda & i\lambda & 0 \\ 0 & -i\omega+\kappa & -i\lambda & -i\lambda & 0 \\ -2i\lambda\langle \bar{J}_z\rangle & -2i\lambda\langle \bar{J}_z\rangle & i\omega_0 & 0 & -2i\lambda\langle \bar{a}+\bar{a}^{\dagger}\rangle \\ 2i\lambda\langle J_z\rangle & 2i\lambda\langle \bar{J}_z\rangle & 0 & -i\omega_0 & 2i\lambda\langle \bar{a}+\bar{a}^{\dagger}\rangle \\ 0 & 0 & -i\lambda\langle \bar{a}+\bar{a}^{\dagger}\rangle & i\lambda\langle \bar{a}+\bar{a}^{\dagger}\rangle & 0 \end{pmatrix}, \tag{6.38}$$

$$\mathbf{D}(\boldsymbol{\zeta}_0) = i\lambda \begin{pmatrix} 0 & 0 & 2\langle \bar{J}_z\rangle & 0 & -\langle \bar{J}_+\rangle \\ 0 & 0 & 0 & -2\langle \bar{J}_z\rangle & \langle \bar{J}_-\rangle \\ 2\langle \bar{J}_z\rangle & 0 & 2\langle \bar{a}+\bar{a}^{\dagger}\rangle\langle \bar{J}_-\rangle & 0 & 0 \\ 0 & -2\langle \bar{J}_z\rangle & 0 & -2\langle \bar{a}+\bar{a}^{\dagger}\rangle\langle \bar{J}_+\rangle & 0 \\ -\langle J_+\rangle & \langle \bar{J}_-\rangle & 0 & 0 & 0 \end{pmatrix}. \tag{6.39}$$

6.2. Haken vs. Holstein-Primakoff representation

6.2.1. Drift Matrix

With the drift and diffusion matrices one might follow the procedure taken in section 5.2.3 and calculate spectra, entanglement and covariances. Such a procedure would reproduce the results of that section up to the limitations of the Haken representation, as we discuss now. In this section we concentrate on the differences between the Holstein-Primakoff and Haken representation, and show where and how they disagree. We make the distinction between the drift and diffusion matrices in each representation by including the superscript ^{HP}, for Holstein-Primakoff, and ^{Ha}, for the Haken representation.

The drift matrix in the Haken representation has one eigenvalue equal to zero; this accounts for a conserved quantity of motion. It can be said, alternatively, that the Haken representation has two linearly dependent eigenvectors that can can be used to express one of the Haken phase-space variables in terms of the remaining four; in short, all the information conveyed in the (5-dimensional) Haken representation is expressed in four variables, corresponding to the Holstein-Primakoff representation. To demonstrate this result we write the linearised expansion of the angular momentum operators in both representations and write down the expressions that map Haken phase-space variables into Holstein-Primakoff phase-space variables, and use such expressions to transform the Haken representation drift matrix. Assuming that $\langle\bar{b}\rangle$ is real we have (from (5.1):

$$\hat{J}_+ \to \xi^* = N\langle\bar{b}\rangle\sqrt{1-\langle\bar{b}\rangle^2} + \frac{N^{1/2}}{2\sqrt{1-\langle\bar{b}\rangle^2}}\left(\left(2-3\langle\bar{b}\rangle^2\right)\beta^* - \langle\bar{b}\rangle^2\beta\right), \quad (6.40a)$$

$$\hat{J}_- \to \xi = N\langle\bar{b}\rangle\sqrt{1-\langle\bar{b}\rangle^2} + \frac{N^{1/2}}{2\sqrt{1-\langle\bar{b}\rangle^2}}\left(\left(2-3\langle\bar{b}\rangle^2\right)\beta - \langle\bar{b}\rangle^2\beta^*\right), \quad (6.40b)$$

$$\hat{J}_z \to \mu = N\left(\langle\bar{b}\rangle^2 - \frac{1}{2}\right) + N^{1/2}\langle\bar{b}\rangle\left(\beta+\beta^*\right), \quad (6.40c)$$

where the operators are expanded as $\hat{b} = N^{1/2}\langle\bar{b}\rangle + \beta$, which supposes we are writing the equations in a P-representation. We compare Eqs. (6.40) with the expansions of the Haken phase-space variables (6.3). By equating mean values, setting the fluctuations to zero, $\langle\beta\rangle = 0$, and using the solutions for $\langle\hat{J}_+\rangle$ and $\langle\hat{J}_z\rangle$ in the steady state of the superradiant phase, we have that

$$\langle b\rangle = \frac{1}{\sqrt{2}}\sqrt{1-\langle\mu\rangle}. \quad (6.41)$$

The expression for the noise becomes

$$\mu = \frac{1}{\sqrt{2}}\sqrt{1-\langle\mu\rangle}\left(\beta+\beta^*\right), \quad (6.42a)$$

$$\xi = \frac{\sqrt{2}}{4\sqrt{1+\langle\mu\rangle}}\left((1+3\langle\mu\rangle)\beta + (\langle\mu\rangle-1)\beta^*\right). \quad (6.42b)$$

We check that these transformations lead $\mathbf{A}^K$ to $\mathbf{A}^H$ by writing the deterministic part

of the equations of motion for the fluctuations in the Haken representation:

$$\dot{\alpha} = -(i\omega + \kappa)\alpha + i\lambda\,(\xi + \xi^*) \tag{6.43a}$$

$$\dot{\xi} = -i\omega_0\xi + 2i\lambda\langle\hat{J}_z\rangle(\alpha + \alpha^*) + 2i\lambda\mu\langle\bar{a} + \bar{a}^\dagger\rangle \tag{6.43b}$$

$$\dot{\mu} = i\lambda(\xi - \xi^*)\langle\bar{a} + \bar{a}^\dagger\rangle \tag{6.43c}$$

The means in the steady state are given by (from Eqs. (6.12) and (6.16))

$$\langle\bar{a} + \bar{a}^\dagger\rangle = \frac{\omega_0}{2\lambda\mu}\sqrt{1-\mu^2}, \tag{6.44}$$

$$\langle\bar{J}_z\rangle = -\frac{\mu}{2}. \tag{6.45}$$

The transformations given by (6.42) are easily summarized in the matrix

$$\mathbf{S} = \begin{pmatrix} 1 & 0 & 0 & 0 & 0 \\ 0 & 1 & 0 & 0 & 0 \\ 0 & 0 & \frac{\sqrt{2}(1+3\mu)}{4\sqrt{1+\mu}} & \frac{\sqrt{2}(\mu-1)}{4\sqrt{1+\mu}} & 0 \\ 0 & 0 & \frac{\sqrt{2}(\mu-1)}{4\sqrt{1+\mu}} & \frac{\sqrt{2}(1+3\mu)}{4\sqrt{1+\mu}} & 0 \\ 0 & 0 & \sqrt{\frac{1-\mu}{2}} & \sqrt{\frac{1-\mu}{2}} & 0 \end{pmatrix}. \tag{6.46}$$

Such that $\mathbf{S}\boldsymbol{\zeta}^{HP} = \boldsymbol{\zeta}^{Ha}$. We note the transformations between the variables cannot be inverted as they are overdetermined – $\mathbf{S}$ has no inverse, but we can define the inverse within the subspaces $\{\xi, \xi^*\} \leftrightarrow \{\beta, \beta^*\}$, which we denote by $\mathbf{s}$:

$$\mathbf{s} = \begin{pmatrix} 1 & 0 & 0 & 0 & 0 \\ 0 & 1 & 0 & 0 & 0 \\ 0 & 0 & \frac{\sqrt{2}(1+3\mu)}{4\mu\sqrt{1+\mu}} & \frac{\sqrt{2}(1-\mu)}{4\mu\sqrt{1+\mu}} & 0 \\ 0 & 0 & \frac{\sqrt{2}(1-\mu)}{4\mu\sqrt{1+\mu}} & \frac{\sqrt{2}(1+3\mu)}{4\mu\sqrt{1+\mu}} & 0 \\ 0 & 0 & 0 & 0 & 0 \end{pmatrix}. \tag{6.47}$$

The 5^{th} column and row are zero, as the equations for $\dot{\mu}$ are of no use; relation (6.42a) is already built-into the Holstein-Primakoff representation. The drift matrix, in the transformed variables, is given by

$$\mathbf{sA}^{Ha}\mathbf{S} = \begin{pmatrix} & & & & 0 \\ & & \mathbf{A}^{HP} & & 0 \\ & & & & 0 \\ 0 & 0 & 0 & 0 & 0 \end{pmatrix}, \tag{6.48}$$

where $\mathbf{A}^{HP}$ is the Holstein-Primakoff drift matrix given by (5.32). This shows the equivalence between drift matrices within the 4×4 subspace in the Haken representation.

6.2.2. Covariance matrix and spectra

With the drift and diffusion matrices we are able to use formula (5.42) to derive the spectra of the fluctuations, and also to use (5.33) to calculate the covariance matrix. To compare the results between the two representations we need to translate the HP variables into Haken variables. We use the expressions (6.42) and the fact that the spectrum matrix

$$\mathbf{S}(\nu) = \frac{1}{2\pi}\left(\mathbf{A} + i\nu\mathbb{1}\right)\mathbf{D}\left(\mathbf{A} - i\nu\mathbb{1}\right), \tag{6.49}$$

is the Fourier transform of the correlations $\langle\xi(\tau)\xi\rangle$ etc. We calculate the correlations in one representation and apply the transformation rules, as for example, noticing that

$$\xi + \xi^* = \frac{\mu\sqrt{2}}{\sqrt{1+\mu}}(\beta + \beta^*), \tag{6.50}$$

we have

$$(\xi + \xi^*)(\xi(\tau) + \xi^*(\tau)) = \frac{2\mu^2}{1+\mu}(\beta + \beta^*)(\beta(\tau) + \beta^*(\tau)); \tag{6.51}$$

by performing a Fourier transform in the correlation function defined above we have that the spectra

$$S_{33} + S_{44} + 2S_{34}, \tag{6.52}$$

in each representation, are proportional to one another. This quantity is plotted in Figure 6.3, where we clearly see that they fail to agree for $\lambda > \lambda_c$. This problem does not occur, however, in the field subspace $\{\mathcal{S}_{11}, \mathcal{S}_{22}, \mathcal{S}_{12}\}$, as we will show explicitly below.

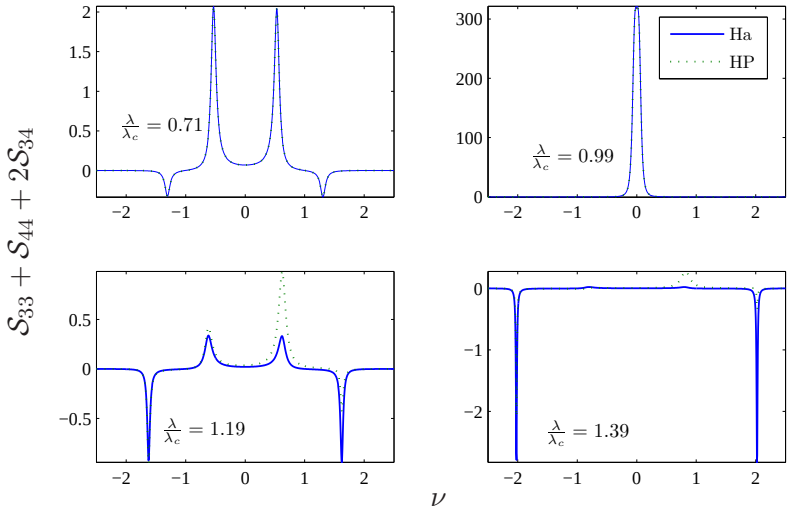

Figure 6.3.: Holstein Primakoff compared with Haken spectra for $\omega = \omega_0$ and $\kappa = 0.1$.

To demonstrate the origin of this problem, we must calculate the second order correlations. We calculate $\langle \mathbf{J}^2 \rangle$ in normal order as $\langle \hat{J}_+ \hat{J}_- + \hat{J}_z^2 - \hat{J}_z \rangle$, using the stochastic differential equations of motion for the linearized set of variables in the Haken representation. We need the matrix $\mathbf{B}$, such that $\mathbf{B}\mathbf{B}^\intercal = \mathbf{D}$, where $\mathbf{D}$ is the diffusion matrix (6.38). We can derive such a matrix by writing the quadractic form $\mathbf{x}^\intercal \mathbf{D} \mathbf{x}$, where

$\mathbf{x} = (x_1, x_2, x_3, x_4, x_5)^\intercal$, as sum of squares. With this procedure we obtain

$$\mathbf{B}^\intercal = \begin{pmatrix} i\frac{\sqrt{2}\langle \bar{J}_z\rangle}{\sqrt{\langle \bar{J}_+\rangle\langle 2\bar{a}\rangle}} & 0 & 0 & 0 & i\frac{\sqrt{\langle \bar{J}_+\rangle\langle 2\bar{a}\rangle}}{\sqrt{2}\langle \bar{J}_z\rangle}\langle \bar{J}_+\rangle \\ 0 & \frac{\sqrt{2}\langle \bar{J}_z\rangle}{\sqrt{\langle \bar{J}_+\rangle\langle 2\bar{a}\rangle}} & 0 & 0 & \frac{\sqrt{\langle \bar{J}_+\rangle\langle 2\bar{a}\rangle}}{\sqrt{2}\langle \bar{J}_z\rangle}\langle \bar{J}_+\rangle \\ 0 & \frac{i2\langle \bar{J}_z\rangle}{\sqrt{2\langle \bar{J}_+\rangle\langle 2\bar{a}\rangle}} & 0 & i\sqrt{2\langle \bar{J}_+\rangle\langle 2\bar{a}\rangle} & 0 \\ \frac{2\langle \bar{J}_z\rangle}{\sqrt{2\langle \bar{J}_+\rangle\langle 2\bar{a}\rangle}} & 0 & \sqrt{2\langle \bar{J}_+\rangle\langle 2\bar{a}\rangle} & 0 & 0 \\ 0 & 0 & 0 & 0 & 0 \end{pmatrix}, \tag{6.53}$$

and the stochastic differential equations are

$$\mathrm{d}\boldsymbol{\zeta} = \frac{\partial}{\partial \boldsymbol{\zeta}^\intercal}\mathbf{A}\boldsymbol{\zeta}\mathrm{d}t + \mathbf{B}^\intercal \mathrm{d}\mathbf{W}, \tag{6.54}$$

where $\mathrm{d}\mathbf{W}$ is a vector of Wiener increments. We write the equations of motion for second order momenta such as $\xi^*\xi$ and μ^2. Using the properties of the Wiener process, namely that $dW_i dW_j = \delta_{ij}$ and matrix (6.53), we have, for the motion of the total angular momenta

$$\frac{\mathrm{d}\langle \mathbf{J}^2\rangle}{\mathrm{d}t} - \mathrm{O}(N^2) = N\frac{\mathrm{d}}{\mathrm{d}t}(\langle \xi\xi^*\rangle + \langle \mu^2\rangle + \langle \mu\rangle) = 2i\lambda\langle \bar{J}_z\rangle\langle(\xi^* - \xi)(\alpha + \alpha^*)\rangle. \tag{6.55}$$

In solving the equations of motion for the means in the steady state, we encountered equations which conserve the mean total angular momentum – $\langle \mathbf{J}^2\rangle = N^2/2$ for $\mathrm{O}(N^2)$. We conclude from this equation that, in the Haken representation, the total angular momentum $\langle \mathbf{J}^2\rangle$ is conserved *only* to order $O(N^2)$, but not to order $O(N)$, corresponding to the noise terms.

On the other hand, in the Holstein-Primakoff representation this conservation law in intrinsic, as we can see by writing $\mathbf{J}^2$, which, in normal order becomes

$$\mathbf{J}^{2\ HP} = \langle \hat{J}_+\hat{J}_- - \hat{J}_z + : \hat{J}_z^2 : + \hat{b}^\dagger\hat{b}\rangle \tag{6.56}$$

With the expansion $\hat{b} = N^{1/2}\langle \hat{b}\rangle + \beta$, using the definitions of $\hat{J}_+$ and $\hat{J}_z$ in equation (5.1),

we have:

$$\begin{aligned}\langle \mathbf{J}^2 \rangle =& \langle \left| N^{1/2}\langle \bar{J}_+ \rangle + \beta \right|^2 \left(N - \left| N^{1/2}\langle \bar{J}_+ \rangle + \beta \right|^2 \right) - \frac{N}{2} + \left(\left| N^{1/2}\langle \bar{J}_+ \rangle + \beta \right|^2 - \frac{N}{2} \right) \rangle \\ =& \frac{N}{2}\left(\frac{N}{2} + 1 \right). \end{aligned} \tag{6.57}$$

This result is independent of linearization, and shows that the Holstein-Primakoff representation is more accurate in describing the linearized system than the Haken representation.

We still have to explain why, despite the lack of total angular momenta conservation in the linearised Haken representation, there is perfect agreement between both representations in the cavity spectra. We can write the equation for the covariance matrix, $\mathbf{C}$, in the Haken representation as

$$\mathbf{AC} + \mathbf{CA}^{\intercal} = -\mathbf{D}, \tag{6.58}$$

where $\mathbf{A}$ and $\mathbf{D}$ are the drift and diffusion matrices given by (6.38) and (6.39) respectively. As $\mathbf{A}$ has a null eigenvalue, the equations for the covariances and correlations are overdetermined, in the same way as we had to use the conservation of total angular momentum to obtain the means in the steady state. Our strategy is to change these equations to a basis where this eigenvalue appears explicitly. We can define the new coordinate system, knowing that $(0, 0, \sqrt{(1-\mu^2)}/2\mu, \sqrt{(1-\mu^2)}/2\mu, 1)$ is the eigenvector of $\mathbf{A}$ with zero eigenvalue. The similarity transformation is given by the matrix:

$$\mathbf{S} = \begin{pmatrix} 1 & 0 & 0 & 0 & 0 \\ 0 & 1 & 0 & 0 & 0 \\ 0 & 0 & \frac{\sqrt{2}(1+3\mu)}{4\mu\sqrt{1+\mu}} & \frac{\sqrt{2}(\mu-1)}{4\mu\sqrt{1+\mu}} & 0 \\ 0 & 0 & \frac{\sqrt{2}(\mu-1)}{4\mu\sqrt{1+\mu}} & \frac{\sqrt{2}(1+3\mu)}{4\mu\sqrt{1+\mu}} & 0 \\ 0 & 0 & \frac{\sqrt{1-\mu^2}}{2\mu} & \frac{\sqrt{1-\mu^2}}{2\mu} & 1 \end{pmatrix}, \tag{6.59}$$

and its inverse

$$\mathbf{S}^{-1} = \begin{pmatrix} 1 & 0 & 0 & 0 & 0 \\ 0 & 1 & 0 & 0 & 0 \\ 0 & 0 & \frac{\sqrt{2}(1+3\mu)}{4\sqrt{1+\mu}} & \frac{\sqrt{2}(\mu-1)}{4\mu\sqrt{1+\mu}} & 0 \\ 0 & 0 & \frac{\sqrt{2}(\mu-1)}{4\sqrt{1+\mu}} & \frac{\sqrt{2}(1+3\mu)}{4\sqrt{1+\mu}} & 0 \\ 0 & 0 & -\frac{\sqrt{1-\mu}}{\sqrt{2}} & -\frac{\sqrt{1-\mu}}{\sqrt{2}} & 1 \end{pmatrix}. \tag{6.60}$$

The transformed matrix $\tilde{\mathbf{A}}$ is given by

$$\tilde{\mathbf{A}} = \mathbf{S}\mathbf{A}^{Ha}\mathbf{S}^{-1}; \tag{6.61}$$

while the diffusion and covariance matrices transform according to

$$\tilde{\mathbf{D}} = \mathbf{S}\mathbf{D}\mathbf{S}^{\intercal}, \tag{6.62}$$

$$\tilde{\mathbf{C}} = \mathbf{S}\mathbf{C}\mathbf{S}^{\intercal}. \tag{6.63}$$

The new matrix $\tilde{\mathbf{A}}$ is written explicitly as:

$$\tilde{\mathbf{A}} = \begin{pmatrix} & & & & 0 \\ & & & & 0 \\ & & \mathbf{A}^{HP} & & \frac{-i\omega_0\sqrt{2(1-\mu)}}{\mu} \\ & & & & \frac{i\omega_0\sqrt{2(1-\mu)}}{\mu} \\ 0 & 0 & 0 & 0 & 0 \end{pmatrix} \tag{6.64}$$

Before calculating $\tilde{\mathbf{D}}$, we note that the correlation function, $\mathbf{c}(\tau)$, obeys the equation

$$\frac{\mathrm{d}\tilde{\mathbf{c}}(\tau)}{\mathrm{d}\tau} = -\tilde{\mathbf{A}}\tilde{\mathbf{c}}(\tau). \tag{6.65}$$

The matrix $\tilde{\mathbf{c}}(\tau)$ will give the correlations directly in the Holstein-Primakoff representation. We use this to study the correlations of the field variables:

$$\frac{\mathrm{d}}{\mathrm{d}t}\begin{pmatrix} \alpha\alpha(\tau) \\ \alpha\alpha^*(\tau) \\ \alpha\beta(\tau) \\ \alpha\beta^*(\tau) \end{pmatrix} = \mathbf{A}^{HP}\begin{pmatrix} \alpha\alpha(\tau) \\ \alpha\alpha^*(\tau) \\ \alpha\beta(\tau) \\ \alpha\beta^*(\tau) \end{pmatrix} + \frac{i\omega_0\sqrt{2-2\mu}}{\mu}\begin{pmatrix} 0 \\ 0 \\ -\alpha\sigma(\tau) \\ \alpha\sigma(\tau) \end{pmatrix}, \tag{6.66}$$

where σ is the constant of motion of the matrix $\mathbf{A}^{Ha}$; therefore the coupling between the extra dimension of the Haken representation is embedded only in the atomic variables when transformed to the Holstein-Primakoff formalism. The spectrum matrix in the Haken variables is shown in Figure 6.4 for $\lambda = 1.2\lambda_c$, so the singularities in the extra dimension, representing the conserved quantity, can be seen clearly. The transformed

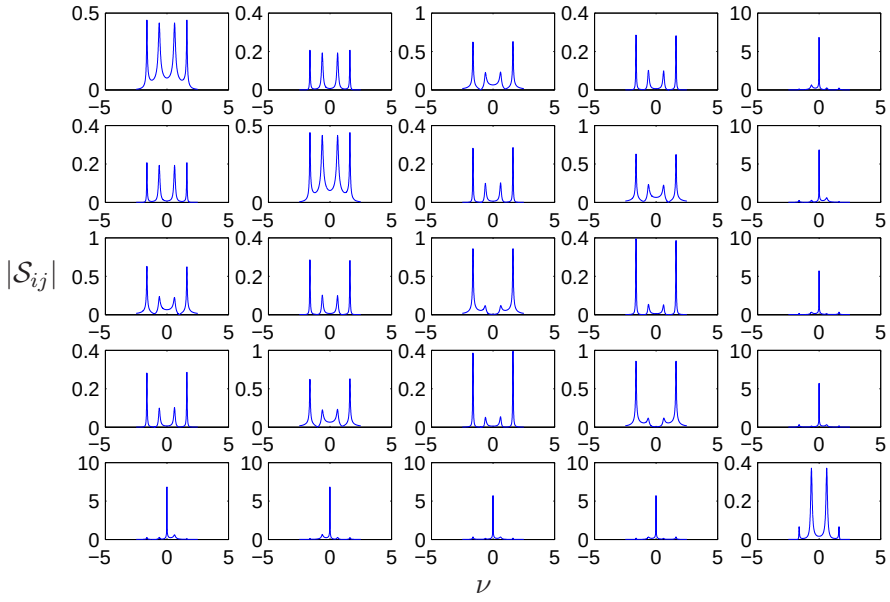

Figure 6.4.: Graphical representation of the spectrum matrix in the Haken representation for $\lambda = 1.2\lambda_c$

diffusion matrix is given by

$$\tilde{\mathbf{D}} = i \begin{pmatrix} 0 & 0 & -\frac{\lambda\sqrt{2}(1+3\mu)}{4\sqrt{1+\mu}} & \frac{\lambda\sqrt{2}(\mu-1)}{4\sqrt{1+\mu}} & 0 \\ 0 & 0 & \frac{\lambda\sqrt{2}(1-\mu)}{4\sqrt{1+\mu}} & \frac{\lambda\sqrt{2}(1+3\mu)}{4\sqrt{1+\mu}} & 0 \\ -\frac{\lambda\sqrt{2}(1+3\mu)}{4\sqrt{1+\mu}} & \frac{\lambda\sqrt{2}(1-\mu)}{4\sqrt{1+\mu}} & \frac{(\mu^2-1)\omega_0}{2\mu^2} & 0 & \frac{\sqrt{2-2\mu}(\mu^2-1)\omega_0}{4\mu^2} \\ \frac{\lambda\sqrt{2}(\mu-1)}{4\sqrt{1+\mu}} & \frac{\lambda\sqrt{2}(1+3\mu)}{4\sqrt{1+\mu}} & 0 & -\frac{(\mu^2-1)\omega_0}{2\mu^2} & \frac{(1-\mu)^{3/2}(1+\mu)\omega_0}{2\sqrt{2}\mu^2} \\ 0 & 0 & \frac{\sqrt{2-2\mu}(\mu^2-1)\omega_0}{4\mu^2} & \frac{(1-\mu)^{3/2}(1+\mu)\omega_0}{2\sqrt{2}\mu^2} & 0 \end{pmatrix}, \tag{6.67}$$

which is not the same matrix as the Holstein-Primakoff representation in the 4×4 subspace, but we see that the extra dimension has no correlation with the field (elements $\tilde{D}_{15}$ and $\tilde{D}_{25}$ are 0). We notice that below λ_c , where $\mu = 1$, the extra dimension vanishes, and the both matrices, $\tilde{\mathbf{A}}$ and $\tilde{\mathbf{D}}$, become identical to the drift and diffusion matrices in the Holstein-Primakoff representation.

6.3. Coherent atomic state representation

In the previous section we dealt with the linearized Haken representation for collective atomic operators and found that it is not a completely accurate description, failing to conserve the total angular momentum in its linearised version; as a consequence the atomic spectra are different from those computed in the Holstein-Primakoff representation. We might consider also an exact treatment of these representations, but, as we mentioned, this would introduce derivatives of all orders in both representations. Ideally, we seek a treatment without transformations in the Hamiltonian, as in the Haken approach, that does not introduce singularities or over-determinacy and intrinsically conserves angular momentum. Such a representation is introduced in this chapter: the atomic coherent states representation. These states are an extension of the field coherent states [62], and have been used in many situations in quantum optics [18, 63].

The atomic coherent states are defined in a similar way to the coherent states. There

are many definitions; we shall use one of the simplest here, defining

$$||\ell,\gamma\rangle = \exp\left[\gamma\hat{J}_+\right]|\ell,-\ell\rangle, \tag{6.68}$$

where γ is a complex number and $\ell = N/2$ is the total angular momentum. The resulting state is unnormalized. The normalization factor can be calculated easily by writing $|\ell, m_z\rangle = |\ell, p\rangle$, where $p - \ell = m_z$, with $0 \leq p \leq 2\ell$, and with this definition noting that

$$\left(\hat{J}_-\right)^p |\ell, 0\rangle = \left(\frac{p!(2\ell)!}{(2\ell-p)!}\right)^{1/2} |\ell, p\rangle. \tag{6.69}$$

Then the unnormalized state can be written explicitly as

$$||\ell,\gamma\rangle = \mathrm{e}^{\gamma\hat{J}_+}|\ell,0\rangle = \sum_{p=0}^{2\ell}\left(\frac{(2\ell)!}{p!(2\ell-p)!}\right)^{1/2}\gamma^p|\ell,p\rangle, \tag{6.70}$$

and the normalization constant is given by

$$\sum_{p=0}^{2\ell}\frac{p!(2\ell)!}{(2\ell-p)!}|\gamma|^{2p} = (1+|\gamma|^2)^{2\ell}. \tag{6.71}$$

We define the normalized *atomic coherent state* by

$$|\gamma\rangle = (1+\gamma\gamma^*)^{-\ell}\mathrm{e}^{\gamma\hat{J}_-}|0\rangle, \tag{6.72}$$

where we omit the index ℓ. This definition highlights the similarities with the coherent states. Indeed, the defined atomic coherent state representation represents the rotation of the state $|-m\rangle$ through an angle θ about the vector $(\sin[\phi], -\cos[\phi], 0)$ on a "Bloch sphere", as depicted in Figure 6.5. The parameter γ is the coordinate of the stereographic projection of the state. With this parametrization, the state can be written as

$$\begin{aligned}|\gamma\rangle &= \mathrm{e}^{i\theta\left(\hat{J}_x\sin[\phi]-\hat{J}_y\cos[\phi]\right)}|-\ell\rangle \\ &= \mathrm{e}^{\gamma\hat{J}_-}\mathrm{e}^{-\hat{J}_z\ln[1+\gamma\gamma^*]}\mathrm{e}^{-\gamma\hat{J}_+}|-\ell\rangle,\end{aligned} \tag{6.73}$$

where $\gamma = \mathrm{e}^{i\phi}\tan[\theta/2]$. We can also see that $|\gamma\rangle$ is an eigenstate of the angular momentum in the direction given by the spherical coordinate angles θ and ϕ, $\hat{\mathbf{J}}(\theta,\phi)$. The

relations leading to these equations are given in [64]. From the parametrization it can be easily shown that the following completeness relation is satisfied:

$$\frac{1}{4\pi}\int \mathrm{d}\phi\mathrm{d}\theta|\gamma\rangle\langle\gamma| = \mathbb{1}. \tag{6.74}$$

With this property we are able to write any state ρ, of the field plus atoms, as a diagonal

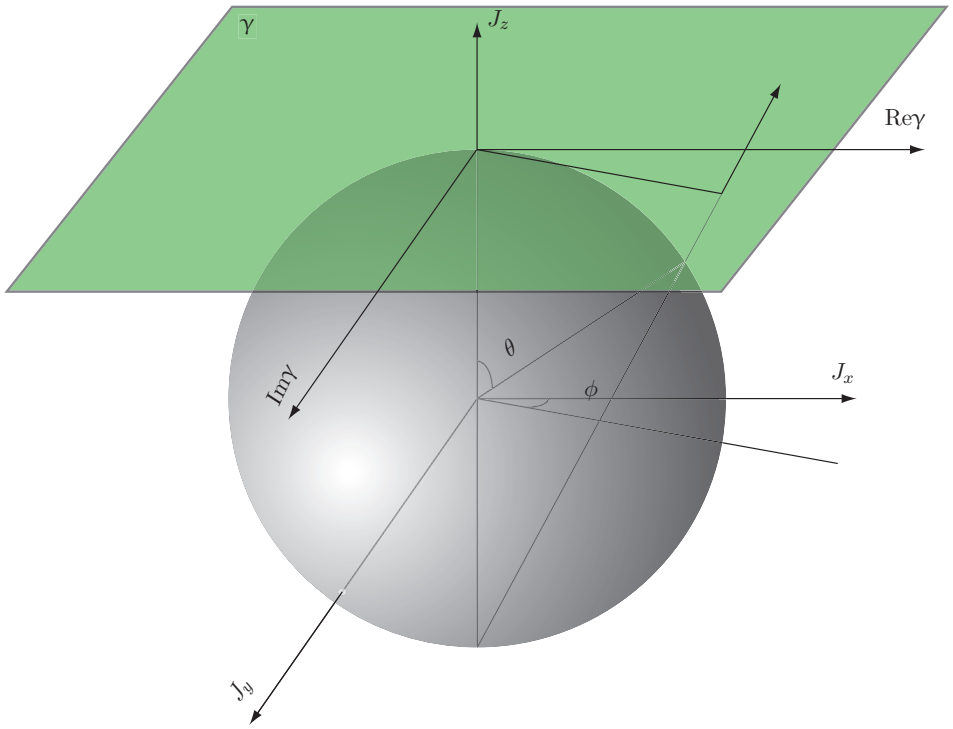

Figure 6.5.: Stereographic projection of the Bloch sphere in the plane γ

expansion of the states $|\gamma,\alpha\rangle$, namely

$$\rho = \int \mathcal{P}(\gamma,\alpha)|\gamma,\alpha\rangle\langle\gamma,\alpha|\mathrm{d}^2\gamma\mathrm{d}^2\alpha, \tag{6.75}$$

where $\mathcal{P}(\gamma,\alpha)$ is a pseudo-probability distribution over the variable γ and field amplitude

α and $\mathrm{d}^2\gamma = \mathrm{dRe}(\gamma)\mathrm{dIm}(\gamma)\mathrm{d}$. The following properties are useful:

$$\hat{J}_-||\gamma\rangle\langle\gamma|| = \frac{\partial}{\partial\gamma}||\gamma\rangle\langle\gamma||, \tag{6.76}$$

$$\hat{J}_+||\gamma\rangle\langle\gamma|| = \gamma\left(2\ell - \gamma\frac{\partial}{\partial\gamma}\right)||\gamma\rangle\langle\gamma||, \tag{6.77}$$

$$\hat{J}_z||\gamma\rangle\langle\gamma|| = \left(\ell - \gamma\frac{\partial}{\partial\gamma}\right)||\gamma\rangle\langle\gamma||. \tag{6.78}$$

The first of these equations is readily proved from Equation (6.70), while for the other two we use, with the help of (6.24),

$$\hat{J}_+\mathrm{e}^{\gamma\hat{J}_-}|\ell\rangle = \mathrm{e}^{\gamma\hat{J}_-}\left(\hat{J}_+ + 2\gamma\hat{J}_z - \gamma^2\hat{J}_-\right)|\ell\rangle = \left(2\ell\gamma - \gamma^2\hat{J}_-\right)\mathrm{e}^{\gamma\hat{J}_-}|\ell\rangle, \tag{6.79}$$

and

$$\hat{J}_z\mathrm{e}^{\gamma\hat{J}_-}|\ell\rangle = \mathrm{e}^{\gamma\hat{J}_-}\left(\hat{J}_z - \gamma\hat{J}_-\right)|\ell\rangle. \tag{6.80}$$

Noting then that the unnormalized states can be written in terms of the normalized states as $(1+\gamma\gamma^*)^{2\ell}|\gamma\rangle\langle\gamma|$, we use these results to write (writing $2\ell = N$)

$$\hat{J}_-|\gamma\rangle\langle\gamma| = \left(\frac{N\gamma^*}{1+\gamma\gamma^*} - \frac{\partial}{\partial\gamma}\right)|\gamma\rangle\langle\gamma|, \tag{6.81a}$$

$$\hat{J}_+|\gamma\rangle\langle\gamma| = \gamma\left(\frac{N}{1+\gamma\gamma^*} - \gamma\frac{\partial}{\partial\gamma}\right)|\gamma\rangle\langle\gamma|, \tag{6.81b}$$

$$\hat{J}_z|\gamma\rangle\langle\gamma| = \left(\frac{N}{2}\frac{1-\gamma\gamma^*}{1+\gamma\gamma^*} - \gamma\frac{\partial}{\partial\gamma}\right)|\gamma\rangle\langle\gamma|. \tag{6.81c}$$

The means of the operators will be some function of γ; for the operators in the same order as the Haken representation, using Equation (6.81), we have

$$\langle\gamma|\hat{J}_+^q\hat{J}_z^r\hat{J}_-^s|\gamma\rangle = (1+\gamma\gamma^*)^{-N}\frac{\partial^{q+s}}{\partial\gamma^{*q}\partial\gamma^s}\left(\frac{N}{2} - \gamma^*\frac{\partial}{\partial\gamma^*}\right)^r(1+\gamma\gamma^*)^N \tag{6.82}$$

We now use these expressions and the master equation for the Dicke model (6.1) to derive an equation of motion for the distribution P. We replace the density operator by its expansion in terms of atomic coherent states, given by Equation (6.75), in the equation of motion for ρ (6.1), namely

$$\frac{\partial\mathcal{P}}{\partial t} = \int\mathcal{P}(\gamma,\alpha)\mathcal{L}|\gamma,\alpha\rangle\langle\gamma,\alpha|\mathrm{d}\gamma^2\mathrm{d}\alpha^2, \tag{6.83}$$

where the Liouvillian operator is defined in (5.23). We then apply the operators as defined in (6.81), and proceed with integration by parts to order the terms such that the differential operators act on $\mathcal{P}$; in summary we have the substitutions:

$$\hat{J}_-\rho \to \left(\frac{N\gamma^*}{1+\gamma\gamma^*} + \frac{\partial}{\partial\gamma}\right)\mathcal{P} \tag{6.84}$$

$$\hat{J}_+\rho \to \left(\frac{N\gamma}{1+\gamma\gamma^*} + \frac{\partial}{\partial\gamma}\gamma^2\right)\mathcal{P}, \tag{6.85}$$

$$\hat{J}_z\rho \to \left(\frac{N}{2}\frac{1-\gamma\gamma^*}{1+\gamma\gamma^*} + \frac{\partial}{\partial\gamma}\gamma\right)\mathcal{P} \tag{6.86}$$

$$\rho\hat{J}_- \to \left(\frac{N\gamma^*}{1+\gamma\gamma^*} + \frac{\partial}{\partial\gamma^*}\gamma^{*2}\right)\mathcal{P} \tag{6.87}$$

$$\rho\hat{J}_+ \to \left(\frac{N\gamma}{1+\gamma\gamma^*} + \frac{\partial}{\partial\gamma^*}\right)\mathcal{P}, \tag{6.88}$$

$$\rho\hat{J}_z \to \left(\frac{N}{2}\frac{1-\gamma\gamma^*}{1+\gamma\gamma^*} + \frac{\partial}{\partial\gamma^*}\gamma^*\right)\mathcal{P} \tag{6.89}$$

Thus, also using (6.28) for the photonic operators, we derive the equation of motion for $\mathcal{P}$, which takes the form of a Fokker-Planck, with the non-linear drift matrix

$$\mathbf{A} = \begin{pmatrix} (\kappa+i\omega)\alpha + i\lambda\frac{\gamma+\gamma^*}{1+\gamma\gamma^*} \\ (\kappa-i\omega)\alpha^* + i\lambda\frac{\gamma+\gamma^*}{1+\gamma\gamma^*} \\ -i\omega_0\gamma + i\lambda(1-\gamma^2)(\alpha+\alpha^*) \\ i\omega_0\gamma - i\lambda(1-\gamma^2)(\alpha+\alpha^*) \end{pmatrix}, \tag{6.90}$$

and diffusion matrix,

$$\mathbf{D} = i\lambda\frac{1}{N}\begin{pmatrix} 0 & 0 & -(1-\gamma^2) & 0 \\ 0 & 0 & 0 & (1-\gamma^{*2}) \\ -(1-\gamma^2) & 0 & 0 & 0 \\ 0 & (1-\gamma^{*2}) & 0 & 0 \end{pmatrix}, \tag{6.91}$$

where we use the scaled variable $\alpha \to N^{1/2}\alpha$. This equation gives an exact phase space representation for a finite number of atoms. The equation has to be interpreted in the

positive-P sense in order for the equation to be called a Fokker-Planck equation, as $\mathbf{D}$ has eigenvalues $\pm N^{-1}\lambda\sqrt{-(\gamma^2-1)^2}$. Thus the diffusion matrix is not positive definite as required by a legitimate Fokker-Planck equation (see [53]). It follows that the stars on the variables do not represent complex conjugates, but independent variables; hence, the phase space becomes 8-dimensional.

This partial differential equation, if interpreted in the positive-P representation sense, thus as a Fokker-Planck equation, has a set of stochastic differential equations given by

$$\mathrm{d}\mathbf{\Gamma} = \mathbf{A}^{\intercal}\mathrm{d}t + \mathbf{B}\mathrm{d}\mathbf{W} \tag{6.92}$$

where $\mathbf{\Gamma} = (\alpha, \alpha^*, \gamma, \gamma^*)^{\intercal}$, $\mathrm{d}\mathbf{W}$ is a vector of Wiener increments, and the matrix $\mathbf{B}$ is defined such that $\mathbf{B}\mathbf{B}^{\intercal} = \mathbf{D}$. Matrix $\mathbf{B}$ is found by completing squares as in Section 6.2.2, Equation (6.53), and is given by

$$\mathbf{B} = \left(\frac{i\lambda}{2N}\right)^{1/2} \begin{pmatrix} 1+\gamma & i\,(1+\gamma) & 0 & 0 \\ 0 & 0 & (1+\gamma^*) & i(1+\gamma^*) \\ -(1-\gamma) & i(1-\gamma) & 0 & 0 \\ 0 & 0 & (1-\gamma^*) & -i(1-\gamma^*) \end{pmatrix}. \tag{6.93}$$

We notice that the fluctuations in these equations scale with $N^{-1/2}$. The equations are highly non-linear, and the difficulties arising in the Positive-P representation are present. For example, the fact that the product $\gamma\gamma^*$ is not necessarily a positive number makes possible the appearance of diverging trajectories during the numerical integration.

We used the technique described in [65] to improve numerical stability. In this method, the vector $\mathbf{\Gamma}$ at a time t is calculated implicitly from $\mathbf{\Gamma}$ in a intermediate position parametrized by $0 < \theta < 1$. The numerical integration has the form

$$\Delta\mathbf{\Gamma}^n = \mathbf{A}(\mathbf{\Gamma}^{n+\theta})\Delta t + \mathbf{B}(\mathbf{\Gamma}^n)\Delta\mathbf{W}, \tag{6.94}$$

where $\Delta\mathbf{\Gamma}^n = \mathbf{\Gamma}^{n+1} - \mathbf{\Gamma}^n$, and Δt and $\Delta\mathbf{W}$ are finite differences of time and the Wiener increment respectively; n is the n-th time step of the integration. The method only

takes into account the deterministic part of the stochastic differential equation, so to find $\mathbf{\Gamma}^{n+\theta}$ we linearize $\mathbf{A}$ as follows

$$\mathbf{A}(\mathbf{\Gamma}^{n+\theta}) = \mathbf{A}(\mathbf{\Gamma}^n) + \mathbf{J}_A^n \theta \Delta\mathbf{\Gamma}^n, \tag{6.95}$$

where $\mathbf{J}_A^n$ is the Jacobian of $\mathbf{A}$ evaluated at $\mathbf{\Gamma}^n$:

$$(\mathbf{J}_A^n)_{ij} = \left.\frac{\partial \mathbf{A}_i}{\partial \mathbf{\Gamma}_j}\right|_{\mathbf{\Gamma}=\mathbf{\Gamma}^n}. \tag{6.96}$$

The value of $\mathbf{A}(\mathbf{\Gamma}^{n+\theta})$ is obtained by inverting (6.95). Substituting the result into (6.94), we obtain.

$$\Delta\mathbf{\Gamma}^n = (\mathbb{1} - \theta \mathbf{J}_{\mathbf{A}}^n \Delta t)^{-1} \left(\mathbf{A}(\mathbf{\Gamma}^n)\Delta t + \mathbf{B}(\mathbf{\Gamma}^n)\Delta\mathbf{W}\right) \tag{6.97}$$

We see that the inverse of a 4×4 matrix has to be obtained at each step of the numerical integration.

In figure 6.6 we plot samples of trajectories for the variable α using $N = 10^3$, $N = 10^4$ and $N = 10^5$ atoms (clockwise). We notice the integration becomes more stable as the number of atoms increases (bottom in Figure 6.6, notice the change in time scale). The coupling λ is varied across the phase transition $\lambda = 0.9\lambda_c$, $\lambda = \lambda_c$ and $\lambda = 1.1\lambda_c$ (top to botton in each Figure respectively). This variable shows a small non zero mean, but is teeming with large excursions from the mean, in the small N case, although, above λ_c, instabilities tend to appear after some time of stable integration. Even for $N = 10^5$ these large fluctuations eventually appear for a long time of integration, necessary to calculate the means. Nevertheless, the simulations can show the large scale chaotic oscillation, as is shown in the semiclassical equations (Figure 6.1), although on a much shorter time scale as they should, and as we see in Figure 6.7 in a sample trajectory for γ. Simulations with $N = 10^5$ atoms were carried out to calculate the means of the angular momentum operators $\hat{J}_x$ and $\hat{J}_z$; the result is shown in Figure 6.8. There we can see that the simulation agrees with the linearized treatment away from λ_c.

Around the critical point the equations succeed, partially, in describing how the fluctuations grow around the phase transition (compare Figure 6.8 with figures 6.2 and 7.1). The number of trajectories needed for convergence becomes of the order of 10^6.

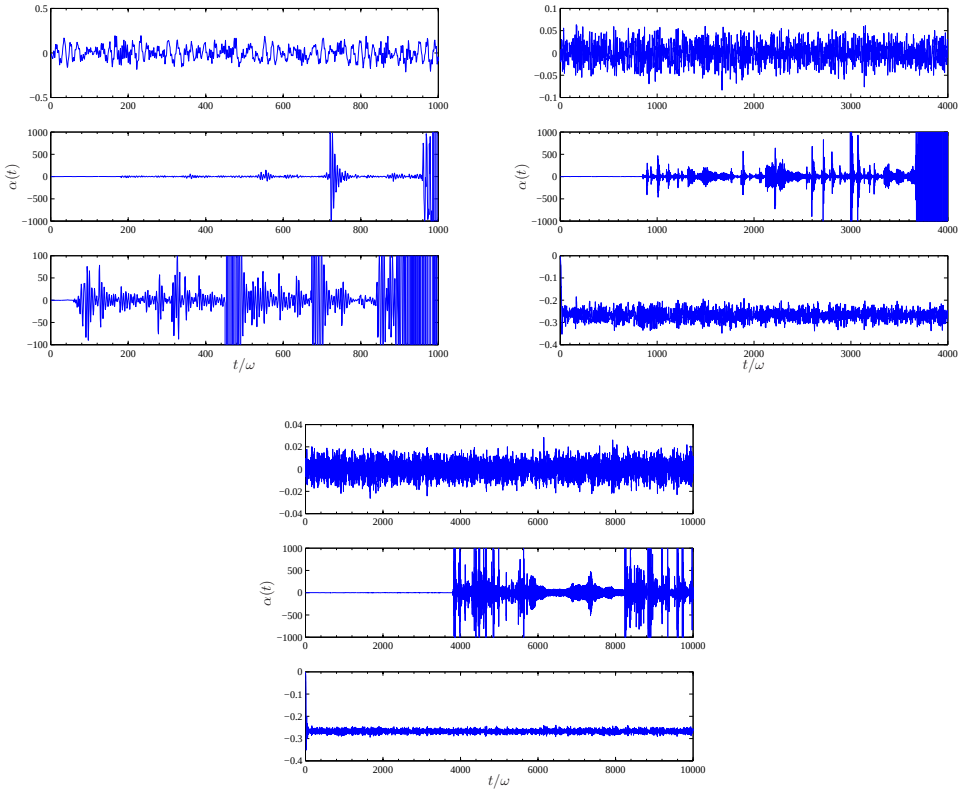

Figure 6.6.: Sample trajectories of α. In clockwise order the number of atoms is increased from $N = 10^3$, $N = 10^4$ and $N = 10^5$. In each plot λ is varied $\lambda = 0.9\lambda_c$, $\lambda = \lambda_c$ and $\lambda = 1.1\lambda_c$ from top to bottom ($\omega = \omega_0 = 1$ and $\kappa = 0.1$).

Similarly to what was done in chapter 5, we linearize these equations around the mean values. Here the linearization is carried out to demonstrate how the means transform from the Holstein-Primakoff representation to the atomic coherent representation. Define the vector of operator mean values $\Theta = (N^{1/2}\langle\bar{a}\rangle, N^{1/2}\langle\bar{a}^\dagger\rangle, \langle\gamma\rangle, \langle\gamma\rangle)^\intercal$, with the fluctuations scaled as $\boldsymbol{\xi} = (z, z^*, N^{-1/2}v, N^{-1/2}v^*)^\intercal$. We calculate the linearized drift matrix as

$$\mathbf{A}_L = \left.\frac{\partial \mathbf{A}}{\partial \boldsymbol{\Gamma}}\right|_{\boldsymbol{\Gamma}=\boldsymbol{\Theta}}, \tag{6.98}$$

The diffusion matrix is simply $\mathbf{D}_L = \mathbf{D}_{\Gamma=\Theta}$. The steady state solutions for the vector $\boldsymbol{\Theta}$ are calculated setting nonlinear drift matrix $\mathbf{A}$ to zero. The mean of the field variable

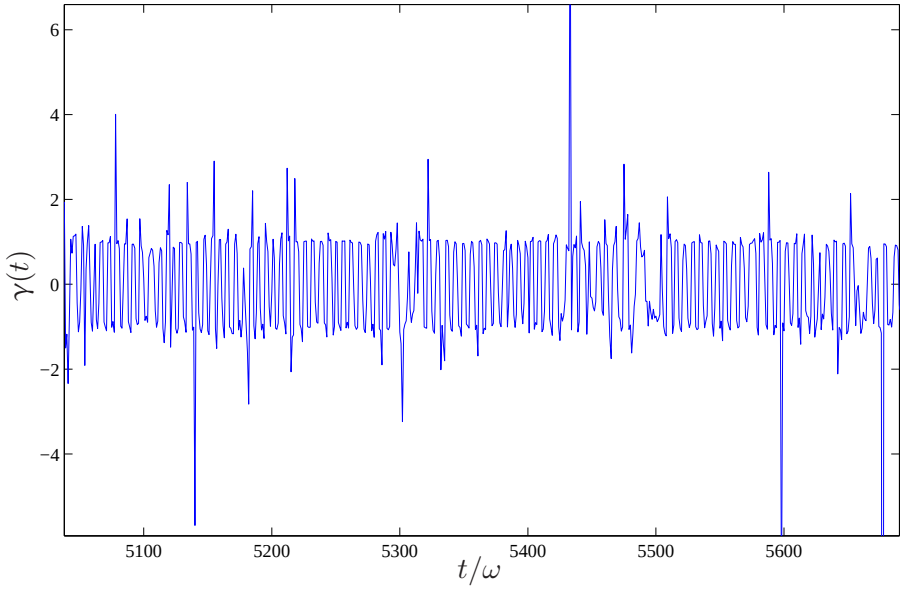

Figure 6.7.: Sample γ for $\lambda = 1.1\lambda_c$, $N = 10^3$ atoms ($\omega = \omega_0 = 1$) and $\kappa = 0.1$.

$\langle \bar{a} \rangle$ is obviously the same as that calculated in the previous section, while for the atomic variables we have:

$$\langle \gamma \rangle = \begin{cases} 0 & \text{if } \lambda < \lambda_c \\ \pm\frac{\sqrt{1-\mu}}{\sqrt{1+\mu}} & \text{if } \lambda > \lambda_c, \end{cases} \tag{6.99}$$

where $\mu = \lambda_c^2/\lambda^2$ as usual. We are able to rederive all results of Chapter 5, and the use of formulae (5.33) and (5.42) return the same spectra and covariance for field variables as the Holstein-Primakoff approach. Instead, we shall use this representation to compute the values of variances for the atomic variables, ΔJ_+^2 and ΔJ_z^2. This is done by expanding the phase-space expressions corresponding to the operators $\hat{J}_z$ and $\hat{J}_+$ to first order:

$$\hat{J}_z \to -\frac{N}{2}\frac{1-\gamma\gamma^*}{1+\gamma\gamma^*} = -\frac{N}{2}\frac{1-\langle\gamma\rangle^2}{1+\langle\gamma\rangle^2} + N^{1/2}\frac{\langle\gamma\rangle(v+v^*)}{(1+\langle\gamma\rangle^2)^2} + \mathrm{O}(N^0), \tag{6.100a}$$

$$\hat{J}_+ \to N\frac{\gamma^*}{1+\gamma\gamma^*} + \frac{N^{1/2}}{1+\langle\gamma\rangle^2}(v - \langle\gamma\rangle^2 v^*) + \mathrm{O}(N^0). \tag{6.100b}$$

The variances are obtained by taking the squares of equations (6.100) and taking the stochastic average, taking into consideration that $\langle v \rangle = \langle v^* \rangle = 0$. We replace $\langle v^2 \rangle \to C_{33}, \langle v^{*2} \rangle \to C_{44}$, and $\langle v v^* \rangle \to C_{34}$, where C_{ij} are solutions of the covariance matrix for

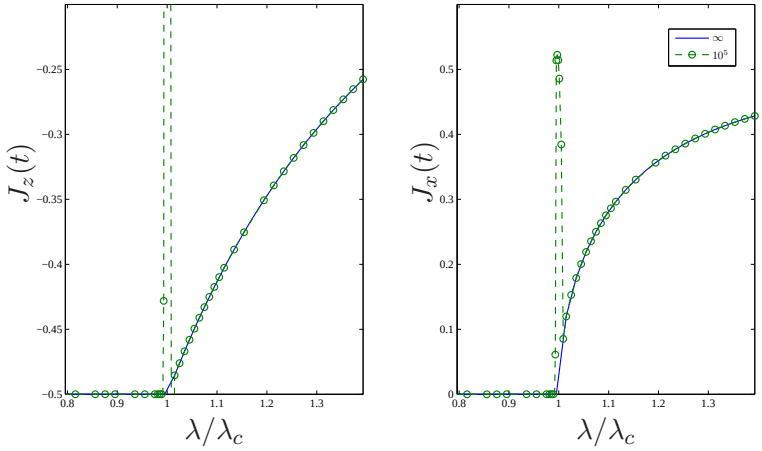

Figure 6.8.: Means of $\hat{J}_z$ and $\hat{J}_x$ for $\omega = \omega_0 = 1$, $\kappa = 1$, $N = 10^5$ atoms. Averaged over 10^6 trajectories.

the atomic coherent state representation. We also have to take into consideration the terms of order N in the expansions of the second order moments in the atomic coherent state representation derived from equations (6.82):

$$\langle \hat{J}_z^2 \rangle = \frac{N^2}{4} \frac{(1-\gamma\gamma^*)^2}{(1+\gamma\gamma^*)^2} + N \frac{\gamma\gamma^*}{(1+\gamma\gamma^*)^2} \tag{6.101}$$

$$\langle \hat{J}_+^2 \rangle = N(N-1) \frac{\gamma^2}{(1+\gamma\gamma)^2}. \tag{6.102}$$

This procedure adds the following terms to the variances

$$\langle \hat{J}_z^2 \rangle \xrightarrow{\mathrm{O}(N)} \frac{\langle\gamma\rangle^2}{(1+\langle\gamma\rangle^2)^2}, \tag{6.103}$$

$$\langle \hat{J}_+^2 \rangle \xrightarrow{\mathrm{O}(N)} -\frac{\langle\gamma\rangle^2}{(1+\langle\gamma\rangle^2)^2} \tag{6.104}$$

We use the solutions for the covariance matrix in the atomic coherent state representation to write the variances above λ_c as

$$\begin{aligned} \frac{\langle \Delta \hat{J}_z^2 \rangle}{N} =& \frac{\langle\gamma\rangle^2}{(1+\langle\gamma\rangle^2)^4} (C_{33} + C_{44} + 2C_{34}) + \frac{\langle\gamma\rangle^2}{(1+\langle\gamma\rangle^2)} \\ =& \frac{(\kappa^2 + \omega^2 - \omega_0^2)\mu^2 + \omega_0^2}{8\mu\omega\omega_0}, \end{aligned} \tag{6.105}$$

and for $\hat{J}_+$,

$$\begin{aligned}\frac{\langle\Delta\hat{J}_+^2\rangle}{N} =& \frac{1}{(1+\langle\gamma\rangle^2)^4}\left(C_{33}+\langle\gamma\rangle^4 C_{44}-\langle\gamma\rangle^2 2C_{34}\right)\\ =& \frac{\mu\left(1-2\mu^2\right)\left(\kappa^2+\omega^2\right)}{8\left(\mu-1\right)\omega\omega_0}+\frac{\left(\mu^2-1\right)\omega_0}{8\mu\omega}\end{aligned} \tag{6.106}$$

These are the same results we get with the equivalent equations for the Holstein-Primakoff representation,

$$\frac{\langle\Delta\hat{J}_{zHP}^2\rangle}{N} = \frac{1-\mu}{2}\left(C_{33}^{HP}+C_{44}^{HP}+2C_{34}^{HP}+1\right) \tag{6.107}$$

$$\langle\Delta\hat{J}_{+HP}^2\rangle = \frac{(\mu-1)^2 C_{33}^{HP}+(1+3\mu)(\mu-1+2(\mu-1)C_{34}^{HP}+(1+3\mu)C_{44}^{HP})}{8(1+\mu)}, \tag{6.108}$$

where C_{ij}^{HP} are the Holstein-Primakoff covariances obtained in Section 5.2.3. For $\lambda<\lambda_c$ the equations have to be expanded up to second order, and the noise in $\hat{J}_z$ is given to order N^0 only. In doing this we have:

$$\begin{aligned}\frac{\langle\Delta\hat{J}_z^2\rangle}{N} =& C_{34}\\ =& \frac{1}{8}\Big(-4+\frac{(\mu^2-2)(\kappa^2+\omega^2)}{(\mu^2-1)\omega\omega_0}+\frac{2\omega_0}{\omega}\Big).\end{aligned} \tag{6.109}$$

The noise in $\hat{J}_+$ is given by (6.106) for $\langle\gamma\rangle=0$,

$$\begin{aligned}\frac{\langle\Delta\hat{J}_+^2\rangle}{N} =& C_{33}\\ =& \frac{\kappa^2+\omega^2}{8\omega\omega_0(\mu-1)}.\end{aligned} \tag{6.110}$$

These are the same results as given by the Holstein-Primakoff representation and are shown in Figure 6.9, and as the solid line in Figure 7.1.

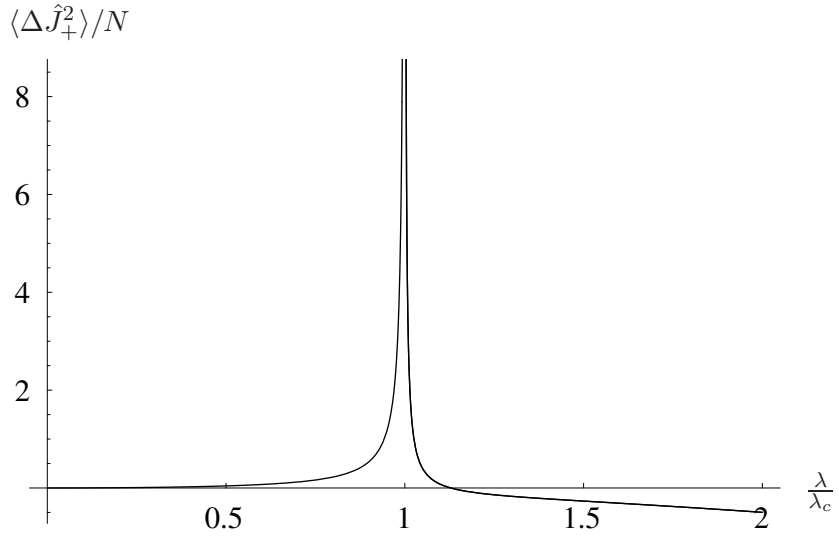

Figure 6.9.: Variance of $\hat{J}_+$ for $\omega = \omega_0 = 1$ and $\kappa = 0.1$

7. Dicke model with finite number of atoms

This chapter is devoted to the study of the Dicke model for a small number of atoms. Experimental techniques allow the precise control of even a single atom in a cavity (see [66] and references therein for a comprehensive review). In experiments with few atoms, quantum fluctuations become of the same order of magnitude as mean values, ruling out linearisation as a valid approximation technique. Using a master equation approach in order to obtain the quantum states of the system is feasible only for a small number of atoms. Alternatively one can use a quantum trajectory approach, which allows the calculation of averages of operators through the simulation of a stochastic Schrödinger equation – i.e. requiring less computational resources as we deal with vectors rather than with matrices. Within the quantum trajectory approach we are able to model the backaction of measurements on the quantum state of the system, as well as providing a measurement of entanglement from the simulated measurement record [67]. With these abilities we can explore the effects of measurements on the entanglement between atoms and photons in the Dicke model; in particular, study how the angle in a homodyne detection scheme alters the degree of entanglement.

More important in this chapter is the study of the dynamics associated with the switching between two possible states of the radiation field. The results in the thermodynamic limit show two possible mean values for the field amplitude and atomic polarization $\hat{J}_x$. After the linearization is made around one of them, this large scale dynamics is lost, whereas, solving the exact (non-linear) equations of motion for the mean values produced the chaotic features shown in Figures 6.1 and 6.7. In a analogous way, the full quantum mechanical treatment gives a more detailed view of the dynamics of the

system.

7.1. Stationary solutions of the master equation for finite N

In Section 5.1, phase space methods were used to describe the statistical properties of the system in the thermodynamic limit with the Holstein-Primakoff representation. The mesoscopic limit of the Dicke model can also be described by the use of the non-linear atomic coherent state representation – which, due to instabilities, failed to describe the means of operators correctly near λ_c for 10^3 atoms.

In treating the quantum system for a low number of atoms – tens of atoms – we expect to recover all features of the phase transition shown in figures 5.4 and 6.2, smoothed out as shown in Figure 7.1; thus the singularities appearing in the covariances will disappear.

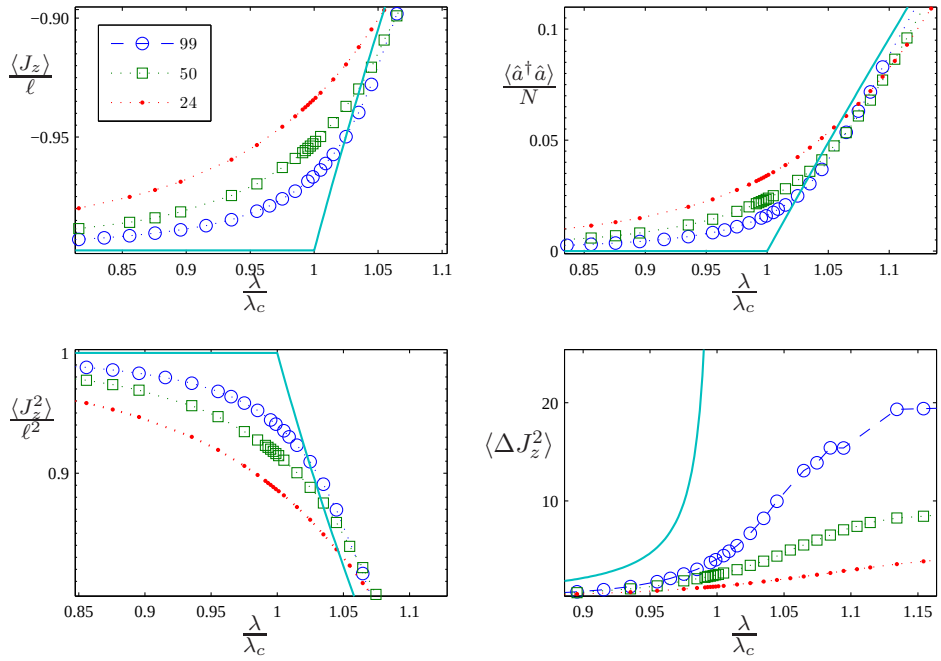

Figure 7.1.: Behaviour of means as N becomes large (solid line: linearized results)

These simulations consider a system using the ring cavity we describe in Section 4.3, where dipole coupling strengths ($\chi/2\pi$) and cavity losses ($\kappa/2\pi$) are considered to be on the order of 50 KHz and 20 KHz respectively. In the situation of Section 4.3, where the number of atoms is 10^6, the laser intensity (Ω_s) and detuning (Δ_s) are chosen so that $\Omega/\Delta_s \approx 10^{-3}$, giving a coupling λ above 10^2 KHz. In this Section we treat a situation where the number of atoms is on the order of 10^2. In order to maintain the atom-field coupling λ at the same order of magnitude one should have, according to Eq. 4.37, a ratio $\Omega_s/\Delta_s \approx 10^{-1}$. This can be achieved by an increase in the intensity of the driving lasers and/or a reduction in the detuning Δ_s. For these parameters, the off-resonant spontaneous emission, given approximately by $\Gamma\left(\Omega_s/\Delta_s\right)^2$, is increased from a few tens of Hz to hundreds of KHz. Under these conditions spontaneous emission would have to be taken into account in the model, or one must use a suitable atom or cavity configuration in order to increase the ratio χ/Γ. For the remainder of this chapter we assume the later and *do not consider spontaneous emission*, using $\omega = \omega_0 = 1$ and $\kappa = 0.1$.

7.1.1. Wigner function

The equations derived in the (positive) P representation in the previous chapters were useful for calculating the spectra and covariances. We were not interested, directly, in the pseudo distribution $\mathcal{P}$, however. In this section the use of a phase space representation has the purpose of giving a simple picture of the state of the system. The Wigner function [51, 68], $\mathcal{W}(\alpha)$, gives rise to well behaved functions, not necessarily true probability distributions, with which we are able to calculate the means of operators in symmetric order. As seen in previous chapters, the phase transition is characterized by a non-analiticity of the mean values $\langle \hat{J}_z \rangle$ and $\langle \hat{a}^\dagger \hat{a} \rangle$ around λ_c. The Wigner function provides a clearer way of characterizing the phase transition, allowing us to extend this concept to the finite number of atoms case. The characteristic function giving rise to this representation is

$$W(z) = \mathrm{Tr}\left[\rho \mathrm{e}^{iz\hat{a}+iz^*\hat{a}^\dagger}\right]. \tag{7.1}$$

The Wigner function $\mathcal{W}(\alpha)$ is the Fourier transform of this expression:

$$\mathcal{W}(\alpha) = \int \mathrm{d}^2 z W(z) \mathrm{e}^{-i\alpha^* z^* - i\alpha z}. \tag{7.2}$$

With these definitions the quantity $\langle \alpha^n \alpha^{*m} \rangle = \int \mathrm{d}^2\alpha \alpha^* \mathcal{W}(\alpha)$ gives the mean of the operator product $\hat{a}^n \hat{a}^{\dagger m}$ arranged in symmetric order, e.g.

$$\langle \alpha\alpha^* \rangle = \frac{1}{2} \left\langle \hat{a}^\dagger \hat{a} + \hat{a}\hat{a}^\dagger \right\rangle, \tag{7.3}$$

$$\langle \alpha^2\alpha^* \rangle = \frac{1}{3} \left\langle \hat{a}^2 \hat{a}^\dagger + \hat{a}^\dagger \hat{a}^2 + \hat{a}\hat{a}^\dagger \hat{a} \right\rangle. \tag{7.4}$$

In particular, the Wigner function gives the probability distributions for the quadrature amplitudes X and Y as marginal distributions, i.e.

$$\int \mathrm{d}X \mathcal{W}(X, Y) = P(Y). \tag{7.5}$$

The Wigner function can be calculated numerically from the expansion of the Fock states in terms of the X coordinate, which are the energy eigenstates of the harmonic oscillator in position representation, i.e., expressed in terms of Hermite polynomials. The calculation proceeds by doing the Fourier transform [68]

$$W(X, Y) = \int \mathrm{d}x' \langle X - x'|\rho|X + x' \rangle \mathrm{e}^{2iYx'}. \tag{7.6}$$

A fast Fourier Transform can be used to implement this algorithm [69]. We use the function provided in the Quantum Optics Toolbox [70]. The density operator, ρ, for the steady state of the system is used to calculate the Wigner functions shown in Figure 7.2. There we can see how the Wigner function behaves as λ increases across the phase transition. The two peaks represent the macroscopic means of the X quadrature amplitude, obtained (approximately) by solving the semi-classical equations. The non-zero macroscopic mean for the Y quadrature amplitude causes the axis joining the two peaks to be tilted in relation to the X axis by an angle $\arctan[\langle Y \rangle / \langle X \rangle] \simeq \arctan[\kappa/\omega]$. This is the same angle which maximizes the squeezing and entanglement as seen in section 5.2.3.

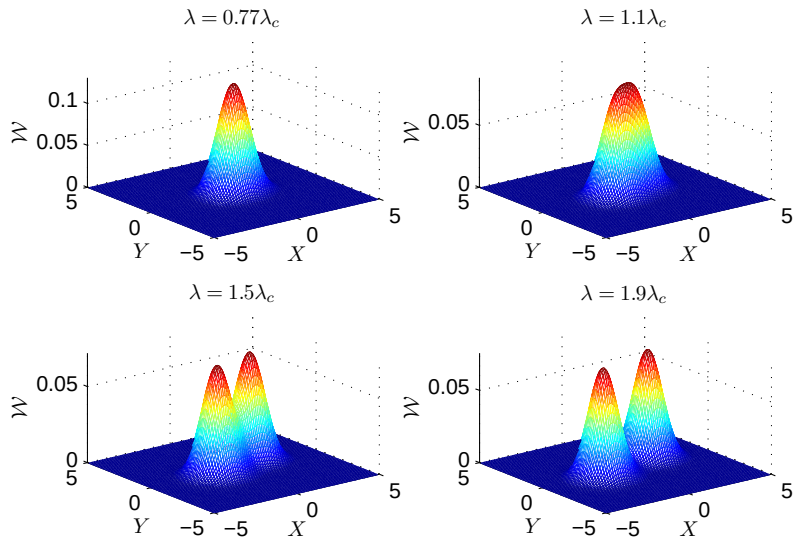

Figure 7.2.: Wigner function for the Dicke model across the phase transition

7.1.2. Spectra

The power spectra can be calculated from the correlation function, as given by equation (5.19). In this case the correlation function can be calculated from the evolution for the density matrix, formally written as

$$\langle \hat{a}^\dagger(\tau)\hat{a}\rangle_{ss} = \mathrm{Tr}_P\left[\hat{a}\mathrm{e}^{\mathcal{L}\tau}\left(\rho_{ss}\hat{a}^\dagger\right)\right], \tag{7.7}$$

where ρ_{ss} is the steady state density operator for the system, and $\mathcal{L}$ is the Liouvillian super-operator given by (5.23). Numerically, it can be calculated by diagonalizing the Liouvillian and expressing the operator $\rho\hat{a}^\dagger$ as a linear combination of its eigenoperators $\rho_1, \rho_2, \cdots$:

$$\langle \hat{a}^\dagger(\tau)\hat{a}\rangle = \mathrm{Tr}[\hat{a}\mathrm{e}^{\mathcal{L}\tau}\rho\hat{a}^\dagger] = \mathrm{Tr}[\hat{a}\sum_i \mathrm{e}^{s_i\tau}C_i\rho_i], \tag{7.8}$$

where s_i are the eigenvalues of $\mathcal{L}$. This will return the solution of $\langle \hat{a}^\dagger(\tau)\hat{a}\rangle$ as an exponential series $\sum_i \tilde{c}_i\mathrm{e}^{s_i\tau}$. The spectrum is then given by the Fourier transform of this

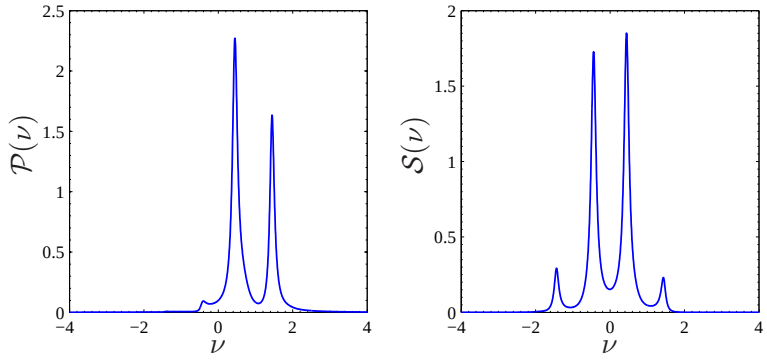

Figure 7.3.: Power and probe spectrum 2 atoms $\lambda = 0.5$

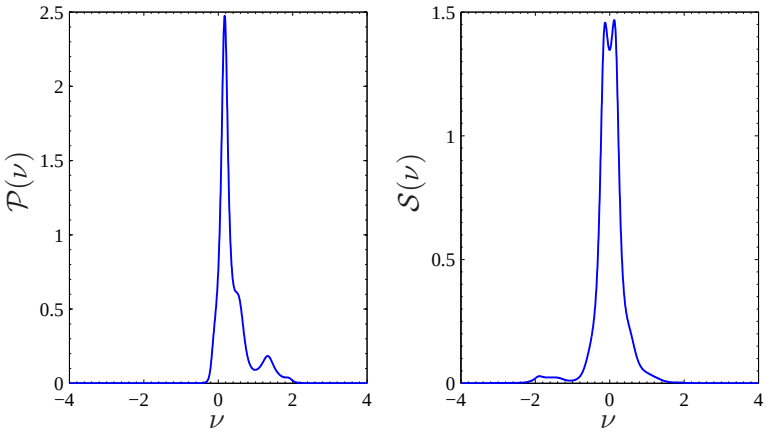

Figure 7.4.: Power and probe $\lambda = 0.7$

function

$$\mathcal{S}(\nu) = \sum_i \frac{\tilde{c}_i}{i\nu - s_i}. \tag{7.9}$$

By using this method we have to calculate the eigenvectors and eigenvalues of the Liouvillian, which is a square matrix of dimension $(M(N+1))^2$, with M the dimension of the truncated Fock space for the field. Alternatively, for larger problems, we can propagate the master equation

$$\frac{\mathrm{d}\left(\rho\hat{a}^\dagger\right)}{\mathrm{d}t} = \mathcal{L}\left(\rho\hat{a}^\dagger\right), \tag{7.10}$$

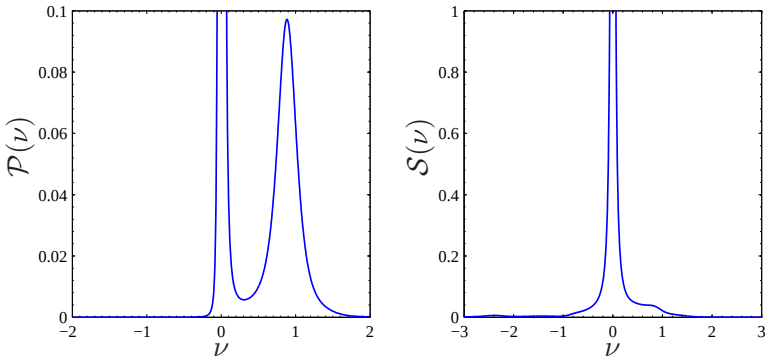

Figure 7.5.: Power and probe spectrum $\lambda = 0.9$

with the initial condition $\rho(0) = \rho_{ss}$, and calculate the mean value

$$\langle \hat{a}(t)\hat{a}^\dagger \rangle = \mathrm{Tr}\left(\hat{a}\left(\rho\hat{a}^\dagger\right)(t)\right)$$

at each time step, avoiding the calculation of eigenvalues of a big matrix. We used the quantum optics toolbox [70] to calculate the power and probe spectra for the Dicke model across the phase transition. The probe spectrum is calculated by propagating (or calculating the exponential expansion of)

$$\frac{\mathrm{d}}{\mathrm{d}t}\left(\rho\hat{a}^\dagger - \hat{a}^\dagger\rho\right) = \mathcal{L}\left(\rho\hat{a}^\dagger - \hat{a}^\dagger\rho\right). \tag{7.11}$$

In Figure 7.3 we show the spectrum for two atoms below the critical λ. The structure is the same as that seen for the thermodynamic limit $\lambda < \lambda_c$; we can define a critical value of the coupling, λ_c, for a finite number of atoms at which the Wigner function develops two maxima. We have no analytical expression for λ_c, however. For coupling sufficiently large the spectra show a peak at zero frequency, signaling the large scale dynamics as the state of the system switches between the two peaks. The dynamical behaviour associated with this switching will be explored in the quantum trajectory theory. The spectrum shows the switches as a peak at $\nu = 0$, corresponding to the degeneracy of the corresponding eigenvalue – zero imaginary part of the eigenvalue of $\mathcal{L}$. The real part of the Liouvillian eigenvalue, which gives the mean time between the switches, determines the broadness of the peak. Well above the critical λ the mean

switching time becomes longer. In the linearized treatment these features do not appear as we are studying the fluctuations around one of the mean values. For a large number of atoms the switching time becomes longer and the system loses this large scale dynamics for $N \to \infty$.

7.2. Quantum trajectory simulations

In this section we present the results obtained from simulations using the quantum trajectory theory. In Appendix B we present the basic ideas of quantum trajectory theory and show the derivation of the equations used to simulate the Dicke model subjected to homodyne and heterodyne measurement schemes. A short description of these measurement schemes is presented below.

7.2.1. Homodyne and heterodyne measurements

The core idea of quantum trajectory theory is to generate a record of possible measurement outcome. To do so we use the information from the system – the probabilities calculated from the state – and introduce measurement feedback into the state of the system, e.g., through the jump operators $\hat{J}$ for the case of photodetection. We obtain the state of the system, but we gain also an extra piece of information: the detection record. The record determines how the measurement affects the state of the system, and the choice of the particular measurement scheme depends on the quantity of interest.

The photo-detection measurement scheme described in Appendix B can give information about photon statistics. For example, to obtain the waiting time distribution, a simulation is carried out and the time interval between photo-detections is recorded. The waiting time distribution obtained this way can be calculated also directly from the master equation [71, Chapter 12], but such approach, however, may not be easily extended for other measurement schemes. Other treatments giving stochastic stochastic Schrödinger equation can be seen for example in [22].

A homodyne measurement allows the experimenter to learn about the quadrature

amplitudes of the field [72]. It is done by introducing a local oscillator field, as shown in Figure 7.6. There, a classical field with complex amplitude $e^{i\theta}\mathcal{E}$ is mixed with the signal

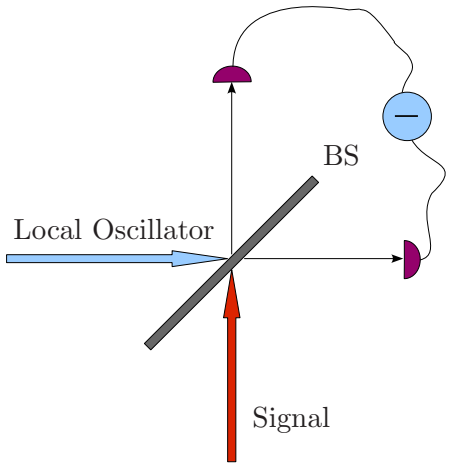

Figure 7.6.: Scheme for homodyne/heterodyne detection

field $\hat{a}$ we intend to measure. The frequency of the local oscilator is the same as that of the mode being detected (homos from the Greek – "the same"). For the two arms of the beam splitter we have, in a rotating frame (and up to a constant factor),

$$\mathbf{E}_+ = e^{i\theta}\mathcal{E} + \hat{a}, \tag{7.12}$$

$$\mathbf{E}_- = e^{i\theta}\mathcal{E} - \hat{a}. \tag{7.13}$$

Each photo-detector measures the quantity $|\mathbf{E}_\pm|^2$, and the photo-currents are subtracted, leaving only the cross terms,

$$\hat{X}_\theta = 2\mathcal{E}\left(e^{i\theta}\hat{a} + e^{-i\theta}\hat{a}^\dagger\right). \tag{7.14}$$

This is the quantity being measured for the case of homodyne detection. The angle θ, which is the phase of the local oscillator, can be adjusted in order to measure any quadrature. Experimentally, the local oscillator field is typically taken from the lasers feeding the experiment by the use of a beam splitter.

For the heterodyne detection scheme the local oscillator field is far-detuned from the signal light. In this case the input signal is added to a high frequency signal (in a rotating

frame of mode frequency ω)

$$\mathbf{E}'_{\pm} = \hat{a} + \mathcal{E}\mathrm{e}^{-i\omega_{LO}t} \tag{7.15}$$

The same process will give the measured quantity

$$\hat{I} = \mathcal{E}\left(\hat{a}^{\dagger}\mathrm{e}^{-i\omega_{LO}t} + \hat{a}\mathrm{e}^{i\omega_{LO}t}\right), \tag{7.16}$$

where ω_{LO} is the local oscillator frequency relative to the mode. In this case, detection at frequency ω_{LO} returns the field amplitude $\hat{a}$, i.e., the intra-cavity field amplitude. The current appears as a carrier signal with amplitude and phase modulated given by $\langle\hat{a}\rangle = \langle X\rangle + i\langle Y\rangle$.

We show the derivation of the quantum trajectory evolution equations for homodyne/heterodyne detection in Appendix B. We obtain a stochastic Schrödinger equation, for the homodyne case, of the form

$$\mathrm{d}|\Psi\rangle = \left[\frac{1}{i\hbar}\hat{H}_C\mathrm{d}t + \mathrm{e}^{-i\theta}\hat{\mathcal{J}}\left(\langle\hat{X}_\theta\rangle(t)\mathrm{d}t + \mathrm{d}W(t)\right)\right]|\Psi\rangle, \tag{7.17}$$

where $\mathrm{d}W$ is a Wiener increment with the property $\mathrm{d}W(t)\mathrm{d}W(t') = \delta(t-t')\mathrm{d}t$, $\hat{\mathcal{J}}$ is the photo-detection operator (see Appendix B) given by

$$\hat{\mathcal{J}} = \sqrt{2\kappa}\hat{a} \tag{7.18}$$

and $\langle\hat{X}_\theta\rangle$ is the conditional (on state $|\Psi\rangle$) expectation value of the quadrature operator $\hat{X}_\theta$. The term $\mathrm{d}Q_{HET} = \langle\hat{X}_\theta\rangle(t)\mathrm{d}t + \mathrm{d}W$ is proportional to the detected homodyne current, which also depends on the intensity of the local oscillator field. The term $\mathrm{d}W$ comes from the shot noise introduced by the local oscillator.

The equation for the heterodyne detection scheme is similar, with

$$\mathrm{d}|\Psi\rangle = \left[\frac{1}{i\hbar}\hat{H}_C\mathrm{d}t + \mathrm{e}^{-i\theta}\hat{\mathcal{J}}\left(\langle\hat{\mathcal{J}}\rangle(t)\mathrm{d}t + \mathrm{d}Z(t)\right)\right]|\Psi\rangle, \tag{7.19}$$

but in this case the noise is complex, $\mathrm{d}Z(t) = \sqrt{1/2}(\mathrm{d}W_x + i\mathrm{d}W_y)$, and the charge deposited in the detector is $\mathrm{d}Q_{HET} = \langle\hat{\mathcal{J}}\rangle(t)\mathrm{d}t + \mathrm{d}Z(t)$. We are interested in recording the corresponding photo-current. We can model the detected photo-current by the equation

$$\mathrm{d}i(t) = -\frac{1}{\tau_D}(i(t)\mathrm{d}t - \mathrm{d}Q), \tag{7.20}$$

where dQ is the infinitesimal charge, whose explicit form depends on the measurement scheme. There are also other measurement schemes we could consider, such as, for example, a conditional detection scheme [73], which mixes photo-counts and homo/heterodyne detection. In that case the photo-current is related to the third order correlation function $\langle \hat{a}^\dagger \hat{a} \hat{X}_\theta \rangle$.

7.2.2. Results

Wigner Function

For the homodyne detection scheme the photo-current is proportional to the conditional expectation of the quadrature amplitude $\langle X_\theta \rangle$. We can calculate the stationary density

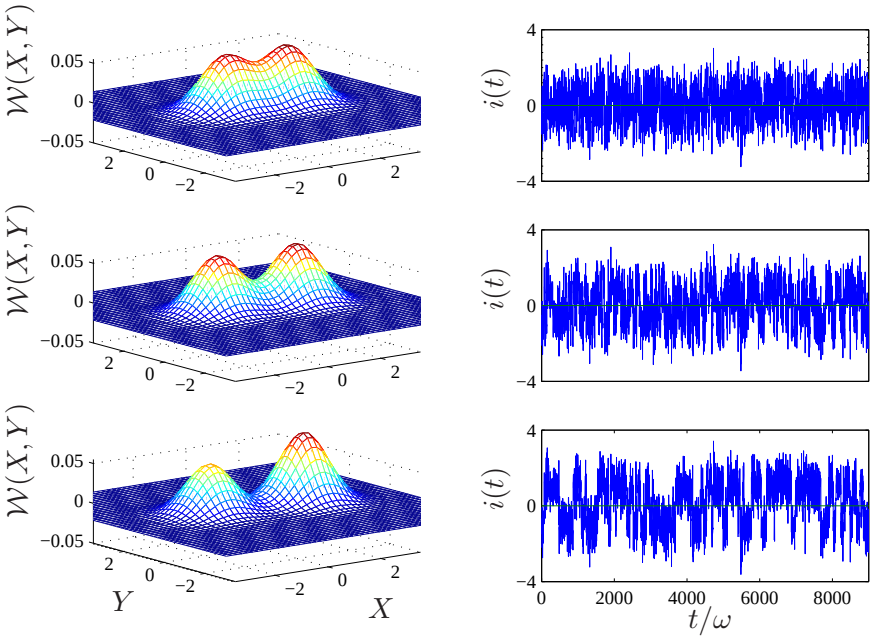

Figure 7.7.: Wigner function calculated in the quantum trajectory theory ($\omega = \omega_0 = 1, \kappa = 0.1$), (from the top: $\lambda = 0.8, 1, 1.2$).

matrix by averaging over the record of conditional states,

$$\bar{\rho}_{SS} = \sum_{REC} |\Psi\rangle\langle\Psi|, \tag{7.21}$$

where the bar denotes that the density matrix is unnormalized. The results are not different from those calculated using the Liouvillian operator formalism, but now we can observe the dynamics. In Figure 7.7 we show the Wigner function calculated from the record average, and the a sample of the homodyne current for $\theta = 0$. At this angle, the distribution of the sampled homodyne current represents the projection of the Wigner function along the X axis. Below λ_c, when the Wigner function has only one peak, the homodyne current, for this angle, shows noise centered at $i(t) = 0$ with dispersion proportional to the width of the Wigner function and the bandwidth of the filter. Once the peak splits, for λ well above λ_c, the current becomes a noisy square wave of amplitude proportional to the separation of the peaks in the Wigner function. We characterize the mean lifetime of each state later, but we see already that each of these states corresponds to a solution of the semi-classical equations, i.e., to the conditional expectation $\langle X \rangle$ having two possible values in the steady state.

Entanglement

The quantum trajectory theory provides a way of quantifying the entanglement between atoms and photons *depending on the measurement scheme*. Instead of following the analysis of section 5.2.3, we pay attention to the entanglement variation with the homodyne detection angle. To do so, we apply the method given in [67]. We aim at measuring the entanglement of a mixed state. As noted by [67] and references therein, the definition of a measure of entanglement for mixed states is based on the decomposition of a mixed state in an ensemble of pure states $|\psi_i\rangle$,

$$\rho = \sum_i p_i |\psi_i\rangle\langle\psi_i|. \tag{7.22}$$

The choice of the basis $|\psi_i\rangle$ is arbitrary and leads to different definitions for the measure of entanglement. The measure of entanglement for pure states, however, is unambiguously defined by the von Neumann entropy, to the advantage of quantum trajectory theory, which expresses mixed states as ensembles of pure states. The entanglement in the quantum trajectory theory is defined as and average over records of the von Neumann

entropy of particular records,

$$E_U = -\mathrm{Tr}_B \left[\rho^B_{REC} \log_2(\rho^B_{REC})\right], \tag{7.23}$$

where $\rho^B_{REC} = \mathrm{Tr}_A(\rho_{REC})$, is the density matrix for one part of the system, calculated for a given realization of the stochastic Schrödinger equation. Such a definition limits the possible decompositions of the density operator to those which are relevant to the chosen measurement scheme.

Entanglement was calculated varying the homodyne detection angle θ. Figures 7.8 and 7.9 show examples of the homodyne current, the entanglement, given by Eq. (7.23), calculated at each time step, and the conditional expectation of $\hat{J}_x$. Note the difference between the two homodyne currents as the angle is changed by 90^o. Close to 5^o the current shows pronounced switches between two distinct values; the homodyne measurement, made essentially along the X axis, is able to distinguish between the two semiclassical amplitudes located at X_0 and $-X_0$. The optimal axis is tilted slightly from 0^o as the losses introduce a small Y component to the steady state amplitudes (in the semi-classical equations $Y = (\kappa/\omega)X$). Specifically, the optimal angle is close to $\arctan[\kappa/\omega] = 5^o$. For an angle close to the Y quadrature, the measurement cannot distinguish between the two amplitudes and the switching behaviour is lost. More interesting is the effect of a change in the homodyne detection angle on the entanglement of the system. We see that the entanglement is destroyed whenever we are able to distinguish, via the measurement, between the two amplitudes. For the intervals where the switching is occurring, both amplitudes "coexist" for a very short time, during which the entanglement is close to one.

The entanglement may also have a persistent non zero mean. In particular, for the angle where the two amplitudes cannot be distinguished, $\theta \approx 95^o$, the measurement preserves the entanglement, avoiding collapse to one of the macroscopic states of the field. We learn also that the state of the atoms is highly correlated with the field. That is, for $\lambda > \lambda_c$, the steady state is described essentially by $|-\ell\rangle_x|X_\theta\rangle + |+\ell\rangle_x|-X_\theta\rangle$, where $|\ell\rangle_x$ is a Dicke state, eigenvector of the operator $\hat{J}_x$, and $|X_\theta\rangle$ is a field state, eigenvector of the quadrature operator X_θ. In the figures, the coupling strength chosen is $\lambda = 1$,

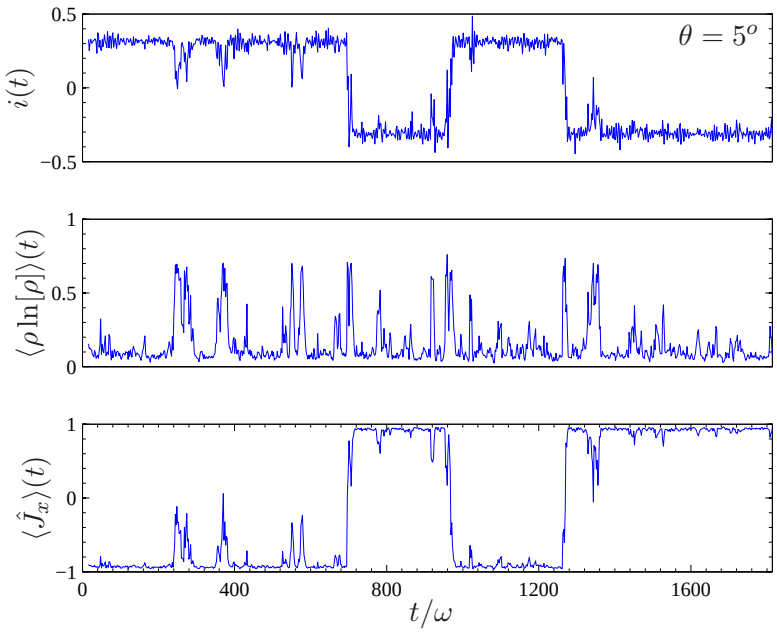

Figure 7.8.: Homodyne current for $\theta = 5^o$ ($\omega = \omega_0 = 1, \lambda = 1, \kappa = 0.1$)

making the amplitudes $\pm X_\theta$ well separated. We can make a study of the entanglement varying the homodyne angle around 95^o. In Figure 7.10 we plot the mean entanglement, E_U, averaged over a long time realization (usually of the order of $10^4/\omega$). We can see that the mean entanglement has a maximum for $\theta \approx \arctan[\kappa/\omega] = 95^o$, which becomes sharper as the separation between $\pm X_\theta$ increases. With the X component becoming larger, the angle of maximum entanglement moves slightly towards 90^o, corresponding to the limit $\kappa \to 0$.

In Figure 7.10 the angle is kept constant while λ is varied. The maximum entanglement occurs close to λ_c, and vanishes as the homodyne measurement for $\theta = 5^o$ selects one of the peaks. Again, the angle that maximizes the entanglement changes as λ increases, as demonstrated in Figure 7.12; there, an increase in λ corresponds to the peaks of the Wigner function being translated along the $\langle X \rangle$ axis (from darker to brighter circles in Figure 7.12). The angle for maximum entanglement, $\theta + \pi/2$, is such that both peaks of the Wigner function, in a coordinate system rotated by an angle θ in relation to the

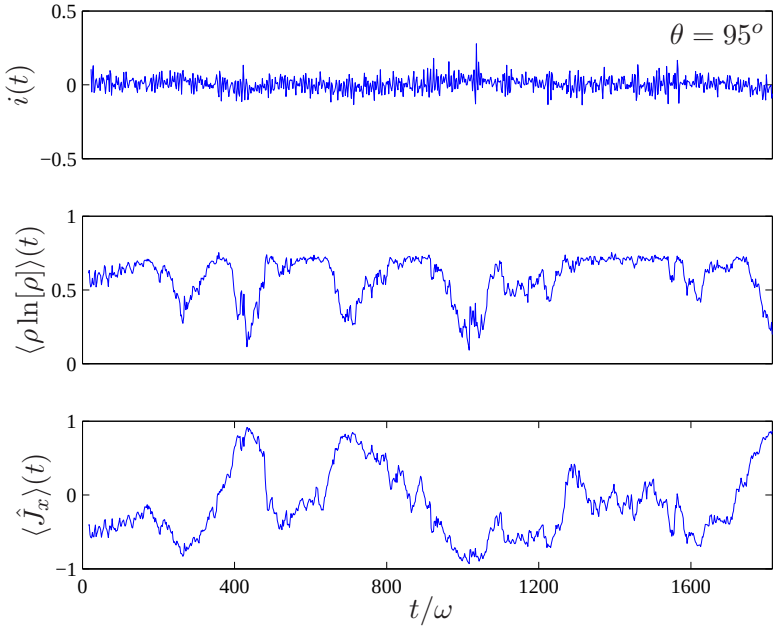

Figure 7.9.: Homodyne current for $\theta = 95^o$ ($\omega = \omega_0 = 1, \lambda = 1, \kappa = 0.1$)

original axis, have the maximum overlap in the ordinate axis $X_{\theta+\pi/2}$. The choice of the homodyne angle becomes more critical as λ increases, this explains the decrease in the entanglement for a fixed angle, as shown in 7.11.

Switching dynamics

The heterodyne scheme measures the intracavity operator $\hat{a}$, and can be used to retrieve the power spectrum (contaminated by shot noise) from the correlation function $\overline{i(t)i(t+\tau)}$. We show in Figure 7.13 the real and imaginary heterodyne current record as λ increases. The current visits the two sites corresponding to the peaks in the Wigner function. The heterodyne current record can be used to reconstruct the Q function from the probability $P(X, Y)$ of the current visiting the site $X + iY$; this measurement, however, is affected by the bandwidth of the filter, $1/\tau$. Large bandwidths allow unwanted noise to come in, while very small bandwidths cut off the quantum fluctuations we are interested in – we find the optimal bandwidth corresponds to $\tau = 1$. Thus, reconstructing

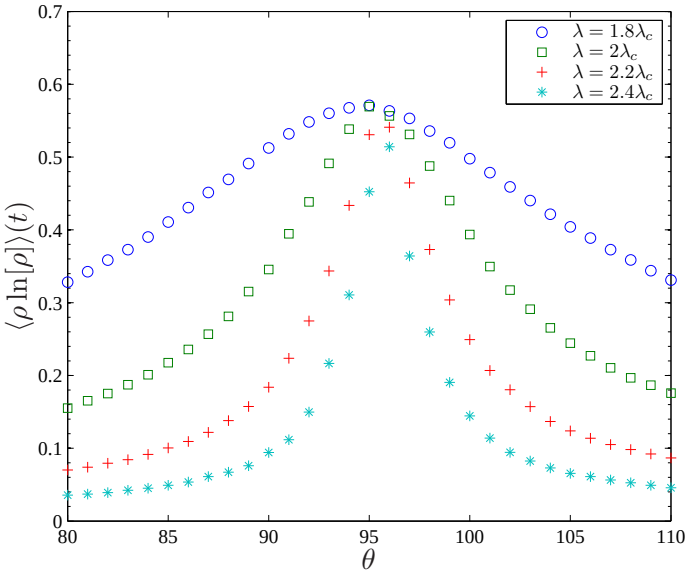

Figure 7.10.: Entanglement vs. θ ($\omega = \omega_0 = 1, \kappa = 0.1$)

the Q function from the heterodyne current is not an straightforward exercise.

In Figures 7.14 and 7.15 we show two dimensional histograms with the counts of the number of visits to the sites of the complex plane. The results become more accurate as the trajectories run longer, as the current visits a larger region in phase space. This brings computational problems for higher numbers of atoms, as the time between the switches becomes larger and more simulation time is needed to get accurate results.

The switching time is also observed to increase with λ. As we saw in Chapter 5, with the inclusion of a reservoir coupled to the system, the eigenvalues of the Liouvillian acquire a real part, introducing an exponential decay in the evolution of the density matrix. The two eigenstates of the system corresponding to the peaks seen in the Wigner function become unstable. On a short timescale, the steady state system presents only one of the peaks, corresponding to one of the X values in the semi-classical equations. As the evolution unfolds over longer times, the state switches, and the sign of X changes – hence the square wave behaviour seen in the heterodyne current. We can study the time distribution of the switches. Define the conditional probabilities of switching, P_{+-},

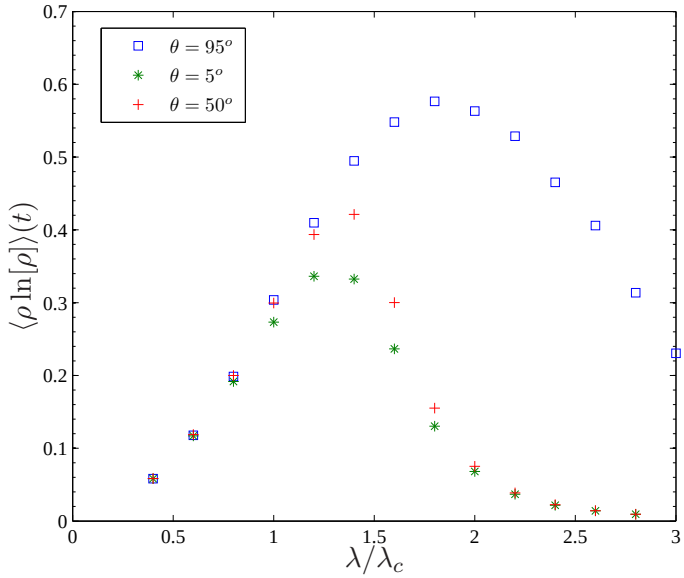

Figure 7.11.: Entanglement vs λ for different θ ($\omega = \omega_0 = 1, \kappa = 0.1$)

and remaining in the state with mean quadrature amplitude $\pm\langle X\rangle_{ss}$, P_{++} or P_{--}, by

$$P_{+-} = P(\pm, t|\mp, t_0 = 0) = 1 - \mathrm{e}^{-st}, \tag{7.24}$$

$$P_{\pm\pm} = P(\pm, t|\pm, t_0 = 0) = \mathrm{e}^{-st}. \tag{7.25}$$

The (inverse) lifetime is given by the eigenvalue of the Liouvillian with the smallest real part, s. The switching probability per unit of time is given by

$$\frac{\mathrm{d}P_{+-}}{\mathrm{d}t} - \frac{\mathrm{d}P_{++}}{\mathrm{d}t} = p_{\mathrm{switch}}(t) = 2s\mathrm{e}^{-st}. \tag{7.26}$$

The mean switching time is then given by

$$\bar{t} = \int_0^\infty t p_{\mathrm{switch}}(t)\mathrm{d}t = 2s\left(-\frac{\mathrm{d}}{\mathrm{d}s}\right)\int_0^\infty \mathrm{e}^{-st}\mathrm{d}t, \tag{7.27}$$

performing the integral and the derivation gives a mean switching time of $2/s$. We simulated the heterodyne measurement scheme, recording the time taken between consecutive switches, and used this data to generate figures like 7.16 and 7.17. In Figure 7.16, $\lambda = 1.05$, defining an operation condition well above the critical point, but small

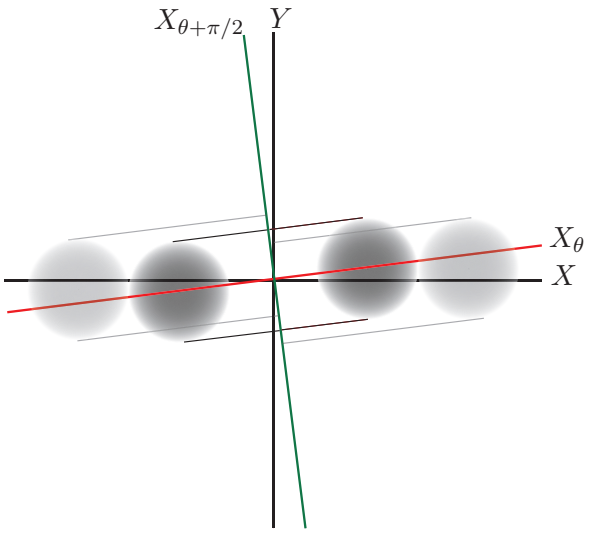

Figure 7.12.: Homodyne Detection and Wigner function

enough so that switching is frequent. The large number of switches allows a good exponential fit. In Figure 7.17, $\lambda = 1.35$, and the average time interval between switches becomes bigger, so the simulation had to run for much longer times in order to obtain a fairly smooth fit (it also required a larger Fock basis, making the computations even slower[1]. In Figure 7.18 we plot the comparison of the mean lifetime obtained from the simulation and $2/s$. Error bars representing the standard deviation from a exponential distribution are included so the quality of the exponential fit is known. Agreement is good at low values of λ, but it becomes computationally harder to obtain convergence for values of λ greater than 1.2. These results shown the equivalence between the quantum trajectory formalism and the full master equation approach.

[1]Problems with the random number generators reaching their repetition period are also a concern for longer simulations

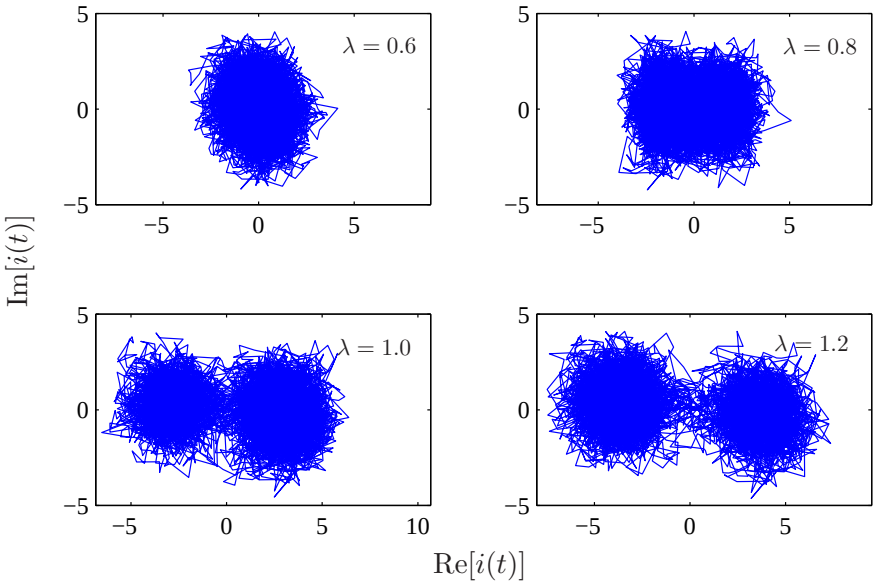

Figure 7.13.: Heterodyne current across the phase transition ($\omega = \omega_0 = 1, \kappa = 0.1$).

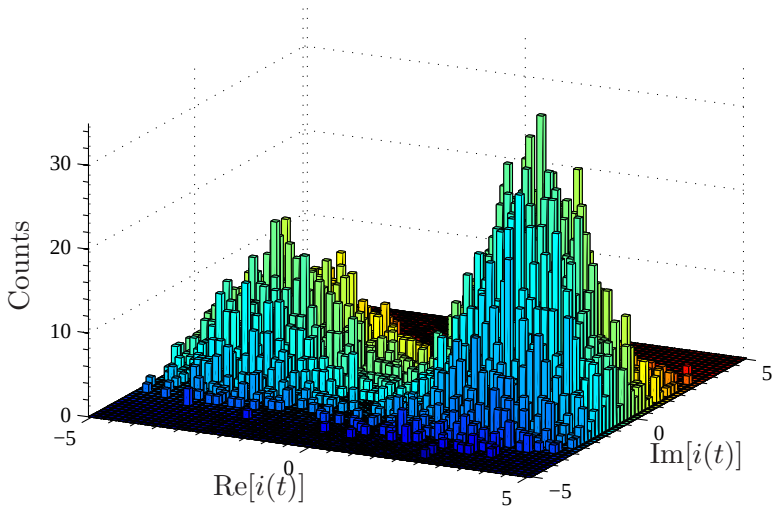

Figure 7.14.: Histogram for heterodyne current ($\omega = \omega_0 = 1, \lambda = 1, \kappa = 0.1$)

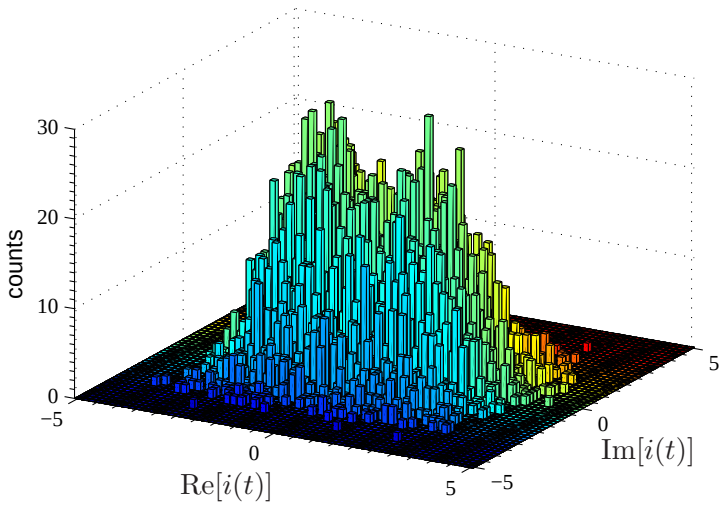

Figure 7.15.: Histogram for heterodyne current ($\omega = \omega_0 = 1, \lambda = 0.8, \kappa = 0.1$)

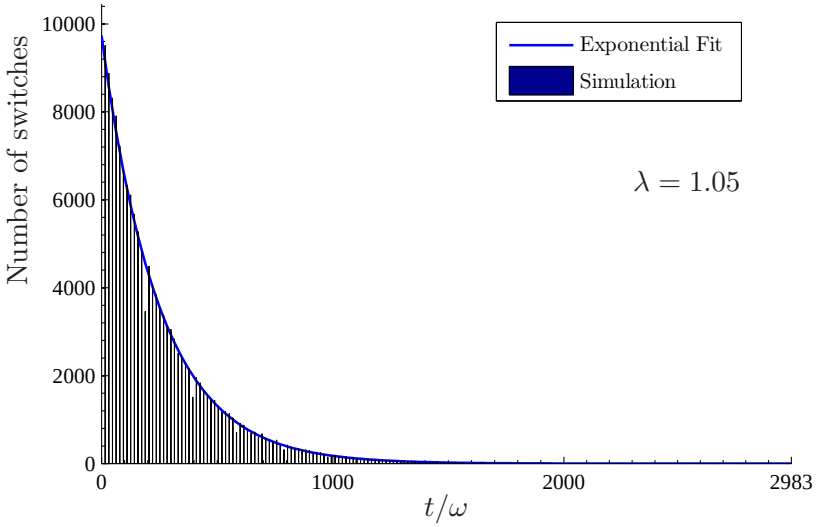

Figure 7.16.: Number of switches vs. time interval ($\omega = \omega_0 = 1, \kappa = 0.1$)

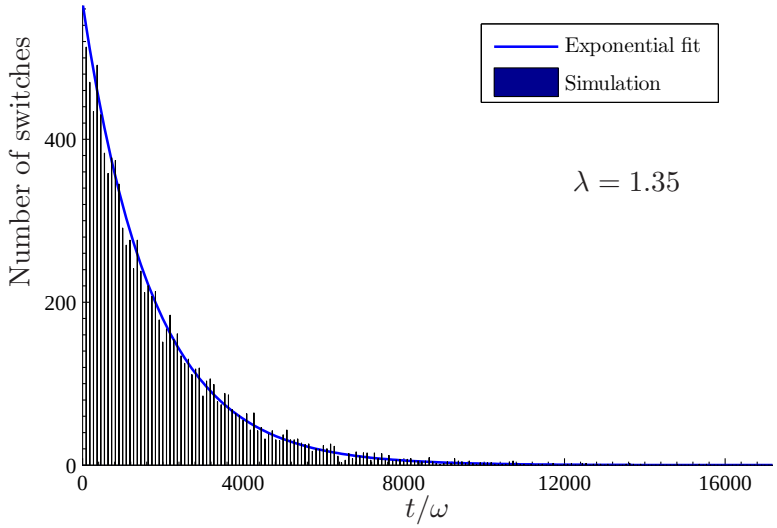

Figure 7.17.: Number of switches vs. time interval ($\omega = \omega_0 = 1, \kappa = 0.1$)

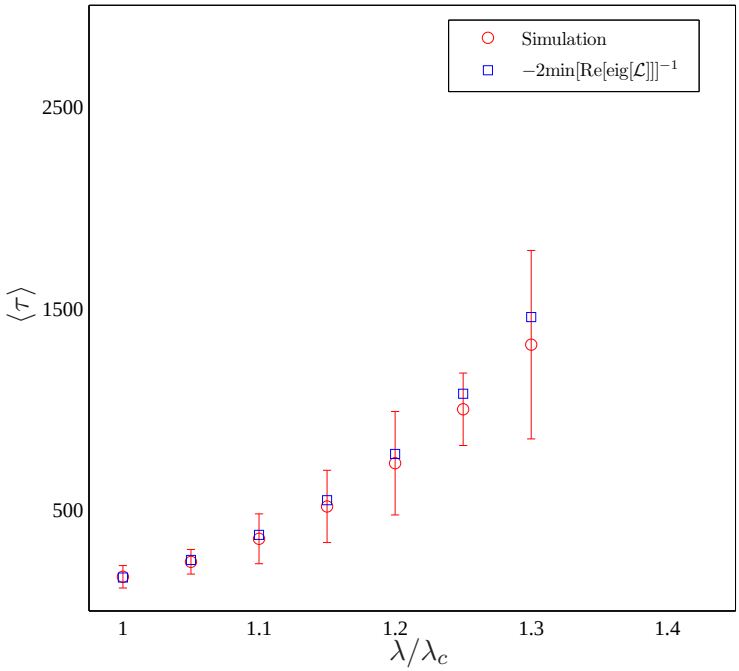

Figure 7.18.: Mean lifetime compared with the real part of eigenvalue of ρ ($\omega = \omega_0 = 1, \kappa = 0.1$)

8. Conclusion

8.1. Summary

In this thesis we presented an extensive account of the Dicke model through several possible quantum optical approaches. Our aim was to investigate this model on several scales and learn different techniques which can be applied to a whole plethora of problems in quantum optics. Our first step was to review the basic Dicke model in quantum optics with the introduction of the Dicke states, Dicke Hamiltonian and master equation. We also stated the problem in its experimental context. Until very recently, it was out of the question to implement a quantum optical system where the rotating wave approximation was not valid. As we explained, the main problem is to achieve the regime where λ is of the order of the field frequency ω. Such a regime still can be pursued, but it would fall outside the scope of this work as other effects would have to be accounted for, e.g. the inclusion of the $\mathbf{A}^2$ term in the Hamiltonian, which destroys potentially interesting effects. The system we envisage still is in the strong coupling regime. The counter rotating terms are included by adding a Raman channel to obtain an effective Hamiltonian with coupling of comparable order of magnitude as the field frequency. The counter rotating terms are non-energy conserving, but the energy non-conservation is accounted for by the external source driving the transitions $\hat{a}^\dagger \hat{J}_+$ and $\hat{a}\hat{J}_-$. This effective Hamiltonian gives rise to a non-equilibrium quantum phase transition. Historically, this phenomenon was first studied in statistical quantum mechanics by Heep and Lieb, for historical consistency, we presented their results for finite temperature.

Our research work started with a phase space study of the Dicke model. We used the Holstein-Primakoff representation in order to obtain an accurate description of the

system in the thermodynamical limit. This was a textbook application of quantum optics techniques for obtaining the spectra and second order momenta, which gave information about spectra, entanglement and squeezing. We carried on the study of the Dicke model in its phase space form by using the extended version of the Haken representation for two level atoms. In this case our aim was to reproduce the results in the Holstein-Primakoff with the advantage of obtaining all moments directly in the atomic variables. In this endeavor we found the linearized version of the Haken representation does not conserve the total angular momentum and therefore fails to reproduce second order moments correctly.

The phase space approach is usually of use for treating problems in the thermodynamic limit, where quantum jumps become small compared to the quantities of interest – more generally, the equations obtained include derivatives of order > 3. The introduction of the atomic coherent states representations gave rise to a Fokker-Planck equation, when interpreted in the Positive-P sense, which could be simulated exactly for any number of atom. The simulations showed the problems usually associated with the use of the Positive-P representation – large fluctuations and numerical instabilities – and were of use to calculate the means of the atomic quantities for N of the order of 10^5 atoms, but teeming with fluctuations for as N as large as $N = 10^3$.

Our last presentation was the quantum trajectory theory applied to the Dicke model. The advantage of this approach is to give a clear picture of the system under a feasible detection scheme – we employed heterodyne and homodyne detection schemes. Its computational advantages allowed us to obtain the averages and variances for as many as 100 atoms. We were able to observe the sharpening of the transition mean values across the phase transition in this case.

The Homodyne detection scheme in the quantum trajectory theory provided a way of measuring how the measurement process preserves/destroys the entanglement in the system. We also used the heterodyne measurement scheme to compute the statistics of the switching times. We explored the technique in some detail and showed how the simulated measurement records may be used to retrieve information about the quantum

state of the system

8.2. Future directions

With the advantage of hindsight we are able to point some the strengths and weaknesses of this work. On the one hand, using such a broad range of techniques to study one subject has the risk of focusing on the methods rather than on the actual physical system. On the other hand, it provides a strong background for pointing future directions. Contemplating all we have done with the present knowledge we see that each chapter could be extended to become a thesis in its own right. We present the possible paths which could have been taken for each chapter

Chapter 2 As we noted, the modeling of the system plus reservoir approach for a system where the rotating wave approximation does not hold is an open problem. With the proposal we presented here this may become an important research topic in the future.

Chapter 3 The similarities with the Ising model can be further explored, following the same lines as were used to show that the optical parametric oscillators have the same universality as a Lifshitz magnetic phase transition [74].

Chapter 4 We can study other implementations of such a system. Figure 8.1 shows a similar switching behaviour in RNA folding experiments, where one observes the same exponential distribution as we verified in our model [1]. The Dicke model also describes polarization waves in active media, as seen in [75]. It is very likely that our model has some common feature with many classical-chaotic systems.

Chapter 5 The Holstein-Primakoff formalism can be applied to the Dicke model with an extra driving field. Alternatively, we can try to express the angular momentum operators as combinations of two bosonic operators, as, e.g., $\hat{J}_z = \hat{b}^\dagger \hat{b} - \hat{a}^\dagger \hat{a}$.

Chapter 6 The linearization in the Haken representation can be done by writing a system of partial differential equations, to replace the terms $\mathrm{e}^{\frac{\partial}{\partial \mu}}$. This could work for

$N \sim 10^3$. We could have used a different approach from the Positive-P representation for the coherent atomic states representation. Indeed, there is a plethora of phase space methods which heal the equations from its instabilities. This representation can be a good opportunity to try to describe the system in a mesoscopic regime.

Chapter 7 We could have studied more extensively the behaviour of the system for large numbers of atoms. We could have used the homodyne and heterodyne current records to calculate the power and squeezing spectrum, for an increasing number of atoms. We could also have implemented conditional homodyne detection scheme in order to observe the giant violation of Bell inequalities as seen in [73].

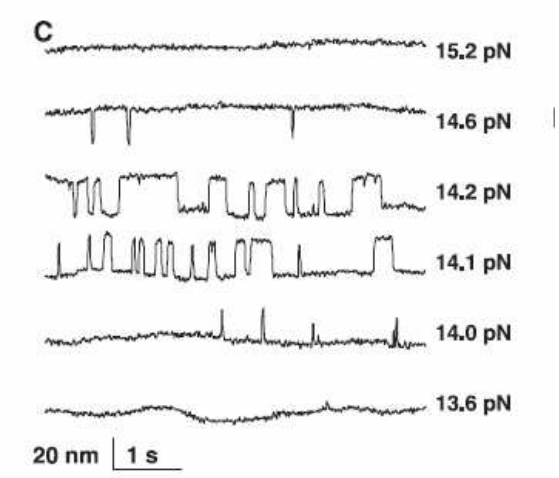

Figure 8.1.: Folding of protein with time (from [1])

In conclusion, we can identify the principal areas of interest of this work as the quantum to classical transition to mesoscopic systems, and the universality and complexity of models in quantum optics.

A. Diagonal operators and symmetry in the Dicke model

A.1. Bogouliubov transformation

In the Holstein-Primakoff representation the general form of the system Hamiltonian is

$$\begin{aligned}\hat{H} =&\omega_a \hat{a}^\dagger \hat{a} + \omega_b \hat{b}^\dagger \hat{b} + \lambda \left(\hat{a}^\dagger + \hat{a}\right)\left(\hat{b}^\dagger + \hat{b}\right) \\ =&\frac{1}{2}\left(\omega_a^2 \hat{x}^2 + \hat{p}_x^2 + \omega_b^2 \hat{y}^2 + \hat{p}_y^2 + 4\lambda\ \sqrt{\omega_a \omega_b}\hat{x}\hat{y}\right) + \text{constants},\end{aligned} \tag{A.1}$$

where $\hat{x}, \hat{y}, \hat{p}_x$ and $\hat{p}_y$ are the normalized position and momentum operators, given by the transformations

$$\hat{x} = \frac{1}{\sqrt{2\omega_a}}(\hat{a}^\dagger + \hat{a}), \tag{A.2}$$

$$\hat{p}_x = i\sqrt{\frac{\omega_a}{2}}(\hat{a}^\dagger - \hat{a}), \tag{A.3}$$

$$\hat{y} = \frac{1}{\sqrt{2\omega_n}}(\hat{b}^\dagger + \hat{b}), \tag{A.4}$$

$$\hat{p}_y = i\sqrt{\frac{\omega_a}{2}}\left(\hat{b}^\dagger - \hat{b}\right). \tag{A.5}$$

This is the general form taken by Hamiltonians (5.6) and (5.10), and it corresponds to two coupled harmonic oscillators. We can put it in diagonal form by considering

$$\hat{H} = \begin{pmatrix} \hat{x} & \hat{y} \end{pmatrix} \begin{pmatrix} \omega_a & 2\lambda\sqrt{\omega_a\omega_b} \\ 2\lambda\sqrt{\omega_a\omega_b} & \omega_b \end{pmatrix} \begin{pmatrix} \hat{x} \\ \hat{y} \end{pmatrix} + \hat{p}_x^2 + \hat{p}_y^2 \tag{A.6}$$

Let us introduce $\hat{q}_1$ and $\hat{q}_2$ as the eigenvectors of the square matrix, with eigenvalues ε_+^2 and ε_-^2 given by equations (5.8) and (5.13), which depend the regime the system is in.

In the diagonal basis the Hamiltonian becomes

$$\hat{H} = \frac{1}{2}\left(\varepsilon_-^2 \hat{q}_1^2 + \varepsilon_+^2 \hat{q}_2^2 + \hat{p}_1^2 + \hat{p}_2^2\right). \tag{A.7}$$

The eigenvectors $\hat{q}_1$ and $\hat{q}_2$ can be written as

$$\begin{pmatrix} \hat{q}_1 \\ \hat{q}_2 \end{pmatrix} = \begin{pmatrix} \cos(\theta) & \sin(\theta) \\ -\sin(\theta) & \cos(\theta) \end{pmatrix} \begin{pmatrix} \hat{x} \\ \hat{y} \end{pmatrix}, \tag{A.8}$$

where the rotation angles are given by

$$\theta = \frac{1}{2}\arctan\left(\frac{4\lambda\sqrt{\omega_a\omega_b}}{\omega_b^2 - \omega_a^2}\right). \tag{A.9}$$

We can now write the modes $\hat{q}_1$ and $\hat{q}_2$ in terms of new quantized operators, written as $\hat{c}_{1(2)}$ in equation (5.7), or $\hat{e}_{1(2)}$ in (5.12), depending on whether we are treating the normal or superradiant phase (we call them $\hat{c}$ for convenience):

$$\hat{c}_{1(2)} = \frac{1}{2}\left(\sqrt{2\varepsilon_{-(+)}}\hat{q}_{1(2)} + i\sqrt{\frac{2}{\varepsilon_{-(+)}}}\hat{p}_{1(2)}\right). \tag{A.10}$$

Written in terms of these operators, the Hamiltonian takes the form of (5.12) and (5.7). The expression for $\hat{c}_{1(2)}$ in terms of $\hat{a}$, $\hat{b}$, $\hat{a}^\dagger$ and $\hat{b}^\dagger$ can be calculated easily as

$$\hat{c}_1^\dagger = \frac{1}{2}\left(\frac{\cos(\theta)}{\sqrt{\omega_a\varepsilon_-}}\left((\varepsilon_- + \omega_a)\hat{a}^\dagger + (\varepsilon_- - \omega_a)\hat{a}\right) - \frac{\sin(\theta)}{\sqrt{\omega_b\varepsilon_-}}\left((\varepsilon_- + \omega_b)\hat{b}^\dagger + (\varepsilon_- - \omega_b)\hat{b}\right)\right), \tag{A.11}$$

$$\hat{c}_2^\dagger = \frac{1}{2}\left(\frac{\sin(\theta)}{\sqrt{\omega_a\varepsilon_+}}\left((\varepsilon_+ + \omega_a)\hat{a}^\dagger + (\varepsilon_+ - \omega_a)\hat{a}\right) + \frac{\cos(\theta)}{\sqrt{\omega_b\varepsilon_+}}\left((\varepsilon_+ + \omega_b)\hat{b}^\dagger + (\varepsilon_+ - \omega_b)\hat{b}\right)\right), \tag{A.12}$$

where $\varepsilon_\pm$ are given by (5.8) and (5.13), depending on the system phase, $\omega_a = \omega$, and $\omega_b = \omega_0$ for the normal phase, while for the superradiant phase,

$$\omega_b = \frac{\omega_0}{2}\left(1 + \frac{\lambda^2}{\lambda_c^2}\right). \tag{A.13}$$

The rotation angle is given by

$$\theta = \begin{cases} \frac{1}{2}\arctan\left(\frac{4\lambda\sqrt{\omega\omega_0}}{\omega_0^2 - \omega^2}\right) & \text{if } \lambda < \lambda_c \\ \\ \frac{1}{2}\arctan\left(\frac{2\mu^2\omega\omega_0}{\omega_0^2 - \mu^2\omega^2}\right) & \text{if } \lambda > \lambda_c \end{cases} \tag{A.14}$$

For $\lambda = 0$ we have $\theta = 0$ in the normal phase, and the operator $\hat{c}_1^\dagger$ depends upon the operators $\hat{a}^\dagger$ and $\hat{a}$ only. At resonance we have that $\theta = \pi/4$ and the normal modes are composed of both $\hat{a}$ and $\hat{b}$ operators.

A.2. Symmetry in the Dicke model

Quantum phase transitions are a result of a break in the symmetry of the system. Above we saw how the operators $\hat{c}_1$ and $\hat{c}_2$ change their nature as the system enters the superradiant regime. We can study the break in symmetry by introducing the parity operator

$$\Pi = \exp\left[i\pi\left(\hat{a}^\dagger\hat{a} + \hat{J}_z + \ell\right)\right] \tag{A.15}$$

This operator commutes with the Dicke Hamiltonian (4.36), having two eigenvalues $\pi = \pm 1$. Thus the eigestates of the Dicke Hamiltonian are divided in two subspaces depending upon the number of excitations, $\hat{a}^\dagger\hat{a} + \hat{J}_z + \ell$, is even or odd. The eigenstates of Π are shown in Figure A.1 for $\ell = 5$, the circles represent $\pi = 1$ and the stars $\pi = -1$.

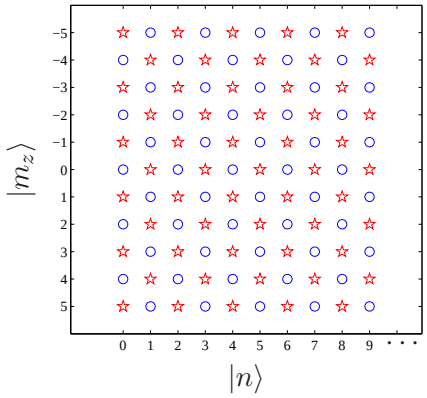

Figure A.1.: Set of eigenstates of Π

The break in the symmetry can be studied by writing Π in the Holstein-Primakoff

representation

$$\Pi = \exp\left(i\pi\left(\hat{a}^\dagger\hat{a} + \hat{b}^\dagger\hat{b}\right)\right). \tag{A.16}$$

Below the critical λ the operators have no displacement, thus the operator given by (A.16) is a conserved quantity for $\lambda < \lambda_c$. In the superradiant phase, however, the operators are displaced, e.g. $\hat{a} \to \langle\hat{a}\rangle + \hat{\alpha}$ and the conserved quantity becomes

$$\Pi_{\text{Super}} = \exp\left(i\pi\left(\hat{\alpha}^\dagger\hat{\alpha} + \hat{\beta}^\dagger\hat{\beta}\right)\right). \tag{A.17}$$

Above the critical point, the operator (A.16) is not a conserved quantity anymore, demonstrating the change in symmetry that occurs at critical coupling.

B. Quantum trajectory theory and heterodyne/homodyne measurement schemes

B.1. Jumps and conditional evolution in quantum trajectory theory

In this appendix, we present a simple explanation of the main ideas behind the quantum trajectory theory [76, 71]. To this end, we apply the quantum trajectory theory to the simple phenomenon of spontaneous emission. The main idea of the quantum trajectory theory is to infer the state of the system from a simulated detection record. One of its advantages is that, in calculating the state of the system from a record of conditional probability, P_{REC}, and state, $|\psi_{\mathrm{REC}}\rangle$, with

$$\rho = \sum_{\mathrm{REC}} P_{\mathrm{REC}} |\psi_{\mathrm{REC}}\rangle\langle\psi_{\mathrm{REC}}|, \tag{B.1}$$

we need to evolve, as we see below, a state vector rather than a density matrix. This was particularly useful for generating Figure 7.1. For 100 atoms and a Fock basis truncated at $n = 100$ we simulated a state with only 100×101 elements, instead of a density matrix of $100^2 \times 101^2$. Also important is the possibility of simulating the experimental setup, taking into account the measurement back action on the system. This is of fundamental importance in quantifying the entanglement in a system subjected to an *actual measurement scheme* (as seen, e.g., in [67, 77] and [20]).

Quantum trajectory theory can be thought of as an application of Bayes' theorem

to quantum physics; the aim of Bayesian inference is to learn future probabilities from prior ones, as expressed by

$$P(A|C) = \frac{P(C|A)P(A)}{P(C)}. \tag{B.2}$$

The event set is determined by the detection scheme we are interested in. For example, if we are interested in detect photons from spontaneous emission of a two level atom, we can define C as the event "no photon is detected", and A as the event "atom in the excited state". In addition, we define the events B_T for "photon detected at time T", and D, for "atom in the ground state". The probabilities $P(A)$ and $P(D)$ at time t can be written as,

$$P(A,t) = P(A|C)P(C) + \int_0^t P(A|B_T)P(B_T)\mathrm{d}t' \tag{B.3}$$

$$P(D,t) = P(D|C)P(C) + \int_0^t P(D|B_T)P(B_T)\mathrm{d}t'. \tag{B.4}$$

Notice that we do not assign a state for the system; we are obtaining information from the measurement events C and B_T only. It is easy to infer the conditional probabilities which make reference to the state of the system once a photon was detected – given that no superpositions of states are allowed – we have simply that

$$P(A|B_T) = 0 \tag{B.5}$$

$$P(D|B_T) = 1. \tag{B.6}$$

On the other hand we cannot infer the state of the system while no detection has happened. All we know is that, as time passes and no detection is made, the more certain it is that the atom is in the ground state. We use Bayes theorem to write

$$P(A|C) = \frac{P(C|A)P(A)}{P(C)} = \frac{P(A)}{P(C)}, \tag{B.7}$$

$$P(D|C) = \frac{P(C|D)P(D)}{P(C)} = \frac{P(D)}{P(C)}, \tag{B.8}$$

where we used the fact that $P(C|A) = 1$ and $P(C|D) = 1$. The probability $P(C)$ is given by $P(A,t) + P(D,t=0)$. We stress the fact that the analysis carried out so far

does not take into consideration coherence. The *conditional* density matrices, used to infer the state,

$$\rho(t) = P(C)\rho_C + \int_0^t P(B_T)\rho_{B_T}(t')\mathrm{d}t, \tag{B.9}$$

given by

$$\rho_C = |+\rangle\langle +|P(A|C) + |-\rangle\langle -|P(D|C), \quad \text{and} \tag{B.10}$$

$$\rho_{B_T} = |-\rangle\langle -|, \tag{B.11}$$

have only diagonal elements – we do not allow cross terms $|+\rangle\langle -|$.

Up to this point it may seem we are walking in circles; notice that the conditional probabilities were calculated in terms of the system probabilities, $P(A)$ and $P(D)$, but at no moment have we mentioned how to obtain these. This is the point where the physical dynamics of the system must be introduced; for the case of no coherence, this is given by the Einstein equations for quantum jumps, and for the full quantum description, by the Schrödinger equation. The events C and B_T are simulated from Monte Carlo rules; the whole process is summarized in the following diagram:

$$\hat{H}|\psi\rangle \underset{\text{State feedback}}{\overset{\text{Probabilities}}{\rightleftharpoons}} \text{Event} \xleftarrow{\text{Monte Carlo rules}} .$$

The system dynamics is used to calculate the probabilities, and Monte Carlo rules decide whether an event happens. This is equivalent to simulating an experimental record with the measurement back-action in the system – coming through ρ_D and ρ_{B_T}. For the jump in the spontaneous emission case, the solution of the Einstein equations gives $P(A,t) = P(A,0)\mathrm{e}^{-\gamma t}$, and $P(D,t) = 1 - P(A,t)$; we use the normalization condition,

$$P(C) + \int_0^t P(B_T)\mathrm{d}t' = 1, \tag{B.12}$$

to calculate $P(B_T,t) = \gamma\mathrm{e}^{-\gamma t}P(A,0)$. With all these probabilities, we can simulate the record by generating a stream of random numbers, r_i, and comparing them with the probability of an emission within a time interval Δt, given, in the Einstein quantum jumps view, by $\gamma\Delta t$. When $r_i < \gamma\Delta t$, the state of the system is assigned ρ_D; when this condition in not satisfied, signaling a photodetection, the system collapses to state

ρ_{B_T}. The process is repeated many times and the states obtained for each realization are summed and renormalized to obtain $\rho(t)$. This is the equivalent of performing the integral (B.9).

As Feynman noted [78], quantum mechanics deals with probability amplitudes rather than probabilities themselves. The approach above has to be extended in order to deal with superpositions. Conditional probability for such states is not a straightforward concept. Say, e.g., we have a photodetection event, B_T. Inference of the state prior to photodetection, i.e., determining the coefficients $c_\pm$ of the state

$$|\psi\rangle = c_+|+\rangle + c_-|-\rangle \tag{B.13}$$

is not easy if superpositions are allowed – in the case where only jumps can occur, we know that the atom should have been in the excited state. On the other hand, it is easy, *given* the state is $|\psi\rangle$, to calculate the probabilities. In order to write an equation like (B.1) allowing coherence, we have to define what the action of the measurement device is. We shall not interpret "measurement device" literally. When we derived the master equation (2.55) we considered the environment to be coupled to the system in such a way that photons could be lost irreversibly. Measuring, in this case, means an output channel to a reservoir that can give information to an observer or not. In any case, the dynamics of a measurement – independent of it providing information or not – is non-unitary. Instead of calculating the dynamics of a state coupled to the reservoir, through a master equation, we simulate many realizations of the *effect* of the reservoir on the system, and infer the state from an average, as we would do in a real experiment. For a simple photo-detection, this effect is described by the operators

$$\hat{H}_C = \hat{H} - i\kappa\hat{a}^\dagger\hat{a}, \tag{B.14}$$

$$\hat{\mathcal{J}} = \sqrt{2\kappa}\hat{a}. \tag{B.15}$$

Here, $\hat{H}_C$ is a non-Hermitian Hamiltonian associated with the terms $-\kappa(\hat{a}^\dagger\hat{a}\rho + \kappa\rho\hat{a}^\dagger\hat{a})$ in the master equation, and $\hat{\mathcal{J}}$ represents the effect of a jump event (photo-emission) on

the system. The full dynamics of the system can be written as

$$\dot{\rho} = (\mathcal{L}_C + \mathcal{L}_J)\,\rho, \tag{B.16}$$

where

$$\mathcal{L}_C\rho = i^{-1}(\hat{H}_C\rho - \rho\hat{H}_C^\dagger) \tag{B.17}$$

and $\mathcal{L}_\mathcal{J}\rho = \hat{\mathcal{J}}\rho\hat{\mathcal{J}}^\dagger$. The evolution of the system density operator can be written as a Dyson expansion,

$$\rho(t) = \mathrm{e}^{\mathcal{L}_C t}\rho(0) + \int_0^t \mathrm{e}^{\mathcal{L}_C(t-t')}\mathcal{L}_\mathcal{J}\mathrm{e}^{\mathcal{L}_C(t')}\rho(0)\mathrm{d}t'. \tag{B.18}$$

The first term of this equation represents the evolution conditioned upon no photon detection,

$$\rho_C = \mathrm{e}^{\mathcal{L}_C}\rho(0) = \mathrm{e}^{-i\hat{H}_C t}|\Psi_0\rangle\langle\Psi_0|\mathrm{e}^{i\hat{H}_C^\dagger t} = |\Psi_t\rangle\langle\Psi_t|. \tag{B.19}$$

The second term gives the evolution conditioned upon a photodetection at time t',

$$\rho_{B_T}(t) = \mathrm{e}^{-i\hat{H}_C(t-t')}\hat{\mathcal{J}}|\Psi_{t'}\rangle\langle\Psi_{t'}|\hat{\mathcal{J}}^\dagger\mathrm{e}^{i\hat{H}_C^\dagger(t-t')} = |\Psi_t'\rangle\langle\Psi_t'|. \tag{B.20}$$

This equation can be rephrased in terms of states. We note that the time evolution given by the non-Hermitian Hamiltonian is non-unitary. The norm of the state $\mathrm{e}^{i\hat{H}_C t}|\Psi_0\rangle$ gives its probability. We can define the normalized conditional states

$$|\psi_C\rangle = \frac{|\Psi_t\rangle}{\sqrt{\langle\Psi_t|\Psi_t\rangle}}, \tag{B.21}$$

$$|\psi_{B_T}\rangle = \frac{|\Psi_t'\rangle}{\sqrt{\langle\Psi_t'|\Psi_t'\rangle}}, \tag{B.22}$$

and redefine the states $\rho_C = |\psi_C\rangle\langle\psi_C|$ and $\rho_{B_T} = |\psi_{B_T}\rangle\langle\psi_{B_T}|$ so that they are normalized. The Dyson expansion becomes

$$\rho(t) = P(C)\rho_C + \int_0^t P(B_T)\rho_{B_T}(t')\mathrm{d}t, \tag{B.23}$$

with $P(C) = \langle\Psi_t|\Psi_t\rangle$ and $P(B_T) = \langle\Psi_t'|\Psi_t'\rangle$. The Monte Carlo rules can be applied in this case to calculate $\rho(t)$ for a single trajectory. In pseudo code it can be written as

Compute $P(B_T) = \langle\Psi'|\Psi'\rangle$

If $r_t < P(B_T)$ **then** $|\Psi(t+\Delta t)\rangle = \hat{\mathcal{J}}|\Psi(t)\rangle$

Else $|\psi(t+\Delta t)\rangle = \mathrm{e}^{i\hat{H}_C\Delta t}|\Psi\rangle$

The process is repeated many times in order to calculate the average (B.1) and obtain the density matrix. The record is created, as in a experiment, by "preparing" the same initial state many times and repeating the measurement. The more we repeat the experiment, the more precise is our knowledge about the state. This treatment can be made very rigorous to include different measurement schemes, as described below.

B.2. Homodyne and heterodyne detection schemes

To introduce the Homodyne/Heterodyne detection schemes in the quantum trajectory theory one have to consider what are the effects of the field of the local oscillator. To account for the extra detector needed by this kind of measurement, we need two output channels, one for each arm of the beam splitter

$$\hat{\mathcal{J}}_P = \frac{1}{\sqrt{2}}\left(\mathcal{E} + \hat{\mathcal{J}}\right), \tag{B.24}$$

$$\hat{\mathcal{J}}_M = \frac{1}{\sqrt{2}}\left(\mathcal{E} - \hat{\mathcal{J}}\right). \tag{B.25}$$

According to the definitions of section B.1, we write the total evolution for the system as a combination of the jumps given above, plus Hamiltonian dynamics, which is given by

$$\mathrm{e}^{\mathcal{L}_C t}\rho = \tilde{B}(t)\rho\tilde{B}^{\dagger}(t), \tag{B.26}$$

where $\mathcal{L}_C$ is the Liouvillian operator defined in equation (B.17), and $\tilde{B}(t) = \mathrm{e}^{-i\hat{H}_B t}$. We add the contribution of the local oscillator field to the non-Hermitian Hamiltonian

$$\hat{H}_B \to \hat{H}_B + i\frac{1}{2}\left|\mathcal{E}\right|^2 \tag{B.27}$$

The addition of the local oscillator will make the detectors fire much faster than in the simple photodetection case. Were we applying Monte Carlo rules in this case the time steps should be much smaller so the probability of photodetection satisfies $\Delta t\gamma|\mathcal{E}|^2 < 1$. Instead, we consider that the back action is continuous over time. We consider the detections occur at regular intervals of time[1], τ, and write the operator giving the state

[1] This is not a fundamental requirement. The interval between the detections can be arbitrary; we opt for a simplified derivation.

of the system at time $\Delta t = N\tau$ as

$$|\Psi(t+\Delta t)\rangle = \tilde{B}(\tau)\hat{\mathcal{J}}_{t_{N-1}}\tilde{B}(\tau)\hat{\mathcal{J}}_{t_{N-2}}\tilde{B}(\tau)\cdots\tilde{B}(\tau)\hat{\mathcal{J}}_{t_1}\tilde{B}(\tau)|\Psi(t)\rangle, \tag{B.28}$$

where $\hat{\mathcal{J}}_{t_n} = \{\hat{\mathcal{J}}_P, \hat{\mathcal{J}}_M\}$, and N is the total number of times the two detectors fired in the interval Δt. Considering that $N \to \infty$, i.e. $\tau \to 0$, we can expand the evolution operator as

$$\left(\hat{\mathcal{J}} + \mathcal{E}\right)\left(1 + i\hat{H}_B\tau\right)\left(\hat{\mathcal{J}} - \mathcal{E}\right)\cdots\left(1 + i\hat{H}_B\tau\right)\left(\hat{\mathcal{J}} + \mathcal{E}\right). \tag{B.29}$$

We denote the number of detections in the channel $\hat{\mathcal{J}}_{P(M)}$ by $N_{P(M)}$, and take the limit $N \to \infty$ with $\Delta t \to 2N_{P(M)}/\left|\mathcal{E}\right|^2$, keeping only terms of order Δt,

$$\left(\frac{\mathcal{E}}{\sqrt{2}}\right)^N \mathrm{e}^{-\frac{1}{2}|\mathcal{E}|^2\Delta t}\left\{\left(1 + i\hat{H}_B\frac{\Delta t}{N}\right)^N + \frac{N_P - N_M}{\mathcal{E}}\hat{\mathcal{J}} - \frac{(N_P - N_M)^2 - N}{2\mathcal{E}^2}\hat{\mathcal{J}}^2\right\} \tag{B.30}$$

The first term in the brackets is the Hamiltonian evolution. The terms with N_P and N_M will depend on the state of the system and will introduce the measurement feedback. They are the intensity of the field in each arm of the beam splitter plus fluctuations, and can be written as

$$N_P = \frac{1}{2}\langle(\mathcal{E}^* + \hat{\mathcal{J}}^\dagger)(\mathcal{E} + \hat{\mathcal{J}})\rangle + \frac{1}{\sqrt{2}}\left|\mathcal{E}\right|\Delta W_P(t), \tag{B.31}$$

$$N_M = \frac{1}{2}\langle(\mathcal{E}^* - \hat{\mathcal{J}}^\dagger)(\mathcal{E} - \hat{\mathcal{J}})\rangle + \frac{1}{\sqrt{2}}\left|\mathcal{E}\right|\Delta W_M(t), \tag{B.32}$$

where $\Delta W_{P(M)}$ are Gaussian distributed random numbers representing the shot noise of the local oscillator, and have the properties $\Delta W^2_{P(M)} = \Delta t$ and $\langle\Delta W_P \Delta W_M\rangle = 0$. The term multiplying the expansion will change the normalization of the state. By replacing the expressions for N_P and N_M into (B.30) we obtain (7.17)

The Heterodyne measurement scheme is obtained in a similar way. First we must consider the local oscillator has noise in both amplitude and phase, we must consider

$$\Delta W \to \Delta Z,$$

where ΔZ is the complex Gaussian noise given in section 7.2.1. We also introduce the time dependency in the local oscillator field $\mathcal{E} \to \mathcal{E}\mathrm{e}^{i\Delta\omega t}$, with $\Delta\omega = \omega - \omega_{LO}$. We follow the derivation, and neglect the high frequency terms $\mathrm{e}^{2i\Delta\omega t}$ to obtain equation (7.19).

Bibliography

[1] J. Liphardt, B. Onoa, S. B. Smith, I. Tinoco, and C. Bustamante, "Reversible unfolding of single RNA molecules by mechanical force," *Science*, vol. 292, no. 5517, pp. 733–737, 2001.

[2] H. J. Kimble, *Structure and dynamics in cavity quantum electrodynamics*. Boston: Academic Press, 1994. Published in *Cavity Quantum Electrodynamics*, Berman, P. R., editor.

[3] R. H. Dicke, "Coherence in spontaneous radiation processes," *Physical Review*, vol. 93, p. 99, 1953.

[4] M. Gross and S. Haroche, "Super-radiance – an essay on the theory of collective spontaneous emission," *Physics Reports-Review Section of Physics Letters*, vol. 93, no. 5, pp. 301–396, 1982.

[5] M. Tavis and F. W. Cummings, "Exact Solution for an N-Molecule Radiation-Field Hamiltonian," *Phys. Rev.*, vol. 170, pp. 379–384, Jun 1968.

[6] G. T. Foster, S. L. Mielke, and L. A. Orozco, "Intensity correlations in cavity QED," *Physical Review A*, vol. 61, no. 5, p. 053821, 2000.

[7] T. J. Osborne and M. A. Nielsen, "Entanglement in a simple quantum phase transition," *Physical Review A*, vol. 66, no. 3, pp. –, 2002.

[8] N. Lambert, C. Emary, and T. Brandes, "Entanglement and entropy in a spin-boson quantum phase transition," *Physical Review A*, vol. 71, p. 053804, 2005.

[9] K. Hepp and E. H. Lieb, "Equilibrium statistical mechanics of matter interacting with quantized radiation field," *Physical Review A*, vol. 8, no. 5, pp. 2517–2525, 1973.

[10] C. Cohen-Tannoudji, J. Dupont-Roc, and G. Grynberg, *Atom-photon interactions: basic processes and applications*. New York: J. Wiley, 1992.

[11] K. Gawędzki and K. Rzążewski, "No-go theorem for the superradiant phase transition without dipole approximation," *Phys. Rev. A*, vol. 23, pp. 2134–2136, May 1981.

[12] I. Bialynicki-Birula and K. Rzaewski, "No-go theorem concerning the superradiant phase transition in atomic systems," *Phys. Rev. A*, vol. 19, pp. 301–303, Jan 1979.

[13] K. Rzążewski and K. Wódkiewicz, "Stability of matter interacting with photons," *Phys. Rev. A*, vol. 43, pp. 593–594, Jan 1991.

[14] K. Rzazewski, K. Wodkiewicz, and W. Zakowicz, "Phase-Transitions, 2-Level Atoms, and A^2 Term," *Physical Review Letters*, vol. 35, no. 7, pp. 432–434, 1975.

[15] K. Rzazewski and K. Wodkiewicz, "Comment on "instability and entanglement of the ground state of the Dicke model"," *Physical Review Letters*, vol. 96, no. 8, p. 089301, 2006.

[16] T. Holstein and H. Primakoff, "Field dependence of the intrinsic domain magnetization of a ferromagnet," *Physical Review*, vol. 58, no. 12, pp. 1098–1113, 1940.

[17] H. Haken, H. Risken, and W. Weidlich, "Quantum Mechanical Solutions of Laser Master Equation. III – Exact Equation for a Distribution Function of Macroscopic Variables," *Zeitschrift Fur Physik*, vol. 206, no. 4, pp. 355–368, 1967.

[18] F. T. Arecchi, H. Thomas, R. Gilmore, and E. Courtens, "Atomic coherent states in quantum optics," *Physical Review A*, vol. 6, no. 6, pp. 2211–2237, 1972.

[19] P. D. Drummond and C. W. Gardiner, "Generalized P-representations in quantum optics," *Journal of Physics A – Mathematical and General*, vol. 13, no. 7, pp. 2353–2368, 1980.

[20] J. Wang, H. M. Wiseman, and G. J. Milburn, "Dynamical creation of entanglement by homodyne-mediated feedback," *Physical Review A (Atomic, Molecular, and Optical Physics)*, vol. 71, no. 4, p. 042309, 2005.

[21] T. Bhattacharya, S. Habib, and K. Jacobs, "Continuous quantum measurement and the emergence of classical chaos," *Phys. Rev. Lett.*, vol. 85, pp. 4852–4855, Dec 2000.

[22] A. J. Scott and G. J. Milburn, "Quantum nonlinear dynamics of continuously measured systems," *Phys. Rev. A*, vol. 63, p. 042101, Mar 2001.

[23] W. Heitler, *The Quantum Theory of Radiation*. London: Oxford University Press, 1944.

[24] M. Sargent, M. O. Scully, and W. E. Lamb, *Laser physics*. Reading, Mass.: Addison-Wesley Pub. Co. Advanced Book Program, 1974.

[25] C. Cohen-Tannoudji, B. Diu, and F. Laloë, *Quantum Mechanics*, vol. 2. New York: Wiley, 2000.

[26] C. Cohen-Tannoudji, B. Diu, and F. Laloë, *Quantum mechanics*, vol. 1. New York: Wiley, 1977.

[27] M. Xiao, H. J. Kimble, and H. J. Carmichael, "Quantum Fluctuations for 2-Level Atoms in a High-Q Cavity with a Spatially Varying Field Mode," *Physical Review A*, vol. 35, no. 9, pp. 3832–3843, 1987.

[28] H. Carmichael, *Statistical Methods in Quantum Optics I: Master Equations and Fokker-Planck Equations*. Springer Verlag, 2002. In this book the comutation relations are different from the ones used in this work, namely: $\left[\hat{J}_+, \hat{J}_-\right] = \hat{J}_z$.

[29] W. H. Louisell, *Quantum statistical properties of radiation*. New York: Wiley, 1973.

[30] M. Lax, "Formal theory of quantum fluctuations from a driven state," *Phys. Rev.*, vol. 129, pp. 2342–2348, Mar 1963.

[31] P. L. Smith, C. Heise, J. R. Esmond, and R. L. Kurucz, "Atomic spectral line database from Kurucz files."
http://cfa-www.harvard.edu/amdata/ampdata/kurucz23/sekur.html, 1995.

[32] L. Moi, P. Goy, M. Gross, J. M. Raimond, C. Fabre, and S. Haroche, "Rydberg-atom masers. I. A theoretical and experimental study of super-radiant systems in the millimeter-wave domain," *Physical Review A*, vol. 27, no. 4, pp. 2043–2064, 1983.

[33] P. Goy, L. Moi, M. Gross, J. M. Raimond, C. Fabre, and S. Haroche, "Rydberg-atom masers. II. Triggering by external radiation and application to millimeter-wave detectors," *Physical Review A*, vol. 27, no. 4, pp. 2065–2081, 1983.

[34] P. Cahuzac, H. Sontag, and P. E. Toschek, "Visible superfluorescence from atomic europium," *Optics Communications*, vol. 31, no. 1, pp. 37–41, 1979.

[35] J. J. Sakurai, *Modern Quantum Mechanics*. Addison-Wesley, 1994.

[36] D. F. Walls and G. J. Milburn, *Quantum optics*. Berlin: Springer, 1994.

[37] S. Sachdev, *Quantum phase transitions*. New York: Cambridge University Press, 1999.

[38] Y. K. Wang and F. T. Hioe, "Phase-transition in Dicke model of superradiance," *Physical Review A*, vol. 7, no. 3, pp. 831–836, 1973.

[39] H. J. Carmichael, C. W. Gardiner, and D. F. Walls, "Higher-order corrections to dicke superradiant phase-transition," *Physics Letters A*, vol. A 46, no. 1, pp. 47–48, 1973.

[40] G. C. Duncan, "Effect of antiresonant atom-field interactions on phase transitions in the Dicke model," *Phys. Rev. A*, vol. 9, pp. 418–421, Jan 1974.

[41] F. T. Hioe, "Phase transitions in some generalized Dicke models of superradiance," *Phys. Rev. A*, vol. 8, pp. 1440–1445, Sep 1973.

[42] R. Pathria, *Statistical Mechanics*. Pergamon Press, 1964.

[43] R. J. Glauber, "The quantum theory of optical coherence," *Phys. Rev.*, vol. 130, pp. 2529–2539, Jun 1963.

[44] G. B. Arfken and H.-J. Weber, *Mathematical methods for physicists*. San Diego: Academic Press, 4th ed., 1995.

[45] P. W. Milonni, J. R. Ackerhalt, and H. W. Galbraith, "Chaos in the Semiclassical N-Atom Jaynes-Cummings Model – Failure of the Rotating-Wave Approximation," *Physical Review Letters*, vol. 50, no. 13, pp. 966–969, 1983.

[46] D. Kruse, M. Ruder, J. Benhelm, C. von Cube, C. Zimmermann, P. W. Courteille, T. Elsässer, B. Nagorny, and A. Hemmerich, "Cold atoms in a high-Q ring cavity," *Phys. Rev. A*, vol. 67, p. 051802, May 2003.

[47] B. Nagorny, T. Elsässer, H. Richter, A. Hemmerich, D. Kruse, C. Zimmermann, and P. Courteille, "Optical lattice in a high-finesse ring resonator," *Phys. Rev. A*, vol. 67, p. 031401, Mar 2003.

[48] C. Emary and T. Brandes, "Chaos and the quantum phase transition in the Dicke model," *Physical Review E*, vol. 67, p. 066203, 2003.

[49] R. J. Glauber, "Coherent and incoherent states of the radiation field," *Phys. Rev.*, vol. 131, pp. 2766–2788, Sep 1963.

[50] E. C. G. Sudarshan, "Equivalence of semiclassical and quantum mechanical descriptions of statistical light beams," *Phys. Rev. Lett.*, vol. 10, pp. 277–279, Apr 1963.

[51] E. Wigner, "On the quantum correction for thermodynamic equilibrium," *Phys. Rev.*, vol. 40, pp. 749–759, Jun 1932.

[52] H. M. Nussenzveig, *Introduction to quantum optics*. Documents on modern physics, London: Gordon and Breach Science Publishers, 1973.

[53] C. W. Gardiner, *Handbook of stochastic methods for physics, chemistry, and the natural sciences*. Berlin: Springer, 3rd ed., 2004.

[54] L.-M. Duan, G. Giedke, J. I. Cirac, and P. Zoller, "Inseparability criterion for continuous variable systems," *Phys. Rev. Lett.*, vol. 84, pp. 2722–2725, Mar 2000.

[55] V. Giovannetti, S. Mancini, D. Vitali, and P. Tombesi, "Characterizing the entanglement of bipartite quantum systems," *Phys. Rev. A*, vol. 67, p. 022320, Feb 2003.

[56] M. J. Collett and C. W. Gardiner, "Squeezing of intracavity and traveling-wave light fields produced in parametric amplification," *Phys. Rev. A*, vol. 30, pp. 1386–1391, Sep 1984.

[57] C. W. Gardiner and M. J. Collett, "Input and output in damped quantum systems: Quantum stochastic differential equations and the master equation," *Phys. Rev. A*, vol. 31, pp. 3761–3774, Jun 1985.

[58] F. Dimer, B. Estienne, A. S. Parkins, and H. J. Carmichael, "Dicke model quantum phase transition in an optical cavity QED system," *Physical Review A*, vol. 75, p. 013804, 2006.

[59] G. S. Agarwal, L. M. Narducci, R. Gilmore, and D. H. Feng, "Optical bistability: A self-consistent analysis of fluctuations and the spectrum of scattered light," *Phys. Rev. A*, vol. 18, pp. 620–634, Aug 1978.

[60] C. Emary and T. Brandes, "Quantum chaos triggered by precursors of a quantum phase transition: The Dicke model," *Phys. Rev. Lett.*, vol. 90, p. 044101, Jan 2003.

[61] N. G. Van Kampen, *Stochastic processes in physics and chemistry.* Amsterdam: North-Holland, Rev. and enl. ed., 1992.

[62] J. Radcliff, "Some properties of coherent spin states," *Journal of Physics Part a General*, vol. 4, no. 3, pp. 313–323, 1971.

[63] R. J. Glauber and F. Haake, "Superradiant pulses and directed angular-momentum states," *Physical Review A*, vol. 13, no. 1, pp. 357–366, 1976.

[64] M. J. Collett, "Exact density-matrix calculations for simple open systems," *Phys. Rev. A*, vol. 38, pp. 2233–2247, Sep 1988.

[65] A. M. Smith and C. W. Gardiner, "Simulations of nonlinear quantum damping using the positive P representation," *Phys. Rev. A*, vol. 39, pp. 3511–3524, Apr 1989.

[66] R. Miller, T. E. Northup, K. M. Birnbaum, A. Boca, A. D. Boozer, and H. J. Kimble, "Trapped atoms in cavity QED: coupling quantized light and matter," *Journal of Physics B-Atomic Molecular and Optical Physics*, vol. 38, no. 9, pp. S551–S565, 2005.

[67] H. Nha and H. J. Carmichael, "Entanglement within the quantum trajectory description of open quantum systems," *Physical Review Letters*, vol. 93, no. 12, p. 120408, 2004.

[68] M. Hillery, R. F. O'Connell, M. O. Scully, and E. P. Wigner, "Distribution functions in physics: fundamentals," *Phys. Rep.*, vol. 106, p. 0121, 1984.

[69] S. Thwaite, "Quantum dynamics of a driven trapped atom," Master's thesis, University of Auckland, 2007.
Available on-line at: *http://www.qo.phy.auckland.ac.nz/*.

[70] S. M. Tan, "Quantum optics toolbox for Matlab®."
http://www.qo.phy.auckland.ac.nz/, 2002.

[71] H. Carmichael, *Statistical Methods in Quantum Optics II: Non-Classical Fields*. Springer Verlag, 2007.

[72] H. P. Yuen and V. W. S. Chan, "Noise in homodyne and heterodyne-detection," *Optics Letters*, vol. 8, no. 3, pp. 177–179, 1983.

[73] H. J. Carmichael, H. M. Castro-Beltran, G. T. Foster, and L. A. Orozco, "Giant violations of classical inequalities through conditional homodyne detection of the quadrature amplitudes of light," *Phys. Rev. Lett.*, vol. 85, pp. 1855–1858, Aug 2000.

[74] P. D. Drummond and K. Dechoum, "Universality of quantum critical dynamics in a planar optical parametric oscillator," *Physical Review Letters*, vol. 95, no. 8, 2005. 083601.

[75] V. V. Zheleznyakov, V. V. Kocharovskii, and V. V. Kocharovskii, "Polarization-waves and superradiance in active media," *Uspekhi Fizicheskikh Nauk*, vol. 159, no. 2, pp. 193–260, 1989.

[76] H. Carmichael, *An open systems approach to quantum optics*. Lecture notes in physics. New series m, Monographs ; m18, Berlin ; New York: Springer-Verlag, 1993.

[77] S. Ghose, P. Alsing, I. Deutsch, T. Bhattacharya, and S. Habib, "Transition to classical chaos in a coupled quantum system through continuous measurement," *Physical Review A (Atomic, Molecular, and Optical Physics)*, vol. 69, no. 5, p. 052116, 2004.

[78] R. P. Feynman, *The Feynman Lectures On Physics: Mainly Mechanics, Radiation, And Heat*, vol. 3 – Quantum Mechanics. Addison-Wesley Publishing Company, 1963.